

# Utilizing the Organizational Power of DNA Scaffolds for New Nanophotonic Applications

Hieu Bui, Sebastián A. Díaz, Jake Fontana, Matthew Chiriboga, Remi Veneziano, and Igor L. Medintz\*

Rapid development of DNA technology has provided a feasible route to creating nanoscale materials. DNA acts as a self-assembled nanoscaffold capable of assuming any three-dimensional shape. The ability to integrate dyes and new optical materials such as quantum dots and plasmonic nanoparticles precisely onto these architectures provides new ways to exploit their near- and far-field interactions. A fundamental understanding of these optical processes will help drive development of next-generation photonic nanomaterials. This review is focused on latest progress in DNA-based photonic materials and highlights DNA scaffolds for rapidly assembling and prototyping nanoscale optical devices. Three areas are discussed including intrinsically active DNA structures displaying chiral properties, DNA scaffolds hosting plasmonic nanomaterials, and fluorophore-labeled DNAs that engage in Förster resonance energy transfer and give rise to complex molecular photonic wires. An explanation of what is desired from these optical processes when harnessed sets the tone for what DNA scaffolds are providing toward each focus. Examples from the literature illustrate current progress along with a discussion of challenges to overcome for further improvements. Opportunities to integrate diverse classes of optically active molecules including light-generating enzymes, fluorescent proteins, nanoclusters, and metal–chelates in new structural combinations on DNA scaffolds are also highlighted.

## 1. Introduction

In the modern era, the impact that optically active devices have on our daily lives is subtle yet cannot be overstated. These devices are integral to an incredibly broad gamut of technologies ranging from televisions, lasers, fiber optics, portable phones, and photovoltaic cells to a myriad of diagnostics, (bio)sensors, and even medical treatments. Similar to the challenge faced by semiconductor chip manufacturers when producing integrated circuits with lithographic techniques, optical device engineers face growing pressure to produce continuously smaller, cheaper, faster, and more powerful, yet still energy efficient devices, if they hope to compete in a rapidly changing marketplace. Depending upon the final product of course, traditional methods of fabricating optical systems also rely to a large extent on lithographic-based approaches where bulk materials are subjected to multiple rounds of pre-defined fabrication procedures to produce and organize the functional components. A major issue currently faced in fabrication of optical devices, is that the Abbe diffraction

limit is reached when devices are scaled or operate on or below the wavelength regime of the electromagnetic radiation they interact with.<sup>[1]</sup> This acts as a major impediment to developing a new generation of smaller devices that function with conventional optically active materials such as dyes, polymers, etc.


Concomitant with the development of the above issues, the burgeoning field of nanotechnology has given rise to a new generation of optically active materials that are on a size scale that is far smaller (<100 nm) than the visible light spectrum. Inspired from nature where atoms and molecules self-assemble to form macromolecules in a very precise order, the field of nanotechnology has been focused on creating new materials by arranging components at the molecular scale, i.e., from the bottom-up as opposed to top-down. Examples of new optically active materials include gold nanoparticles (AuNPs) and gold nanorods (AuNRs), which manifest unique size- and shape dependent plasmonic resonance bands when interacting with light,<sup>[2]</sup> and semiconductor quantum dots (QDs) which demonstrate size-tunable quantum confined photoluminescent spectra.<sup>[3]</sup> Other even newer materials include luminescent gold nanoclusters,<sup>[4]</sup>

Dr. H. Bui, Dr. S. A. Díaz, Dr. J. Fontana, M. Chiriboga, Dr. I. L. Medintz  
Center for Bio/Molecular Science and Engineering, Code 6900

U.S. Naval Research Laboratory  
Washington, D.C. 20375, USA  
E-mail: igor.medintz@nrl.navy.mil

Dr. H. Bui  
Research Associate Program  
National Research Council  
Washington, D.C. 20001, USA

M. Chiriboga, Prof. R. Veneziano  
Department of Bioengineering  
Institute for Advanced Biomedical Research  
George Mason University  
Manassas, VA 20110, USA

 The ORCID identification number(s) for the author(s) of this article can be found under <https://doi.org/10.1002/adom.201900562>.

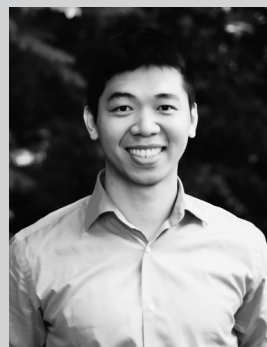
© 2019 The Authors. Published by WILEY-VCH Verlag GmbH & Co. KGaA, Weinheim. This is an open access article under the terms of the Creative Commons Attribution-NonCommercial License, which permits use, distribution and reproduction in any medium, provided the original work is properly cited and is not used for commercial purposes.

DOI: 10.1002/adom.201900562

nanodiamonds,<sup>[5]</sup> and various types of carbon allotropes.<sup>[6]</sup> Indeed, some of these materials such as QDs, for example, have already even seen preliminary commercial application with incorporation into televisions.<sup>[7]</sup> These, and other related nanomaterials (NMs), show great promise for developing new nanoscale optical devices and probes.<sup>[8]</sup> For example, plasmonic NMs have utility in photo-thermal devices and switches,<sup>[9]</sup> while QDs are being developed for solar energy conversion and quantum computing.<sup>[10]</sup> Much of the untapped potential for such new NMs lies in their ability to interact with each other or other types of materials when placed in nanoscale proximity. Employing a variety of unique optical materials with different photophysical properties together is one method of modulating device function. Nanoscale proximity will also allow them to access both near- and far-field interactions, engage in different types of energy transfer, plasmonic interactions or enhancement, along with other types of optical processes. It is here that these materials share much in common with current optical devices, that is the desire to both scale them in size below the diffraction limit and to also place them in very close proximity to each other where they can be further enhanced by combining them with more conventional optical materials such as organic dyes and chiral molecules. The interface of these materials provides new exciting opportunities to sense and signal at nanometer length scales for energy harvesting, heat transfer, photodetection, light sources, and nanomedicine applications.<sup>[11]</sup> Reliable, accurate, and precise fabrication methods are absolutely critical for such device function, however, the challenge remains in how to accomplish this repeatedly in a carefully controlled and prescribed fashion.

The nanoscale scaffolding, arrangement, or bread-boarding, if you will, needed to accomplish the above has some very specific requirements associated with it. First, it must provide access to 1D, 2D, and 3D architectures that can assume any arbitrary shape or configuration as desired. The spacing between each of the optical elements needs to be controllable and ideally would have sub-nanometer resolution since changes in the relative distance between functional groups can manifest dramatic changes in device output. For example, organic dyes may need to be placed at a distance close enough to allow for resonance dipole coupling but should be far enough to allow for the uncoupling of electron orbitals that create “energy sinks.”<sup>[12]</sup> Moreover, the orientation and flexibility of each discrete element should also be controlled if needed. These assembly capabilities should also extend across many different optical materials, be reproducible, scalable, be somewhat facile to implement, and not be egregiously expensive. Conventional top down methods of fabrication include optical and electron beam lithography suffer from high costs, low throughput for prototyping radically new configurations, and, as mentioned, resolution limitations.<sup>[13]</sup> Furthermore, lithography techniques can damage metallic NPs causing surface defects that interfere with plasmonic output or other desirable optical properties.<sup>[14]</sup>

Although a variety of nanofabrication techniques are available for creating different nanophotonic materials,<sup>[15]</sup> a solution to all these fabrication challenges may be found in the field of DNA nanotechnology. As will be described in further detail below, structural DNA nanotechnology approaches utilize the intrinsic chemical and physical properties of the DNA structure to provide a stable and predictable scaffold on which to arrange



**Hieu T. Bui** received his Ph.D. in Computer Science from Duke University in May 2017 under Prof. John Reif. He is currently a National Academies of Sciences, Engineering, and Medicine – National Research Council Postdoctoral Fellow at the Center for Bio/Molecular Science and Engineering of the U.S. Naval Research Laboratory in Washington, D.C. His research is focused on programming and engineering nucleic acid systems with DNA nanotechnology and synthetic biology for addressing engineering, health, and energy applications.



**Sebastián Díaz** received his Licentiate in chemistry from the University of Buenos Aires (Argentina) and a Ph.D. in chemistry from the Georg-August Universität Göttingen (Germany) while working at the Max Planck Institute for Biophysical Chemistry. He is currently a research chemist at the Center for Bio/Molecular Science and Engineering of the U.S. Naval Research Laboratory in Washington, D.C. His research focuses on the functionalization of nanoparticles for probe development, controlling energy transfer pathways at the nanoscale, and interfacing plasmonics and biology for novel materials and catalysis.



**Remi Veneziano** received his Ph.D. in Health Biology from the University of Montpellier II (France) in 2013. He was Postdoctoral Associate in the Department of Biological Engineering at MIT (Mass., USA) until he joined the Department of Bioengineering in the Volgenau School of Engineering at George Mason University (Virginia, USA) in 2018 as an Assistant Professor. He is currently focusing his research on designing and synthesizing new DNA-based nanomaterials and using DNA nanotechnology to investigate the role of biomolecules nanoscale organization in various cell membrane interaction events.

chromophores and other optically active (nano)materials. Self-assembling DNA techniques pioneered by Seeman, Rothemund, and many others now provide a nanoscale designer “bread-board” which can be used to prototype DNA based devices.<sup>[16]</sup>

Self-assembling DNA techniques such as DNA origami, provide a single pot, enormously parallel, bottom-up fabrication method driven just by reaction thermodynamics. The parallel nature of DNA synthesis makes the reaction process high throughput while the simplicity of the technique means there is low overhead costs and a lower margin of error associated with many aspects of it. When combined with open source computational modeling software tools, nearly any nanoscale volumetric 3D structure can be fabricated while incorporating either rigidity or even varying degrees of flexibility if needed.<sup>[17]</sup>

This perspective provides an overview of what structural DNA technology has to offer for developing new optical devices and functionalities by highlighting recent progress in three prototypical DNA-based optical materials: i – what DNA itself offers as an intrinsically optically active NM; ii – DNA as a nanoscaffold for arranging plasmonic NPs that give rise to plasmonically active materials; and iii – DNA as a platform for arranging diverse types of fluorescent molecules that engage in Förster resonance energy transfer (FRET). To provide a proper context for both the progress and the challenges we begin by briefly discussing pertinent aspects such as how structural DNA technology works, how DNA structures are designed, and how DNA is modified with NPs or fluorophores for photonic applications. As a preface to each of these optical applications, a contextual motivation is

provided which briefly describes the optical process(es) utilized in that section and then what may be ideally accomplished if this DNA-driven approach can be fully realized; the latter represents, in essence, the ultimate vision or goal for that material to some extent. Utilizing examples from the literature allows us to compare where actual progress is in this nascent field relative to this vision. Although a large number of excellent examples are available in the literature, this is not meant to be an exhaustive review and we, unfortunately, only discuss a select few example and our apologies are extended for any and all omissions. Lastly, we highlight a list of remaining challenges, potential routes to address those challenges, and provide an outlook on how integrating diverse classes of optically active molecules in new structural combinations on DNA scaffolds may represent a largely untapped but powerfully enabling technology that can facilitate new applications in this field.

## 2. Structural DNA Technology

Nucleic acid molecules are the carriers of genetic information for all known living organisms. These molecules are also biopolymers displaying exceptional structural properties from a biomaterials perspective. Functionally, DNA hybridization

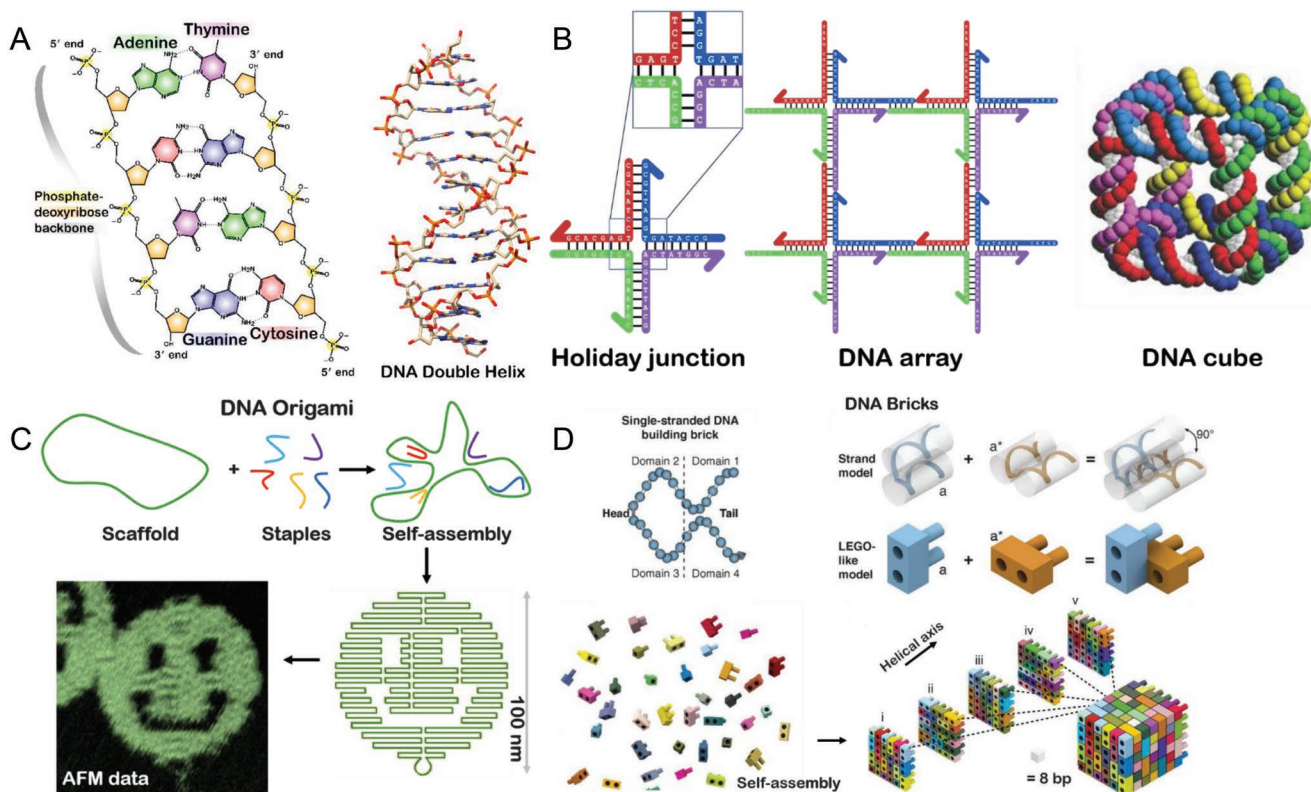


**Figure 1.** Structural DNA nanotechnology. A) Conventional Watson–Crick hybridization such that adenine (A) binds to thymine (T) and guanine (G) binds to cytosine (C) in order to form DNA double helix. Image in the public domain, via Wikimedia Commons. B) Adding sticky ends to the natural Holliday junction enables a new approach to create a 2D DNA array or 3D DNA cube. Reproduced with permission.<sup>[21]</sup> Copyright 2003, Springer Nature. C) Scaffolding methods such as DNA origami enables users to create large nanoscale objects with arbitrary shapes. Reproduced with permission.<sup>[16b]</sup> Copyright 2006, Springer Nature. D) Modular methods such as DNA bricks enable users to create any arbitrary nanoscale objects similar to Lego. Reproduced with permission.<sup>[40]</sup> Copyright 2012, The American Association for the Advancement of Science.



follows the Watson–Crick base pairing rules<sup>[18]</sup>—where adenine (A) binds with thymine (T) and cytosine (C) binds with guanine (G), see **Figure 1A**. The basic building block of DNA nanotechnology is the B-form DNA double helix with the following generalized characteristics: a right-handed turn with a periodicity of 10.5 base pairs (bps)  $\approx$ 3.4 nm in length, a helix diameter of 2 nm, and a persistence length of  $\approx$ 147 bps (50 nm).<sup>[19]</sup> Other forms of DNA such as the A-form (obtained with an RNA/DNA duplex) and left-handed Z-form exist naturally but are not typically utilized and thus remain underrepresented in the structural DNA nanotechnology field.<sup>[20]</sup> DNA's unique molecular specificity makes it an ideal material for controlling self-assembly, predicting structural changes, and programming DNA nanoarchitectures with exquisite complexity and functionality at the nanoscale. Following elucidation of the DNA double helical structure by Watson and Crick in 1953,<sup>[18]</sup> a series of sequential landmark discoveries were made that would eventually lead to the foundation that would give rise to the structural DNA nanotechnology field.

The term structural DNA nanotechnology defines a specific branch of materials science that takes advantage of the specific chemical and structural properties of DNA for engineering artificial nanostructures and devices at the molecular scale<sup>[21]</sup> while still preserving essential DNA molecular functionalities and biocompatibility. The field was first pioneered by Nadrian Seeman at New York University in the early 1980s who created the first artificial DNA junctions (**Figure 1B**).<sup>[16a,22]</sup> His work was inspired by the discovery of the Holliday Junction,<sup>[23]</sup> a naturally occurring DNA branched structure observed during DNA recombination in cells. Using analogs of these branched structures, Seeman demonstrated the possibility of creating discrete DNA nano-objects and large-scale 2D and 3D lattices. From the beginning, his initial objective was to use DNA scaffolds to organize biomolecules with unprecedented nanoscale precision for further structural analysis by X-ray crystallography. Using branched structures, he was notably able to assemble a 3D 7 by 7 nm DNA cube (see **Figure 1B**);<sup>[24]</sup> this would subsequently pave the way for the fast development and expansion of the DNA nanotechnology field.

After three decades, many techniques have now been developed to effectively fold DNA into well-defined 1D, 2D, and 3D structures in a highly programmable manner as highlighted in **Figure 1**,<sup>[16c,25]</sup> demonstrating the feasibility of manipulating and organizing materials beyond the diffraction limit as is desired, in particular, in the semiconductor/lithography industry. Some of the best known examples of early 1D and 2D structures include DNA junctions and various DNA tiles<sup>[26]</sup> and lattices.<sup>[27]</sup> These structures often consist of a finite set of oligonucleotide sequences (or oligos, this terminology is sometimes used interchangeably) which are programmed to hybridize to one another to form the prescribed patterns by means of complementary sticky ends as illustrated in **Figure 1B**. The oligonucleotide sequences are programmed to conceptually fold in any given shape using single DNA duplex multiarm junctions<sup>[28]</sup> or various connected knot or junction types such as a double crossover (DX-Tile)<sup>[29]</sup> or triple crossover (TX-Tile).<sup>[30]</sup> Growing from a few nanometers, the largest structure has been shown to periodically extend to several micrometers in length,<sup>[27d]</sup> an increase of approximately three orders of magnitude. Besides

forming large 2D lattices, DNA tiles were also exploited for DNA computing by programming DNA hybridization reactions to direct self-assembly,<sup>[31]</sup> for creating 3D discrete nanostructures<sup>[32]</sup> and for initially organizing inorganic materials with potential in optical electronic applications.<sup>[33]</sup> In general, DNA tile-based constructs are often periodic structures and consist of a limited number of sequences with repeated motifs, thus limiting the sequence space for integrating other materials beyond the given sequences. In addition, annealing DNA tile-based structures (i.e., self-assembly by temperature driven hybridization) requires optimization of annealing time and an extreme control of the stoichiometry of DNA strands in order to fold correctly. Critically, the yield of folding is known to decrease drastically as the complexity of the final assembly increases.

By early 2000, the need to create a next generation of non-periodic and discrete DNA structures for future applications became apparent. In 2006, Rothemund reported his seminal approach to create discrete DNA nanostructures<sup>[16b]</sup> using the bacteriophage M13mp18 genome, which exists as a circular single-stranded DNA (ssDNA) plasmid of 7249 nucleotides, as a scaffold to assemble DNA nanostructures. Excess complementary synthetic short DNA oligonucleotides (known simply as staple strands) are added to initially drive formation by proscribed crosshybridization events and then hold the structure together by forming stable DNA double helices arranged in any designed shapes. He coined the term “DNA origami” and the technique has now been used extensively to make any arbitrary DNA nanostructure with high yield and robustness, as illustrated in **Figure 1C**. Pertinent to the current context, some initial examples of DNA origami application for assembling nanophotonic circuits were amongst the first translational demonstrations of this approach to be highlighted, see ref.[34] and therein. Additional structural options were later added to fold DNA into twisted and curved nanoscale shapes,<sup>[35]</sup> to fold and cut DNA into reconfigurable topological nanostructures,<sup>[36]</sup> and to assemble discrete 2D and 3D wireframe structures.<sup>[37]</sup> Moreover, to overcome the original size limitations of DNA origami that utilized the original M13mp18 scaffold and to increase production scale, different methods have been explored,<sup>[38]</sup> including a hybrid lambda-M13 virus phagemid system that yielded a scaffold of 51 466 basepairs (bps) in size,  $\approx$ 7 times larger than the original M13mp18.<sup>[39]</sup>

Recognizing that different DNA origami nanostructures will require new scaffold routing designs and a different set of staple strands, Yin et al. recently reported on a new approach to make modular self-assembly of finite-sized, discrete DNA nanostructures and coined it “DNA bricks” as illustrated in **Figure 1D**.<sup>[40]</sup> Unlike DNA origami techniques, the DNA brick approach self-assembles thousands of distinct ss bricks by interbrick binding interactions and thus no intrinsic partner scaffold strand is required. DNA brick structures are composed entirely of short unique strands and many distinct shapes can be derived from the master 3D canvas. Overall, the master 3D canvas is a collection of up to 30 000 strands ( $\approx$ 500 MDa), resulting in 3D DNA structures with various dimension. Similar to DNA origami nanostructures, sophisticated geometries, surface patterns, hollow shapes, and cavities can be designed in DNA brick nanostructures.<sup>[41]</sup> With carefully implemented designs, both DNA origami<sup>[16b]</sup> and DNA brick<sup>[40]</sup> techniques, along with other

**Table 1.** Representative labeling chemistries available for deriving DNA-dye and DNA-NP conjugates (NHS – *N*-hydroxysuccinimide, EDC – 1-ethyl-3-(3-dimethylaminopropyl) carbodiimide, NTA – nitrilotriacetic acid).

Conjugation strategy	DNA	Dye/NP	Notes	Refs.
Dye fluorophores				
Direct synthetic insertion	Phosphoramidite bases	Modified phosphoramidite or fluorescent nucleic acid analog	Dye inserted during DNA synthesis, requires deprotection and purification, limited choice of dyes available	[50]
Labeling of modified DNA	Modified to display amine, thiol labeling site	Reactive dyes such as NHS esters or maleimide activated	Dyes attached post synthesis to nucleotide analog or replacement, wider choice of dyes available	[46]
Intercalation	Native DNA	Monomeric or dimeric homo or heterofunctional intercalating dyes	Standard way to view dsDNA in gels and during capillary electrophoresis	[55a]
Nanoparticles and quantum dots				
Thiol–Au interaction	Thiolated DNA sequence	Gold NPs	Applicable to other noble metal NPs to some extent	[56]
Biotin–avidin chemistry	Biotinylated DNA	Streptavidin-functionalized NPs and QDs	Many streptavidin functionalized NPs are available commercially	[61a]
Electrostatic interactions	Native DNA	Positively charged NPs	Lacks fine control over DNA-NP stoichiometry and orientation	[47]
Covalent modification of NP ligands	Amine/thiol functionalized DNA	NPs and QDs displaying cognate functional groups on their ligands	Multistep chemistry, requires purification, lack of fine control, can include click-type and EDC chemistry	[48]
Metal-affinity coordination	Polyhistidine appended DNA	QDs with available ZnS surface or NPs displaying NTA groups	Ratiometric binding, provides for some control over DNA orientation	[61a]

related approaches,<sup>[17,37c]</sup> enable the creation of larger discrete DNA nanostructures by stitching together multiple discrete DNA nanostructures which can, in turn, accommodate or display macromolecules or host other microarchitectures.<sup>[27,42]</sup> DNA nanotechnology also directly benefits from having multiple open source design and visualization tools such as CanDo, Cadnano, DAEDALUS, V-Helix, and others, which allow for the design and visualization of almost any arbitrary 2D or 3D structure a user can imagine in silico.<sup>[17,37b,c,43]</sup> Though yields typically decrease with increased complexity, recent reports are also starting to address this issue and have noted 90% structural conformity ( $\approx 1\%$  total yield) for 3D structures containing  $>10^8$  individual components.<sup>[41]</sup> Overall, this represents an amazing jump from where the structural DNA field was only 10 years ago, with further increased efficiency still clearly feasible and expected.

### 3. Attachment of Dyes, Nanoparticles, and Other Optically Active Materials to DNA Sequences

Two of the main advantages of utilizing DNA as a nanoscale structural building block over other polymeric materials are found in its addressability coupled to its programmability or the ability to be assembled into prescribed nanostructures. Indeed, within origami and other similar structures, the spatial coordinate of each individual base is known (addressability) for every structure designed and sequence specificity allows for precise conjugation at a resolution that potentially approaches the sub-nanometer scale. Building on this, DNA nanostructures have been utilized to

arrange different materials ranging from organic molecules (e.g., proteins, peptides, and lipids) to inorganic materials such as NPs, allowing realization of even more complex materials with novel properties at the molecular level that are targeted toward diverse applications ranging from drug delivery to nanoelectronics.<sup>[44]</sup> For the current discussion, DNA sequences need to be conjugated with two specific classes of molecules, namely, organic fluorophores and inorganic NPs that include both semiconductor QDs and AuNPs for example. DNA bioconjugation chemistry can be quite complicated and nuanced with many different conjugation chemistries available depending upon what type of molecule is to be attached—extended discussions are available, yet are beyond the current scope of this review.<sup>[45]</sup> See **Table 1** for a representative list of available chemical strategies used to attach dyes and NPs to DNA.<sup>[46–48]</sup> There are, however, several salient points to be appreciated about how the labeled DNA structures are formed since this directly influences their subsequent performance. Primary amongst these are the relative size scales involved.

Organic fluorophores are typically on a size scale comparable to a nucleotide while the NPs can be orders of magnitude larger. Organic dyes can be chemically inserted into DNA during synthesis using two main approaches. The first approach is a two-step method where a specific functional group (e.g., amine, thiol, carboxyl, or alkyne) or modified base (e.g., thymine analog displaying an extended free amine group) is inserted into the DNA sequence at a specific site on some type of linker and then acts as a functional chemical handle for subsequent labeling with a reactive dye (e.g., *N*-hydroxysuccinimyl ester dye derivative for amines, maleimide dye derivative for thiols),

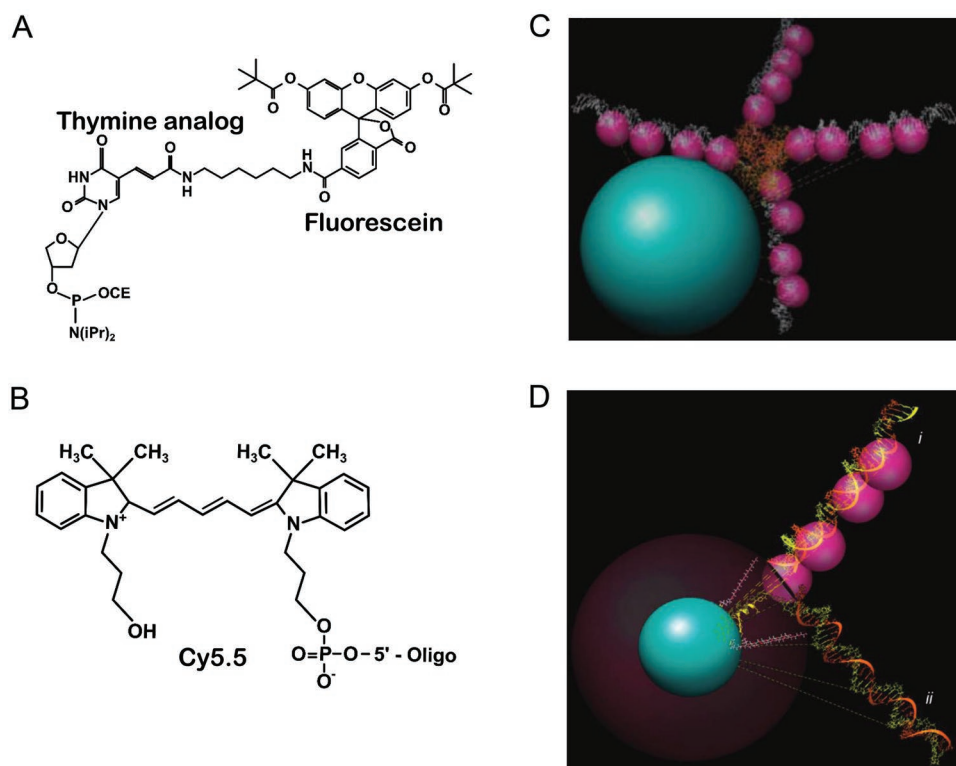


**Figure 2.** Functionalization of DNA with dyes and quantum dots. A) Structure of a fluorescein dye attached to the primary amine on a thymine analog using a six-carbon linker by postsynthetic modification. B) Structure of Cy5.5 dye inserted into DNA during synthesis as a double phosphoramidite, the dye would be attached to the nascent DNA strand by the pendant OH group which functions as a 3'OH analog for attachment to the next base. C) Biotinylated DNA bound to 605 nm emitting streptavidin QDs. The QD core/shell/polymer is simulated by a blue sphere of 75 Å radius according to manufacturer specifications. The streptavidin is shown in orange with DNAs (white) attached at all four binding sites. Fluorescent extensions of putative dye molecules are shown by the magenta spheres. Two possible orientations of the DNA relative to the QDs are shown and are derived by changing the orientation of the streptavidin relative to the QD surface. Note that regardless of orientation, several dyes at all possible acceptor sites are always in close proximity to the QD surface. D) Model of a (His)<sub>6</sub>-peptide-DNA bound to the surface of 530 nm emitting QDs. The QD is shown as the central blue sphere with a radius of 28 Å. The QDs PEGylated surface ligand which provides colloidal stability is indicated by the crimson halo with an estimated extension of 30 Å in an energy-minimized conformation are shown within the crimson sphere. The (His)<sub>6</sub> portion of the peptide is shown with a yellow ribbon. Individual DNA strands within the dsDNA structure are shown in orange and yellow. The rotational extension of putative dye molecules are shown by the magenta spheres. Two possible orientations of the DNA relative to the QDs are shown. (i) DNA extending linearly outward from the QD surface and (ii) DNA adjusted to be at a right angle to that. These represent the maximum extensions available to the DNA. Reproduced with permission.<sup>[58]</sup> Copyright 2010, American Chemical Society.

see **Figure 2A**.<sup>[49]</sup> In the second approach, an appropriately protected version of a dye is directly inserted into the nascent DNA strand during phosphoramidite synthetic chemistry and essentially replaces a nucleotide, see **Figure 2B**.<sup>[50]</sup> Another viable approach is that of incorporating nucleic acid base analogues as epitomized by the work of the Wilhelmsson Group at Chalmers University who synthesized phosphoramidite-protected quadracyclic 2-deoxyadenosine analogues and incorporated them into DNA using standard synthetic chemistry.<sup>[51]</sup> This work was actually an extension of their previous work that synthesized and characterized 1,3-diaza-2-oxophenoxazine nucleobase analogs.<sup>[52]</sup> Some of the issues surrounding this type of chemistry are the length of the linkers to which the dye is attached as extended flexibility can affect dipole orientation during energy transfer and allow interactions with other nucleotides that can quench fluorescence.<sup>[53]</sup> Placing two dyes very close to each other in this manner can also affect fluorescence through dimer formation.<sup>[53b,54]</sup>

Following labeling, the dye incorporating sequences are then utilized in the assembly of larger DNA structures in a manner analogous to unlabeled sequences; that is they are typically added to an origami reaction pot with all the other strands to yield structures with dyes at specified DNA addresses. Although not as prevalent for photonic applications, fluorescent labeling of DNA is often accomplished with intercalating dyes as well. These are usually added to a given DNA sequence or structure in some fixed ratio relative to the number of bps present. This results in an average DNA labeling efficiency without precise addressability. Thus, this approach is by far more commonly used for visualizing DNA in gels or in cells and real-time PCR as opposed to labeling of photonically active structures.<sup>[55]</sup>

In stark contrast to the small size of the above fluorophores, many NPs are far larger than a small DNA oligonucleotide and so the NP, in essence, displays the oligo, and, quite often, several repeated copies of it around its surface. Fortunately, for

AuNP-DNA conjugation the ubiquitous thiol-Au interaction serves as a very effective way to coordinate a thiol-modified oligo to the AuNP surface.<sup>[56]</sup> Moreover, oligos modified with terminal thiols are quite common and easily obtained commercially. There can, however, be issues of oligo dissociation under reducing conditions and these are sometimes remedied by having the oligo display multiple thiols.<sup>[57]</sup> For QDs, the primary DNA conjugation chemistry relies on biotinylated DNA to bind to streptavidin functionalized QDs. This, however, brings with it the issue of control over relative DNA orientation as each “box-like” streptavidin proteins has four almost orthogonally placed biotin binding sites and the DNA oligo can assume one of many configurations relative to the QD, see Figure 2C.<sup>[58]</sup> This issue can be exacerbated as there are typically multiple streptavidins attached to each QD and becomes critical in the case of FRET as fluorophores closest to the QD surface will dominate the interactions. Utilization of polyhistidine modified DNA sequences to coordinate directly to the Zn<sup>2+</sup> on the QD surface by metal-affinity coordination can help alleviate this issue to some extent, see Figure 2D.<sup>[59]</sup> For both NPs and QDs, DNA orientation relative to the particle and control over the number of conjugated DNA sequences attached to their surface are important issues as they factor into any subsequent plasmonic or energy transfer processes. Moreover, the net conformation of the DNA on the NP is an equally important issue as it will also strongly influence where the fluorophores are placed relative to a NP.<sup>[59]</sup> Monothiolated AuNPs and QDs are not easily obtained and may require both a careful chemical design strategy and stringent purification.<sup>[60]</sup> The interested reader is referred to several more focused discussions and reviews on this topic.<sup>[3a,59a,61]</sup>

## 4. Intrinsically Active DNA Materials

### 4.1. Contextual Motivation

DNA is generally considered a stable and economically viable biopolymer for nanoapplications with no significant observable optical absorbance throughout the visible portion of the spectrum. Based on these properties, research has developed around exploiting DNA films as optical memory materials and optical amplifiers.<sup>[62]</sup> For example, DNA films show favorable characteristics as a saturable absorber, a material whose absorbance decreases at higher light power, and as such have been used to passively mode-lock a fiber laser cavity.<sup>[63]</sup> Another successful application of DNA films is as an electron blocking layer in organic light-emitting diodes.<sup>[64]</sup> This area of research is quite extensive and we recommend several recent reviews to the interested reader.<sup>[65]</sup>

In the following brief section, we begin by examining a more bio-oriented utility where the DNA's intrinsic optical properties are primarily used as a readout of its local environment and or localized interactions. The particular advantage that DNA has over other types of biopolymers for this application is its powerful structural capabilities built into the bp matching code, which can give rise to programmable, yet extraordinarily complex, nanoscale architectures in high copy number. At the single molecule level, DNA's inherent light-matter interactions,

its broad range high optical transparency, and responses to environmental cues are extremely subtle and often undetectable unless the DNA is acting as a structural matrix for display of other optically active components (vide infra).<sup>[66]</sup> By contrast, at the ensemble level hierarchical DNA structures do display some inherent and useful photonic properties. Pertinently, the double helical structure of dsDNA allows it to act as a polarizer of light.<sup>[67,68]</sup> DNA's capability to polarize light can be utilized as a reporter of environmental conditions (pH, ions, temperature, solvent polarity, etc.)<sup>[68,69]</sup> as well as to sense more complex biomolecular interactions.<sup>[70]</sup> This is typically observed using circular dichroism (CD) techniques with the basic underlying mechanism or relationship described by

$$\Delta A = (\epsilon_L - \epsilon_R)Cl \quad (1)$$

Here, the difference in absorbance ( $\Delta A$ ) is given by the difference in molar extinction coefficients for left and right circularly polarized light ( $\epsilon_L$  and  $\epsilon_R$ , respectively) multiplied by the concentration,  $C$ , and pathlength,  $l$ , of the cell. The most commonly reported form of CD data is in units of molar ellipticity ( $\theta$ , deg cm<sup>-2</sup> dmol<sup>-1</sup>), which is of particular use for biomolecules and which is typically given as

$$\theta = \frac{I_R^{1/2} - I_L^{1/2}}{I_R^{1/2} + I_L^{1/2}} = 3298.2(\epsilon_L - \epsilon_R) \quad (2)$$

where  $I_R$  and  $I_L$  are the right and left circularly polarized detected intensities, respectively. As is apparent from Equations (1) and (2), the greater the change in  $\epsilon$  of the structure, the greater the signal within the CD measurement. Due to the nature of its helices and strands, DNA displays inherent chirality. As often repeated, chirality is the stuff of life as many of the monomeric precursor building blocks of biology and the enzymes that utilize them display specific chiral requirements.<sup>[71]</sup> Moreover, chirality is critical to the desired effects of many drugs.<sup>[72]</sup> As such monitoring and characterizing chiral systems is of considerable interest and CD spectroscopy in combination with nanostructured DNA scaffolds appears to be a developing tool in this regard.<sup>[64,73,74]</sup> The magnitude of DNA CD signals can be increased by adding underlying structure to the DNA making this methodology a small volume, label-free, nondestructive, aqueous environment compatible sensing, and readout strategy.<sup>[75]</sup> It is also here where most of this nascent field is currently focused and a brief overview is provided on three areas to highlight the potential by showing some preliminary applications. This includes biosensing and potential drug delivery vehicles where CD is more prominent and then concludes with utilizing optical transformations in DNA as a mechanism to drive nanomechanical systems.

### 4.2. Biomolecular Sensors

Researchers have begun constructing biomolecular sensors that utilize the unique structure of different DNA forms and their interchangeability as the basis for sensing. Since the discovery of the left-handed Z-form of DNA in the late 1970s,<sup>[76]</sup> the ability to induce and transition from the native B-form to



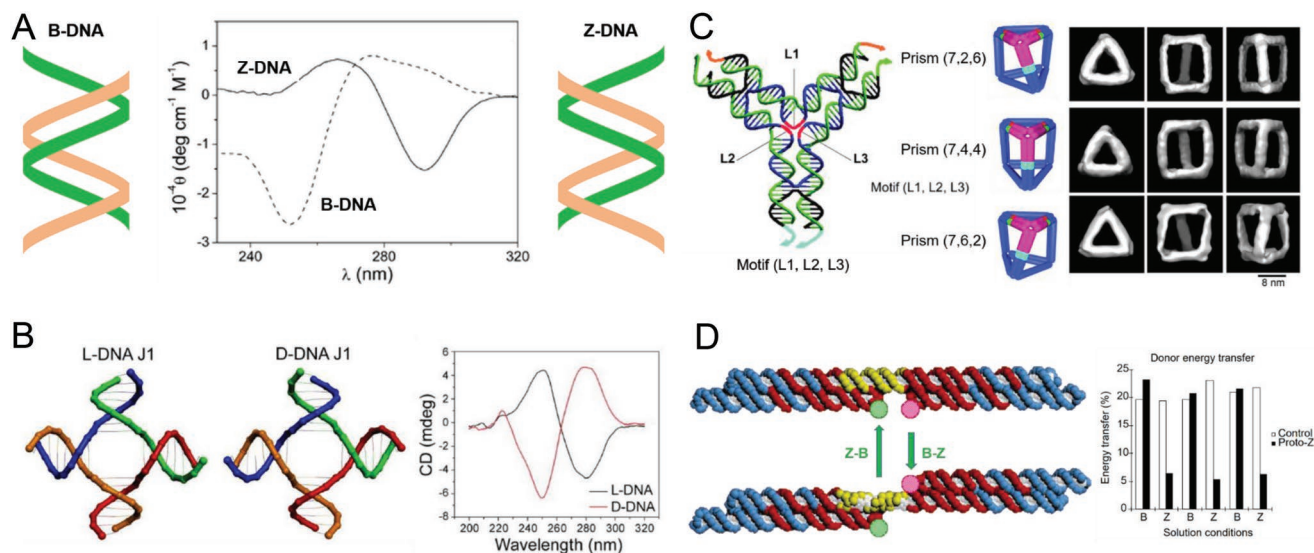


**Figure 3.** Optically active DNA. A) Depending on the handedness of DNA, distinct circular dichroism spectra show dramatic differences between B- and Z-DNA. Reproduced with permission.<sup>[77]</sup> Copyright 2010, The Royal Society of Chemistry. B) Inheriting the handedness of DNA, L-DNA, and D-DNA possess the same duplex conformation except for their opposite chirality. Circular dichroism measurements clearly reveal the opposite chirality of the two distinct four-arm junctions. Reproduced with permission.<sup>[75b]</sup> Copyright 2009, American Chemical Society. C) Self-assembly of chiral DNA triangular prisms out of asymmetric three-point-star motifs. CryoEM characterization of the self-assembled DNA prisms by purposely removing 2D rotation symmetry from the DNA motif in order to control the 3D chirality of the DNA prisms. Reproduced with permission.<sup>[90]</sup> Copyright 2012, Wiley-VCH. D) A nanomechanical system based on the B-Z transition of DNA. The switching between the two systems is read-out as a FRET value. Reproduced with permission.<sup>[91]</sup> Copyright 1999, Springer Nature.

Z-form (or vice versa) as a function of the surrounding environmental conditions including through changes in ions, solvents, and organic molecules has been studied. Because the B-form orients as a right-handed twist and the Z-form DNA as a left-handed twist, their optical responses can, in turn, be observed and used to sense the local environment or its changes. With this concept in mind, Turriani et al. examined the effects of temperature, salt, and ethanol content on the B- to Z-DNA transitions.<sup>[77]</sup> Under normal UV absorption conditions, the right-handed and left-handed DNA were not much different, however the CD signatures showed drastically different signal changes as illustrated in **Figure 3A**. The presence of  $Mg^{2+}$  and ethanol (16% v/v) induced the B- to Z-conformational change, while use of both as a mixture created an aggregate of the latter form known as Z\*-DNA. Turriani also studied the effect of the cyanine dye thiazole orange (an intercalating dye which emits weakly by itself but is strongly enhanced after intercalation into DNA) on the conformational changes.<sup>[78]</sup> Addition of thiazole orange caused a quick return from the Z-form to the B-form DNA. A similar methodology was then utilized by the Subudhi group to report on  $Ce^{+3}$  and  $La^{+3}$  levels based on their interaction with DNA, down to  $7.5 \times 10^{-3}$  M concentrations with clear shifts in the CD spectra from 280 to 260 nm.<sup>[79]</sup> The ability to induce and observe such conformational transitions in DNA suggests this as an excellent optical reporter probe of how drugs interact with DNA, especially given that many chemotherapeutics and several other drug classes including some antibiotics target and interact with DNA.<sup>[80]</sup> Predicting and understanding interactions between DNA and potential treatment candidates would further efforts in developing novel drugs. The work of Alarcón et al. actually utilizes the DNA as

an optical probe to characterize the lipophilic property of drugs, demonstrating that highly lipophilic intercalating drugs such as benzydamine and propranolol greatly modify the structure of DNA as revealed with CD spectroscopy.<sup>[81]</sup>

### 4.3. Potential for Utility in Drug Delivery Vehicles

A great deal of research effort has been invested in understanding the pathophysiology of neurodegenerative diseases and scientists have found that some non-native B-DNA forms could be associated with alterations in the normal functions of cells. In addition, Z-form DNA may participate in gene expression and could also be involved in DNA transcription.<sup>[82]</sup> Other studies have found a high concentration of Z-form DNA in the hippocampal regions of Alzheimer disease patients.<sup>[83]</sup> Being able to measure the different DNA conformations through their intrinsic optical responses could facilitate both understanding of these processes and the synthesis of structurally selective drugs. In this vein, Lin et al. reported on the construction of two four-arm DNA junctions for testing of their intrinsic nuclease-resistance in a biological environment; the latter is critical for any subsequent medical application of DNA structures since endogenous nuclease activity will degrade free DNA *in vivo*.<sup>[75b]</sup> The two junctions (*L*-DNA and *D*-DNA) were mirror images of each other as they had the same duplex conformation but their chirality were opposite as shown in **Figure 3B**. They found that *L*-DNA was far more stable than the *D*-DNA to enzymatic degradation and suggested that small interfering RNA-based drugs could be incorporated within the junctions of such structures for delivery to tumor cells since they would be



less susceptible to degradation. This is another prime example of the aforementioned preference of biological processes for a specific chirality.

It has been demonstrated that DNA nanostructures are capable of providing enhanced cellular delivery for drugs and gene therapy.<sup>[84]</sup> DNA can also interact with lipids to form assemblies that function as cellular delivery structures, in this case the active drug molecule may be the DNA itself, though intercalating and hydrophobic drugs are other reasonable deliverables.<sup>[85]</sup> Importantly the structure of the DNA is strongly modified upon formation of the lipo-complexes, and given the many variables surrounding use of a further exogenous probe (polarity, hydrophobicity, hydrogen bonding) interrogating the DNA structure itself through absorbance and CD spectroscopy is often the best choice.<sup>[86]</sup> For example, Zuidam et al., found that positively charged (dioleoyl-trimethylammoniumpropane) and neutral lipids (dioleoyl-phosphatidylethanolamine), induced DNA to transform from B-form to C-form, upon reaching ratios of lipid/DNA > 1 and a chiral cholesteric-like  $\Psi$ -phase was observed as well.<sup>[87]</sup> These conformational changes could be followed through CD spectroscopy, but more importantly, the conformation/lipid combination was found to be a more effective cellular transfecting agent.<sup>[87]</sup> Subsequent studies found that increased liposome hydrophobicity correlates with greater DNA transformation from B to C-form.<sup>[88]</sup> Standard DNA/liposomes have limited periods of intracellular viability and, in turn, limited chromosomal integration,<sup>[89]</sup> thus it is potentially feasible that specific DNA nanostructures, especially if they have additional functionality, may provide the ideal combination of lipid formulation along with DNA composition to surpass these barriers.

#### 4.4. Nanomechanical and Related Systems

With the goal of creating a building block for future optical materials, Zhang et al. created various chiral DNA triangle prisms using asymmetric DNA three-point-star motifs as the core, illustrated in Figure 3C.<sup>[90]</sup> Using cryogenic electron microscopy (cryoEM) in conjunction with gel electrophoresis, they were able to observe and validate the chiral formations at high resolution. Although it was not explicitly shown, the authors postulate that fabrication of chiral metamaterials could be achieved by utilizing their structures as biotemplates.

Driven from an energy source such as ATP, many protein-based molecular machines have shown intricate motion and perform complex tasks ranging from controlling biosynthesis to coordinating the partitioning that takes place during cellular division. Drawing inspiration from this, development of nanomechanical systems (NAMS) are being pursued to provide a mechanism to sense and harness similar types of properties in a controlled manner on the nanoscale. Beyond nanoscale motion per se, it is postulated that such NAMS could be exploited for sensing of almost any potential target including temperature, pressure, chemical species, magnetic fields, etc. The Seeman group constructed a prototypical nanomechanical systems using two rigid DNA double crossover molecules as illustrated in Figure 3D.<sup>[91]</sup> They utilized the transition between the B- and Z-forms of DNA to show switchable motion as their NAMS

underwent multiple successive cycles of B-promoting and Z-promoting conditions. The Z-promoting condition contained high magnesium chloride ( $100 \times 10^{-3}$  M), moderate sodium chloride ( $100 \times 10^{-3}$  M), and low hexaamminecobalt (III) chloride ( $250 \times 10^{-6}$  M) with  $10 \times 10^{-3}$  M cacodylate buffer (pH 7.5) whereas the B-promoting condition contained low magnesium chloride ( $10 \times 10^{-3}$  M), moderate sodium chloride ( $100 \times 10^{-3}$  M), and no hexaamminecobalt(III) chloride. By integrating a FRET pair at the location where the transition occurs, they measured the mechanical motion indirectly via changes in FRET transfer efficiency.<sup>[92]</sup> A slightly more complex system based on a similar B–Z transition was realized by the Sugiyama group, in this case a rotor system was integrated onto a DNA origami.<sup>[93]</sup> By changing the salt conditions (above  $5 \times 10^{-3}$  M  $Mg^{+2}$ ) the rotor direction was controlled, with a saturation point of 75% desired rotor direction achieved at  $20 \times 10^{-3}$  M  $Mg^{+2}$ . Due to the extensive size of the structure, light interactions with the DNA could confirm the structural B–Z transition, but most of the evidence was gathered through direct AFM observation.<sup>[93]</sup>

The above examples are provided mainly to illustrate the potential that pure DNA nanostructures have for some optically based applications based upon their inherent chirality and the ability to switch it based on their structure. These examples also show that this aspect is still nascent and quite far from maturity and much remains to be developed here as the change in optical properties are most often used as an indirect readout for some type of sensing. In this context, the converse may be more interesting where an added chemical could drive a change in optical properties. We also note that many new and relevant DNA structures are being reported where their potential optical properties are not yet fully realized or explored in this area. For example, the Yan group recently reported on the self-assembly and structural verification of a 3D DNA crystal with sixfold symmetry and right-handed chirality; clearly this construct may have much to offer for these types of applications.<sup>[94]</sup>

## 5. Plasmonically Active DNA-Based Materials

### 5.1. Contextual Motivation

Fluorescent organic dyes and more recently QDs have been used to couple light to and from biological systems, enabling imaging and various types of biosensing.<sup>[95]</sup> However, the use of these materials limit spatial, spectral, and temporal information due to complex photobleaching, blinking, and broadband absorption/emission issues.<sup>[96]</sup> In direct contrast to this, plasmonic NPs have the largest light–matter coupling in nature, leading to resonances with relatively large Q-factors (dimensionless parameter describing how undamped the resonator is and is used to characterize its bandwidth relative to the center frequency) and efficient energy transfer via bright or dark mode coupling.<sup>[17,96,97]</sup> They are also generally made of biocompatible materials (coinage or noble metals), which do not suffer from many of the aforementioned dye and QD photophysical limitations. Moreover, their optical properties including absorption, transmission, reflection, and scattering are fundamentally based on resonance phenomena. This has led to the use of plasmonic NMs as a fundamental nanotechnology building

block.<sup>[98]</sup> A simple harmonic oscillator model can be used to qualitatively understand the response of plasmonic NPs when irradiated with light.<sup>[99]</sup> When light is irradiated onto metallic nanometer sized particles, it penetrates the entire volume, since the size of the NPs are comparable to the penetration depth of the electric field. The free electrons in the metal respond to the electric field, forcing the free electrons to the NPs surface creating a depolarization field inside the NP. The light wave leads to the electrons coherently oscillating on the surface on the NP, which is referred to as a localized surface plasmon resonance. The confinement of the electron on the surface leads to local electric fields becoming orders of magnitude larger than the incident light's field, which can effectively serve to squeeze light down below the Abbe diffraction limit, providing opportunities to create next generation materials with new properties and functionalities on a size regime that was not previously accessible.<sup>[11d,h,j,100]</sup> Using this straightforward description, the surface plasmon resonance frequency, and most ensuing optical properties, only depend on two intrinsic parameters

$$\omega = \sqrt{L}\omega_p \quad (3)$$

where  $L$  is the depolarization factor and is related to the shape of the NP and  $\omega_p$  is the material dependent plasma frequency which is proportional to the free electron density. Tuning the plasma frequency has been thoroughly explored over the last decade using a wide variety of plasmonic materials ranging from aluminum to doped oxides, shifting the resonance wavelength across thousands of nanometers, from the ultraviolet to infrared.<sup>[101]</sup> By contrast, the depolarization factor is the ratio of the induced electric field inside the materials to the applied (optical) electric field and is determined by the shape of the individual plasmonic elements, offering an alternative means to control the resonant wavelength.<sup>[99b]</sup> For a given metallic NP material, it has historically been challenging to efficiently synthesize them beyond basic geometric shapes, leading to only hundreds of nanometers in wavelength tunability.<sup>[102]</sup> To a lesser extent, the absolute size of the NPs and surrounding dielectric environment can also shift the resonance wavelength, but typically by only a few tens of nanometers.<sup>[103]</sup>

In contrast to engineering intra-NP parameters as described above, another approach to tailor the resonance wavelength, or rather the plasmon mode of NPs is by controlling inter-NP parameters via positional and/or orientational order. The organization of multiple closely packed plasmonically active NPs can lead to plasmon coupling and a further increase in control and tunability over the desired plasmonic effect.<sup>[104]</sup> As the distance between two plasmonic NPs decreases, their local electric fields begin to capacitively couple due to dipolar interactions. This capacitive coupling results in the plasmon mode hybridizing into an in-phase (bright) and out-of-phase (dark) mode.<sup>[105]</sup> Dark modes cannot be easily excited by optical means making them challenging to study and are not discussed further. The bright mode couples strongly to light leading to the two NP resonances oscillating in-phase and resulting in a red-shift of the plasmon mode wavelength when probed with light polarized parallel to the interparticle axis. The plasmon wavelength shift as a function of interparticle separation can be a useful tool to optically determine nanometer scale distances extremely

accurately. The empirical relationship on which this is based is known as the plasmon ruler equation and is given by<sup>[96,106]</sup>

$$\frac{\Delta\lambda}{\lambda_0} = Ae^{-\left(\frac{g/D}{\tau}\right)} \quad (4)$$

where  $\Delta\lambda/\lambda_0$  is the fractional plasmon wavelength shift,  $g$  is the interparticle gap, and  $D$  is the NP diameter. It is worth noting that the enhancement of the local electric field in the NP gap due to the plasmon coupling is closely approximated by  $D/g$ .<sup>[107]</sup> The local field decays with a universal constant,  $\tau$ , and only the magnitude,  $A$ , is influenced by the NP size, shape, material, or surrounding medium. Plasmon wavelength shifts along with color changes in a given colloidal sample as a result of the aggregation state have formed the basis of numerous NP-based biosensors including those that are DNA-based (vide infra). Here the biological activity, some other related event, or even just the presence of a target is the key that triggers the desired change to the colloidal state.

If the material in the NP dimer gap changes from insulating to conducting, then charge can flow between the NPs at optical frequencies, and a charge transfer plasmon mode emerges.<sup>[108]</sup> Specifically, if the NP dimers are connected with a thin metallic bridge through the gap, then the depolarization factor of the entire dimer nanostructure can be significantly modified, since the plasma frequency is constant, shifting the plasmon mode wavelength over thousands of nanometers.<sup>[99b]</sup> To realize these materials, first the interparticle positional and orientational symmetries must be controlled with repeatable nanometer scale gap resolution. Next, the materials need to be bridged uniformly with metal across the gaps, conductively linking the NPs, and thereby enabling the ability to tune the intraparticle properties of the new composite high order structure. Such composite NPs have recently been experimentally realized using high-throughput chemical assembly strategies.<sup>[102c,109]</sup> For example, AuNRs were assembled end-to-end forming capacitively coupled dimers using directed self-assembly techniques. The evolution of the absorption spectra of the AuNR suspensions transitioning from monomers to dimers was monitored in situ. When the maximum dimer population was reached, the suspension was irradiated with femtosecond laser pulses at the same wavelength as the capacitively coupled dimer absorption peak, nonthermally welding the dimers together with gold bridges. These structures form nanoantennae with the largest plasmon-based wavelength tunability reported to date.<sup>[102c,109b]</sup> While such nanoantennae open up exciting opportunities to sense and signal at the nanometer size scale, they are limited to 1D structures. If two- or even 3D nanostructures could be accessed, then even broader opportunities could emerge.

The inability to translate plasmonic properties into designer structures having complex 3D prescribed architectures is now impeding the developmental progress of these materials.<sup>[110]</sup> Structural DNA nanotechnology could potentially provide an ideal platform to control interparticle symmetries by arranging them on carefully prescribed architectures; this could also help to elucidate or confirm many of the plasmonic phenomena hypothesized to arise when very complex NP geometries are formed. In two dimensions, DNA origami assembled

nanostructures could control the NPs orientational and positional order, enabling transformative optics,<sup>[111]</sup> energy harvesting,<sup>[112]</sup> or nanocircuitry elements.<sup>[113]</sup> Furthermore, these nanostructures could be extended to three dimensions, facilitating high-density plasmonic hot-spot nanostructures, which may be useful for plasmonic-based photocatalysis,<sup>[114]</sup> and sensing on substrates,<sup>[115]</sup> in suspensions,<sup>[116]</sup> and/or as aerosols.<sup>[117]</sup> However, many of the above list applications remain just speculative or very crudely shown in preliminary proof-of-concept experiments because a means to produce the requisite structure(s) in high fidelity is still not yet available. In the following section, we look at progress in three types of plasmonic devices that have been facilitated by DNA scaffolds, namely, colorimetric detectors, devices created with added metallization, and dynamic devices. These, in essence, represent an important start toward the full potential. As this is a relatively rich area, we only describe representative examples and refer the interested reader to several other excellent reviews.<sup>[104b,118]</sup>

## 5.2. Colorimetric Detectors and Plasmonic Devices

DNA has been experimentally shown to be an attractive material for arranging periodic metallic NP arrays of various sizes.<sup>[119]</sup> See **Figure 4** for three representative examples of how AuNPs and AuNRs are assembled into higher composite structures using DNA scaffolds.<sup>[120–122]</sup> As shown in Figure 4A, 5 and 10 nm diameter AuNPs are arrayed on a flat mica surface using a DNA scaffold while a discrete DNA triangle approach is used in Figure 4B, and a far smaller DNA tetrahedron is the basis of Figure 4C. Interestingly, the DNA tetrahedron has proved a popular scaffold for capturing many types of NPs.<sup>[67]</sup> The first major example of plasmonic DNA-based detectors utilized in a dedicated biological context originated from the work of the Mirkin group and was based on the arrangement of individual gold NPs with 13 nm diameters, resulting in the formation of a network of NPs with red-to-purple color changes.<sup>[123]</sup> The optical properties (i.e., color changes) of the NP network depended

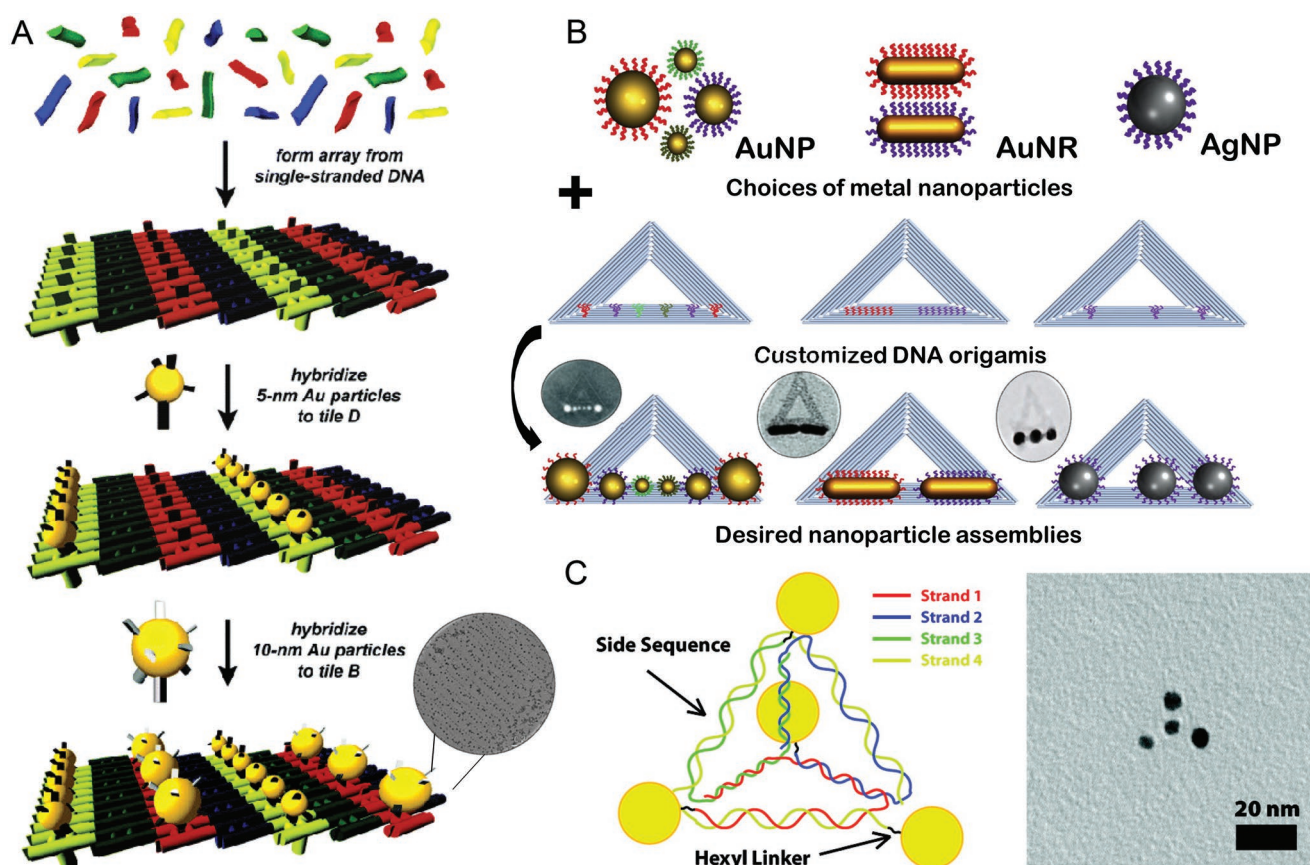


**Figure 4.** Plasmonic materials constructed via DNA scaffolds. A) Representative example of attaching AuNPs to DNA in arrays. The DNA scaffolding is first assembled in solution from the set of 22 strands. A suspension of the DNA scaffolding is deposited on mica, allowing the scaffolding to attach to the surface. The scaffolding is composed entirely of double-stranded DNA, except for the open single-stranded hybridization sites. The scaffolding is combined with DNA-encoded nanocomponents, which attach to the open hybridization sites on tile. Although this diagram shows one nanocomponent occupying each site, single nanoparticles can also attach to multiple sites via hybridization of multiple nanoparticle-bound strands. (Inset: TEM image of the two-particle array). Adapted with permission.<sup>[120a]</sup> Copyright 2005, American Chemical Society. B) Using a DNA origami triangle to organize different-sized metal NPs/NRs with well-controlled orientation and spacing. Adapted with permission.<sup>[120b]</sup> Copyright 2014, Elsevier. Inset: Reproduced with permission.<sup>[124a]</sup> Copyright 2010, American Chemical Society. Reproduced with permission.<sup>[124b]</sup> Copyright 2011, American Chemical Society. Reproduced with permission.<sup>[121]</sup> Copyright 2010, Wiley-VCH. C) Using a dsDNA tetrahedron as a scaffold to control the placement of chiral AuNPs. Reproduced with permission.<sup>[122]</sup> Copyright 2009, American Chemical Society.



on their spacing within the aggregate and were controlled by DNA hybridization. These striking results created an alternative method to detect target molecules with high sensitivity down to a remarkable 10 fmol of target mutant oligonucleotide while still being visible to the unaided eye. By controlling the distance between NPs, the optical properties could be further tuned beyond the constraint of the DNA double helix. For instance, by coupling with DNA tiles, AuNP arrays of periodic square-like configurations were self-assembled on prescribed nanogrids,<sup>[119a]</sup> enabling the ability to control the collective properties of the NPs with respect to their interparticle spacing's and hierarchical organizations. Complex architectures with artificial control of precision at nanometer scales were demonstrated by Yan et al.<sup>[119c]</sup> They created 3D NP architectures by placing 5 and 10 nm particles inside the spiral of DNA tubules and this control allowed for left- and right-handed structures as well as more complex double-helix like structures in which the 5 nm NPs and 10 nm NPs appeared to complement each other. These results not only show the capability of tuning optical properties of NP but also open up other possibilities to create other small-scale devices such as nanoinductors or logical cellular nonlinear networks.

With discrete DNA nanostructures like DNA origami and DNA bricks, metallic materials with various degrees of aspect ratios have been placed on predefined locations with high spatial resolutions.<sup>[124]</sup> In particular, Bokor et al. used the scaffolded DNA origami to organize six AuNPs in the same plane with less than 10 nm separations between NPs.<sup>[124a]</sup> Since the particles were gradually decreased from 15 to 10 and then 5 nm in diameter, this particular structure should generate extremely high field enhancement (though this was not shown) and could work as a nanolens if the structures can be replicated over larger size scales. Although optical NPs have unique optical properties, creating higher order assembly of photonic arrays with anisotropic optical materials such as nanorods could result in better optical responses. In particular, Pal et al. programmed AuNRs that could precisely be immobilized on the surface of DNA origami nanostructures.<sup>[124b]</sup> By organizing anisotropic gold NMs on a DNA origami triangle, they created discrete, well-ordered hybrid gold-based nanoarchitectures with controllable plasmonic properties.

### 5.3. Devices Achieved by Metallization

Instead of fabricating nanometer size optical components using the top-down approach, researchers have demonstrated that one can achieve a similar goal via metal-seeding of DNA nanostructures. In particular, DNA scaffolds can be used as small-scale molds in which seeded materials are introduced and used to develop higher order controllable geometrical metallic structures via chemical methods.<sup>[125]</sup> Although not fully realized in terms of plasmonic tuning capabilities, several examples are described here in order to highlight the strong potential this approach may provide if fully exploited. Using DNA origami templates, Pilo-Pais et al. seeded templates with gold NPs.<sup>[125a]</sup> For the metallization step, they placed seeded DNA templates on a SiO<sub>2</sub> substrate and reduced silver ions from solution, resulting in controllable metallic lines such as

parallel structures or H-shapes with ≈50 nm thick lines. Using similar technique, Schreiber et al. placed 1.4 nm Au nanoclusters within DNA nanotubes and then used the seeded growth to create AuNRs of defined length up to 438 nm.<sup>[125b]</sup> These structures could be further grown into continuously metalized objects of arbitrary size and shape. These results support the formation of extended metal structures, such as μm-long gold nanowires with much higher uniformity than obtained in previous metallization procedures. Using mold elements with different shapes, more structural complexity can be introduced that could lead to the flexibility to construct reconfigurable nanostructures. DNA-based molds to synthesize metallic NPs via a seeded-growth procedure could present an alternative approach complementary to the top-down approach as already conceptually demonstrated by Yin and co-workers.<sup>[126]</sup>

### 5.4. Dynamic Plasmonic Devices

As described in the previous section, natural chiral molecules exhibit optical activities mainly in the UV range, however, these have had limited potential applications beyond that specific energy range. Recently, it has been shown that DNA nanostructures are a potentially ideal template to control metallic material placements to generate tunable CD responses extending beyond the UV to the visible and near IR regions.<sup>[127]</sup> For instance, Kuzyk et al. constructed two DNA origami gold NP helices with left-handed and right-handed helical arrangements.<sup>[127a]</sup> Their CD measurements exhibited the signatures corresponding to their chiral structures in the visible region and using either 10 or 16 nm diameter AuNPs they detected differences in the CD signals of 0.75 mdeg at 524 nm or 50 mdeg at 545 nm for the two sizes, respectively, see **Figure 5A**. The fact that the larger AuNPs had collective plasmonic effects greatly enhanced the overall signal of the structures. Interestingly, for both structures the detected signal was about 75% of the theoretical signal, this demonstrates the excellent formation efficiency and precision placement of the structures. Similarly, Shen et al. created left- and right-handed structures incorporating AuNRs on rectangular origami where the CD response was shifted to the NIR, **Figure 5B**.<sup>[128]</sup> The CD response of the left-handed sample was stronger than that of the right-handed one. Furthermore, a smaller CD response was observed around 520 nm, which corresponded to the AuNRs transverse resonance. Lan et al. were able to extend this approach to include multiple rods stacked between origami rectangles that had fixed angles between neighboring NRs.<sup>[129]</sup> Moreover, by changing the AuNR/origami molar ratio in the assembly system, they could tune the number of AuNRs and the corresponding CD signal, see **Figure 6A,B**.

Initial studies on the plasmonic CD response were done on structures which are nondynamic and irreversible thus limiting future applications. To add reversibility to DNA-based chiral structures, Li et al. conjugated reversible oligonucleotides to AuNRs and subsequent plasmonic CD responses were based on the dynamic assembly and disassembly of the DNA modified AuNRs.<sup>[127b]</sup> By changing the temperature as well as concentration, they were able to control the hybridization of those oligonucleotides thus changing the formation of AuNR networks



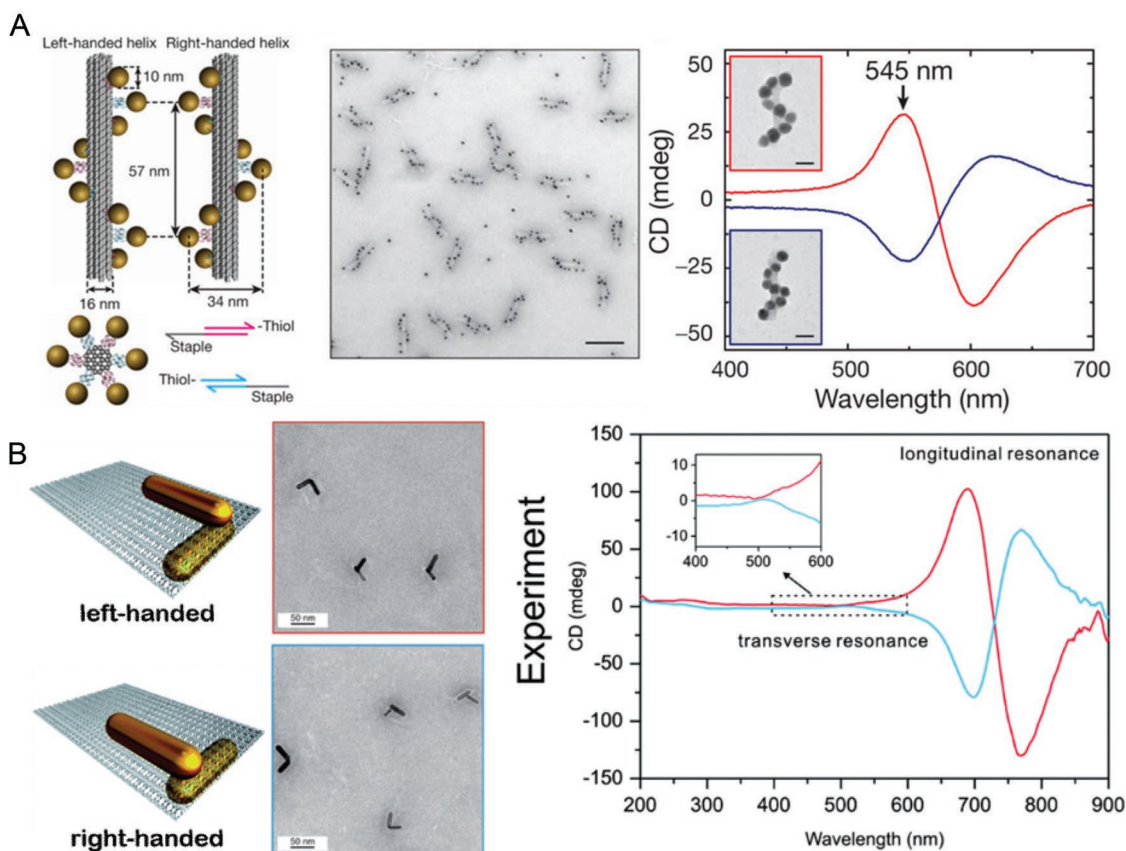


**Figure 5.** Construction of chiral plasmonic materials. A) Left: the left- and right-handed nanohelices (diameter 34 nm, helical pitch 57 nm) are formed by nine AuNPs each 10 nm diameter that are attached to the surface of DNA origami 24-helix bundles. Middle: TEM image of assembled left-handed gold nanohelices (scale bar, 100 nm). Analysis of the TEM data yields a 98% success rate for directed attachment. Right: experimental CD spectra of left-handed (red lines) and right-handed (blue lines) helices of 9 AuNPs showing the characteristic bisignate signatures in the visible. Reproduced with permission.<sup>[122a]</sup> Copyright 2012, Springer Nature. B) Left: AuNRs with corresponding complementary DNA strands are assembled at the pre-designated locations on the origami template through DNA hybridization, forming left- and right-handed structures, respectively. Middle: representative TEM images confirming the structures formed. Measured CD spectra of the left- (red) and right-handed (blue) crossed AuNRs. Right: strong CD is observed around 730 nm, which corresponds to the longitudinal resonance of the AuNRs. The CD response of the left-handed sample is stronger than that of the right-handed one. Smaller CD is observed around 520 nm, which corresponds to the transverse resonance of the AuNRs. Reproduced with permission.<sup>[128]</sup> Copyright 2014, The Royal Society of Chemistry.

and giving rise to different CD responses and the ability to detect a DNA target at  $75 \times 10^{-9}$  M in a proof of concept sensing demonstration. Recently, Elbaz et al. constructed dynamic and fuel-driven mechanical DNA machines which enabled the formation of prescribed NP assemblies.<sup>[127d]</sup> In particular, they first created a three-ring catenane system and demonstrated the dynamic, reversible, and switchable conversion of the three-ring system across three different configuration. They then applied the system as a carrier for AuNPs with 5 or 10 nm diameters and from 1 up to 4 AuNP per system. The distances between the AuNP could vary from 1 to 15 nm depending on the chosen design and initial placement of the AuNP. Within the dynamic nature of the system they demonstrated distance changes of  $\approx 4.6$  nm between two locations (from 7.3 to 2.7 nm). Their molecular fuels are based on additional DNA strands, yet considering DNAs recognition capability (e.g., aptamers) this could be expanded to other fuels/antifuels. Their machines could be employed in nanomedicine and intracellular diagnostics by generating programmed dynamically reconfigurable structures

of AuNPs perhaps through the incorporation of target specific aptamers.

Rather than having a reconfigurable design to achieve reversible plasmonic responses, Schreiber et al. took a contrasting approach and controlled the alignment of chiral objects on a substrate in order to generate reversible optical responses.<sup>[127e]</sup> They created chiral DNA origami templated helices with 10 nm AuNPs that were tethered to a surface through biotin-DNA and streptavidin glass. The structures orient vertically in a liquid buffer medium but then orient horizontally in a dried air environment. By using  $N_2$  gas to dry the system or rehydrating the system with buffer they could choose the spectral read-out and were able to show a reversible signal with a change of 8 mdeg in the CD signal at 540 nm. However, they were unable to show multiple cycles due to the degenerative nature of the switching strategy where the structures would get stuck to the surface or wash away going through the dry-rehydrate process. Nevertheless, the alignment process led to an amplified optical response compared to that from randomly oriented objects at

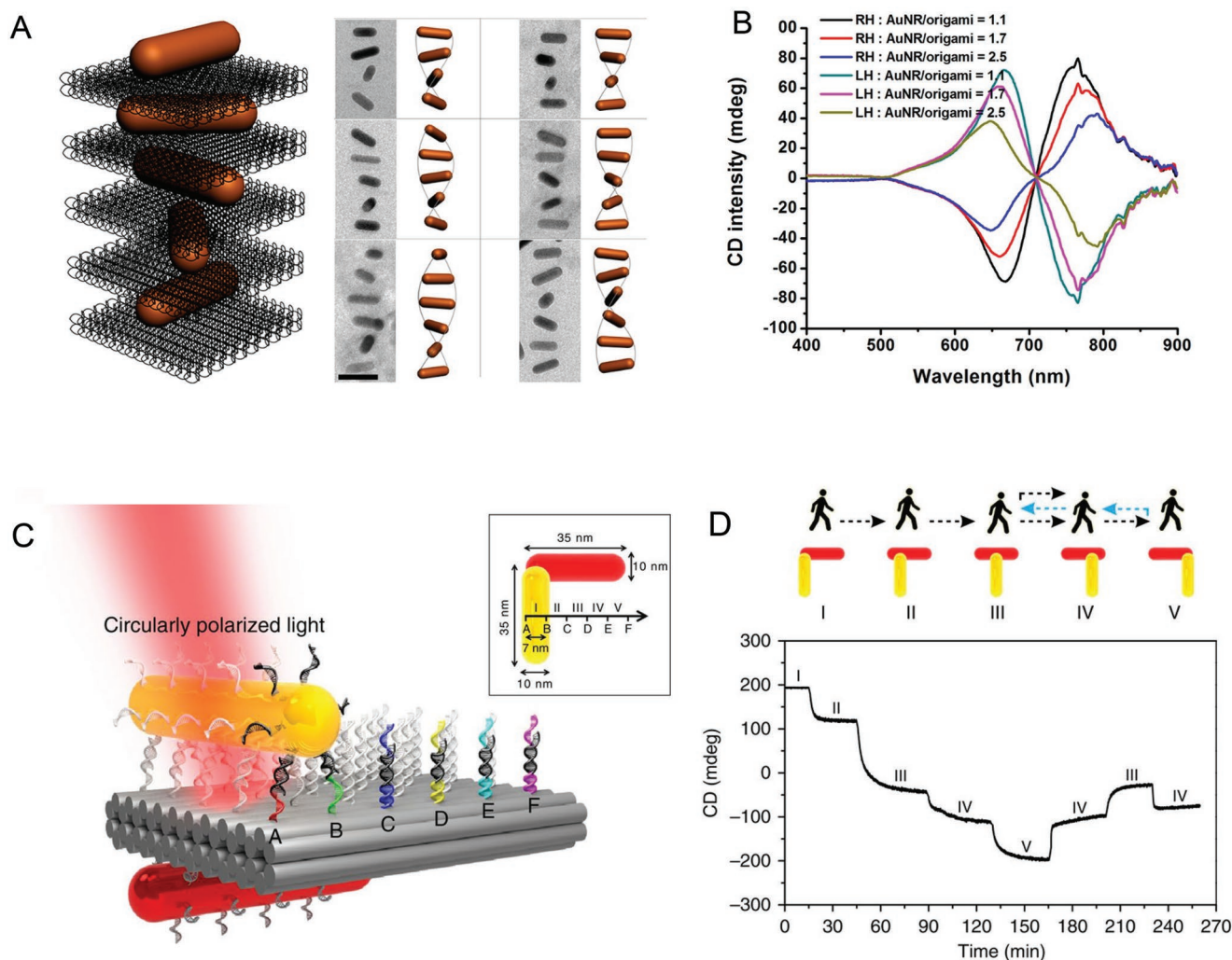


**Figure 6.** Superstructures and active plasmonic devices. A) Schematic illustration of the self-assembly of right handed (RH)-AuNR helices. This design enables one-pot assembly of AuNR helices. Rotation of the intermediate origami may happen as each side of the origami can bind to AuNRs, but the handedness of the helices stays unchanged. Cryo-TEM images of the assembled AuNR helices with varying number of AuNRs. B) The measured CD spectra of RH- and left handed (LH)-AuNR helices containing varying numbers of AuNRs. With the AuNR/origami ratio increasing from 1.1 to 1.7 and 2.5, the statistical number of AuNRs in the resulting superstructures decreases from 9 to 4 and 2, respectively. The CD intensity is normalized according to the concentration of origamis in the assembly system. Reproduced with permission.<sup>[129]</sup> Copyright 2015, American Chemical Society. C) Two gold AuNRs are assembled perpendicularly to one another on a double-layer DNA origami template, forming a left-handed configuration at station I. The yellow AuNR on the top surface represents the “walker” and the red AuNR on the bottom surface represents the “stator.” The walking track comprises six rows of footholds (A–F) extended from the origami surface to define five walking stations (I–V). The distance between the neighboring stations is 7 nm, which also corresponds to the step size. In each row, there are five binding sites with identical footholds. Only the footholds in the front line are colored to highlight the different strand segments. The walker AuNR is fully functionalized with foot strands. To enable robust binding, the walker steps on two rows of neighboring footholds at each station. The red beam indicates the incident circularly polarized light. D) CD intensity was monitored at a fixed wavelength of 685 nm, while the walker performs stepwise walking, following a route I–II–III–IV–V–IV–III–IV. Reproduced under the terms of the CC-BY license.<sup>[132]</sup> Copyright 2015, The Authors, published by Springer Nature.

equal concentrations. Recently, Greybush et al. demonstrated a dynamic plasmonic pixel that can control the spatial, spectra, and temporal properties of light on demand.<sup>[8]</sup> These dynamic pixels can rapidly and reversibly control the alignment of the gold nanorods in liquid suspensions.<sup>[130]</sup> The possibility to control the orientational order, in addition to the positional order provided by the DNA-NP assemblies, using external fields may provide additional degrees of freedom to tune the optical response of these systems.

The two plasmonic resonance modes of AuNRs can be further exploited by accessing 3D chirality given that the orientation of multiple rods can be controlled in an orientation-dependent manner. As discussed in the above motivation and based on theoretical models, the enhanced optical activity of such metal dimers relies directly on their orientations and the interrod gap distances. Using a DNA origami rectangle as a controllable template, Rao et al. demonstrated spatial control of plasmonic nanostructures including both AuNPs and AuNRs in

this vein. For example, they were capable of consistently varying the gap between two parallel AuNRs (40 by 12 nm in size) from 3 to 12 nm. The AuNR dimers demonstrated nearly a tenfold increase in the CD signal as compared to a single AuNR. When combining a AuNR with a AuNP on the origami template changes in ~20 mdeg at 800 nm were measured as compared to the AuNP alone.<sup>[127f]</sup> In addition, dynamic plasmonic CD systems have been demonstrated with the capability of reversing the CD responses by utilizing hybridization driven by different conjugated DNA sequences.<sup>[127b,d,k]</sup> An alternate example was based on a pH sensitive DNA origami structure that allowed the system to be tuned from 6.5 to 9.5 pH with a maximal change in CD signal at 780 nm.<sup>[131]</sup> Interestingly, the system is not required to start from an enantiomerically pure mixture, differences of 10% were enough to get a strong signal as the structures reacted preferentially to the different pH and maximized or minimized their individual signal. Anisotropic assemblies using DNA origami nanostructures have also been shown to enhance Raman resonance.<sup>[127j]</sup> In a fascinating example of both the elegance and subtleties afforded to such systems by dynamic DNA structures, Zhou et al. constructed a plasmonic nanorod system that could “walk” on the DNA scaffold while simultaneously changing its CD response, see Figure 6C,D.<sup>[132]</sup> Each iterative step, as fueled by the addition of a specific DNA oligo, corresponded to a ≈7 nm rearrangement of one rod relative to the other across the whole structure. An almost 400 mdeg change in CD signal was produced by this system. Overall, this last area is a prime example where the interface of biomolecules in the form of DNA with inorganic materials such as AuNRs can lead to an emergent property, namely, de novo designer nanoscale assemblies with dynamically active structures and CD responses in the visible and even extending to the NIR.

## 6. Fluorescently Labeled DNA Materials

### 6.1. Contextual Motivation

Natural photosynthetic antennae in green plants and many other diverse phototrophic species are the prime examples of efficient light harvesting systems.<sup>[133]</sup> Great efforts continue to be made to understand these natural systems by studying the correlated structural and optical properties of their photoactive machinery.<sup>[134]</sup> The primary mechanism by which photosynthetic antenna absorb, transfer, and direct light energy to their reaction centers for conversion to chemical energy is widely understood to be FRET.<sup>[92,135]</sup> Though other energy transfer mechanisms are potentially feasible (e.g., Dexter energy transfer and electron transfer), FRET is also the most extensively studied energy transfer mechanism in fluorescently labeled DNA structures.<sup>[136]</sup> FRET is the nonradiative energy transfer through long range dipole–dipole interactions from an excited state donor fluorophore to a proximal ground state acceptor molecule; the latter can also be fluorescent and sensitized or a dark quencher.<sup>[137]</sup> FRET only occurs when certain key criteria are met by the system in question. Primary amongst these are that the donor and the acceptor must share spectral overlap; that is the donor emission energy levels must align with the acceptor molecule’s absorbance levels. The

degree of spectral overlap between a given donor–acceptor is typically characterized by their Förster distance ( $R_0$ ) which is the separation distance between the donor and acceptor where FRET will occur with 50% efficiency.  $R_0$  (in nm) can be estimated empirically using

$$R_0^6 = C_0 \kappa^2 J n^{-4} \Phi_D \quad (5)$$

where  $\kappa$  is the dipole orientation factor (typically assumed to be random or 2/3 for most ensemble systems),  $\Phi_D$  is the quantum yield of the donor,  $n$  is the refractive index of the medium, and  $J$  is the spectral overlap integral in units of  $\text{nm}^4 \text{M}^{-1} \text{cm}^{-1}$ .<sup>[92,137]</sup> In general, FRET is usually feasible in the 1–10 nm range for most donor–acceptor pairs but can occur at significantly longer distances in special circumstances.<sup>[3a]</sup> FRET efficiency ( $E_{\text{FRET}}$ ) is typically measured experimentally using

$$E_{\text{FRET}} = 1 - \frac{I_{\text{DA}}}{I_{\text{D}}} = 1 - \frac{\tau_{\text{DA}}}{\tau_{\text{D}}} \quad (6)$$

Here,  $I_{\text{D}}$  and  $I_{\text{DA}}$  are the fluorescent intensity of the donor in the absence and presence of acceptor while  $\tau$  is the corresponding excited state lifetime of the donor in the same respective configurations. The FRET mechanism results in  $E_{\text{FRET}}$  correlating directly to donor–acceptor separation distance ( $r_{\text{DA}}$ ) with an inverse sixth power dependency.

$$E_{\text{FRET}} = \frac{nR_0^6}{nR_0^6 + r_{\text{DA}}^6} \quad (7)$$

Here  $n$  accounts for the presence of multiple equivalent acceptor for a given donor. This ability to optically measure separation distances is the reason FRET is also called a molecular scale ruler.<sup>[92,137]</sup> Of course, this is just a very brief generalization meant to be sufficient for this discussion and there are many other important caveats and variables that normally need to be considered with FRET. The interested reader is directed to refs. [92] and [138] and therein for more detailed treatises on FRET and its applications.

One of the many remarkable properties of photosynthetic systems is the near perfect efficiency with which they are able to utilize FRET to accomplish energy transfer simultaneously across both a wide swath of the visible spectrum and significant spatial distances. Evolutionary selection over countless eons has provided for system designs where not only are the intrinsic fluorophore properties hyperoptimized but also their relative spacing, orientation (for optimized dipole orientation), stoichiometry (i.e., number of donors to acceptors), etc.<sup>[134]</sup> Given this remarkable naturally occurring design, there has long been a desire to recapitulate these properties in artificial FRET systems so that they can be applied to not only research in artificial light harvesting systems, but also a myriad of application such as biosensing, optical computing, solar energy conversion, imaging, etc.

From a purely idealistic perspective, one would like to have intimate control over all pertinent variables in designing and assembling such artificial FRET systems including donor–acceptor ratios, relative placement, orientation (for dipole alignment), separation spacing, and especially the ability to array the fluorophores and test their functionality in any 1D,



2D, or 3D architecture as desired in a rapid manner.<sup>[139]</sup> The latter, however, has been extremely hard to achieve with perhaps only photoactive dendrimers providing access to a very limited number of these desirable features but at the expense of exceedingly intensive chemical synthetic requirements.<sup>[140]</sup> The recent development of structural DNA technology has truly been disruptive in this regard as it now provides a potential capability to achieve all of the features desired in a prototypical FRET system and these capabilities are, in turn, leading to extensive growth in the development of such systems.<sup>[25c,136,138c,141]</sup> DNA allows for the rapid design and assembly of almost any scaffolded FRET architecture as desired. Moreover, almost any iteration(s) of a given structure (e.g., moving a dye location or removing a given dye) can be coassembled in parallel and concurrently examined in the same experiment. The structures created by combining DNA with fluorescent components have three general applications of interest to the current discussion: the first are molecular photonic wires (MPWs), the second is light harvesting, and the third is molecular actuators (sensing and computation). We note that there are extensive examples of DNA and dyes combined for characterization of structures, imaging, and other biophysical applications such as use of molecular beacons in diagnostics.<sup>[53a,142]</sup> The latter configurations are, of course, of great importance but lie outside of the scope of this perspective which focuses on nanophotonics in the DNA world.

## 6.2. Molecular Photonic Wires

Conceptually, MPWs are nanoscale devices composed of individual optically active constituents that permits the flow of light. The constituents in this case have typically been fluorescent dyes that are either homogenous (same dye used for donor and acceptor) or heterogeneous (different donor–acceptor dyes). MPWs in all their forms are of interest as they allow for the manipulation of photons below the diffraction limit and as such can be incorporated into optoelectronic systems. This will allow for the continued miniaturization of technologies, but for these applications the systems must first reach higher transfer efficiencies as well as demonstrate consistency in both formation efficiency and dye placement with sub-nanometer resolution and this is where much of the current research is focused. Within this section transfer efficiency across multiple single donor–acceptor pairs will be defined as the fraction of photons absorbed by the initial input (donor) dye that are detected as emitted photons from the final output (acceptor) dye.

The first examples of scaffolds used for MPWs were based on organic chemistry and porphyrin dyes,<sup>[12]</sup> but researchers quickly found that dsDNA was an excellent template to study MPWs. The first DNA-based MPW were described by Ohya et al. who used an extended unlabeled template strand and subsequent addition of shorter (10 bp or one DNA pitch  $\approx 3.4$  nm) dye-labeled DNAs (eosin, tetramethylrhodamine or TAMRA, and Texas Red) that complemented different sections of the template to create photonic wires of up to 10 nm in length yielding a 6% overall transfer efficiency.<sup>[143]</sup> The next iteration of interest used dsDNA, but only two strands that were multilabeled with three different dyes (6-carboxyfluorescein, 5-(and-6)-carboxyTAMRA, and Cy5) achieving a higher transfer

efficiency of  $\approx 10\%$  over 14 nm.<sup>[144]</sup> The advantage of the latter system was that by limiting the number of strands required, the formation efficiency of the structure was much higher. Design of dsDNA MPWs continued to evolve as additional dyes were added to the system with up to five different dyes allowing for spectral shifts of 200 nm from an initial rhodamine green donor to a terminal Atto680 acceptor with a reported transfer efficiency of 8% over four sequential energy transfer steps.<sup>[145]</sup> More advanced tools beyond just steady state spectra were included in these newer studies including single particle microscopy which allowed for an understanding of the heterogeneity in MPW formation and how this could be a critical limiting factor in ensemble photon transfer efficiency.<sup>[145,146]</sup> Differences in formation efficiency along with slight structural variation yielded assemblies that were functional along with those that were either partially function (lower ET efficiency) or even nonfunctional in the ensemble.

Another advantage of utilizing DNA as the template for the MPW is that users are not strictly limited to covalently bonded dyes and, in fact, a variety of DNA intercalating dyes have been utilized in this role.<sup>[147]</sup> These dyes can be added directly to unlabeled DNA to create self-assembled MPWs or as relays between covalently bound fluorophores.<sup>[148]</sup> The primary issue with using intercalating dyes is that the benefit of site-specific labeling is lost as these dyes label in an indistinct manner. Thus an average labeling efficiency is the primary description utilized in this case. For example, if a ratio of 1 intercalating dye per 5 bp is added, then this is also considered the average labeling efficiency and average distribution of dye locations if positional information is further required. Investigations into altering FRET directionality by the controlled inclusion of particular FRET pairs have been reported by multiple groups using various strategies such as inclusion of intercalating components including dyes or pyrrole-imidazole polyamides or altering components on the DNA origami structures.<sup>[148a,149]</sup> The inclusion of the intercalating YO dye (oxazole yellow) in **Figure 7A** transformed a null-transfer wire into one with nearly 20% transfer efficiency at higher dye loading densities (0.4 YO per bp).<sup>[148b]</sup> In another example, the DNA origami structure utilized was planar allowing it to act as a true nanoscale breadboard and changes to the dye placement in the structures not only controlled the efficiency of the MPW transfer but could also modify the direction of the energy transfer, either toward the red dye (Atto647) or the IR dye (Alexa750) by the choice of including or not a particular intermediary dye (ATTO565) (see **Figure 7B**).<sup>[149a]</sup>

As described earlier, DNA structures are not limited to the double stranded helix and much more complex and rigid structures are available even when simply considering just DNA wires. For example, a crossover tile motif was utilized by Spillmann et al. to increase the rigidity of the wire system and allow for the investigation of longer, more complex MPWs (up to 22 nm) displaying up to seven different sequentially arrayed dyes that were meant to function as an integrated FRET cascade, see **Figure 7C**.<sup>[150]</sup> This study demonstrated a confounding problem with such DNA-based MPWs that was to be confirmed repeatedly in subsequent studies; within the context of DNA dye FRET pairs, especially those consisting of covalently attached fluorophores, the photophysical properties expected from studies of parent non-DNA conjugated dye-alone in organic media did not



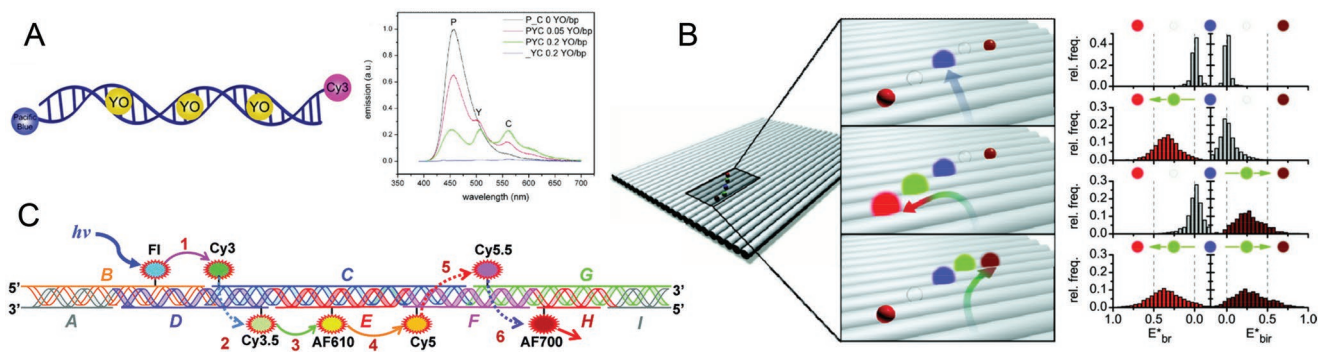


**Figure 7.** Representative MPW structures. A) Schematic representation of the multichromophoric DNA wire with attached Pacific Blue (injector) and Cy3 (reporter) and intercalated YO. Along with emission spectra of the MPW for various YO concentrations (excited at 380 nm). P\_C is the wire with only Pacific Blue and Cy3, \_YC is the wire with YO and Cy3 and PYC is the complete wire containing all three chromophores. Reproduced with permission.<sup>[148b]</sup> Copyright 2008, American Chemical Society. B) Fluorophores on DNA origami and visualization of alternative energy-transfer pathways from the blue input to either the red or the IR output depending on green-dye localization. To the right: single structure microscopy histograms detailing the relative frequency of FRET efficiency of each structure from blue to red and from blue to IR for the four different origami samples. Reproduced with permission.<sup>[149a]</sup> Copyright 2011, American Chemical Society. C) Schematic of MPW containing seven different covalently conjugated dyes. Reproduced with permission.<sup>[150]</sup> Copyright 2014, The Royal Society of Chemistry.

always apply to the final DNA incorporating configuration. For example, while the Cy3–Cy3.5 FRET pair is excellent and maintains high  $R_0$  values in the 6–7 nm range independent of the DNA construct,<sup>[151]</sup> dyes such as Alexa610 or Cy5 can and often do act as energy sinks limiting transfer efficiency.<sup>[150,152]</sup> Indeed, placing Alexa610 in the 4th position of the aforementioned 7 dye cascade,<sup>[150]</sup> diminished  $E_{\text{FRET}}$  through that point to <5% while its removal unexpectedly tripled  $E_{\text{FRET}}$  to the next but far more distantly placed acceptor dye. Insight from molecular modeling has found that conjugated dyes interact with the DNA backbone, entering DNA grooves or engaging in  $\pi$ – $\pi$  stacking, for example, and as such their use may require considerably more study to understand the experimental results.<sup>[153]</sup>

Limitations in accessing arrangement of multiple high-efficiency DNA conjugated FRET donor–acceptor pairs in a sequential manner to create more complex arrangements and cascades has stimulated investigation of alternative fluorophore types going beyond just use of organic dyes or in finding design principles that could overcome these limitations. Some, individual FRET parameters were looked at including: the optimal  $r_{\text{DA}}/R_0$  ratio by positioning dyes at different distances;<sup>[154]</sup> modifying the apparent spectral overlap ( $J$ ) by creating multiacceptor systems, which proportionally increase the FRET acceptor absorption cross-section and thus  $R_0$ ;<sup>[53a]</sup> improving donor QY through attaining cryogenic conditions;<sup>[155]</sup> and fixing dye dipole orientations into optimal transfer alignments.<sup>[156]</sup> These studies did indeed show incremental enhancements but were always limited by the characteristic limitations of the heterogeneous FRET mechanism, i.e., the requirement for an energetically downhill arrangement.

One viable option that could potentially bypass this issue was to exploit homogenous FRET (HomoFRET) with organic dyes.<sup>[152]</sup> HOMO FRET has the limitation of being nondirectional (following a random-walk model of energy hopping), however, if the transfer steps are particularly efficient between the identical dyes and they are optimally arranged this can still compensate for the lack of directionality. To study this possibility in greater detail, custom linear MPWs were assembled

that incorporated up to a total of 6 modular HomoFRET repeat sections within them yielding structures with a total of 16 dyes, see **Figure 8A–C**. These MPWs allowed for photonic transfer over more than a 31 nm distance with an efficiency of  $\approx 2\%$ , whereas no transfer took place when the repeats were removed. Subsequent studies on structurally similar constructs placed on solid substrates under cryogenic conditions demonstrated that these efficiencies could be increased by  $\approx 3$ -fold by minimizing the number of alternative and parasitic relaxation pathways.<sup>[155]</sup> Work realized by the Hanley group used DNA templates to align fluorescent proteins (monomeric teal fluorescent protein or labeled bovine serum albumin) to also look at HomoFRET transfer, finding that the total fluorescence was not the sum of the individual components and confirming the existence of parasitic traps.<sup>[157]</sup> Liedl and collaborators looked at HomoFRET within the context of a DNA origami that displayed non-linearly arranged HomoFRET regions (see **Figure 8D**).<sup>[158]</sup> Their relay was more triangular shaped, but still showed efficient relay capabilities with the HomoFRET section increasing transfer from 0% to 5% over 16 nm. The theoretical applicability of incorporating HomoFRET sections into MPWs is, in general quite large, but increased dye density is still required for optimal transfer. Paradoxically, increasing dye density (and therefore the total number of dyes) has its own inherent limitations as the possibility of energetic traps increases and if the dyes are brought too close together the dye can no longer be considered a point-dipole and FRET assumptions may break down.<sup>[154b,157b]</sup> Moreover, increasing an acceptor dye's density increases its direct absorption cross-section and thus its ability to be directly excited at the more blue-shifted donor excitation wavelength.

Inorganic NPs, and especially semiconductor QDs, can provide a photoluminescent alternative to organic dyes where their brightness and sharp emission bands contribute to and even augment FRET processes.<sup>[3a]</sup> Their high extinction coefficients, especially as the excitation wavelength shifts toward the blue wavelengths, in conjunction with their longer excited state lifetimes typically limit them to light harvesting and initiating donors within MPWs (except in the specific case of

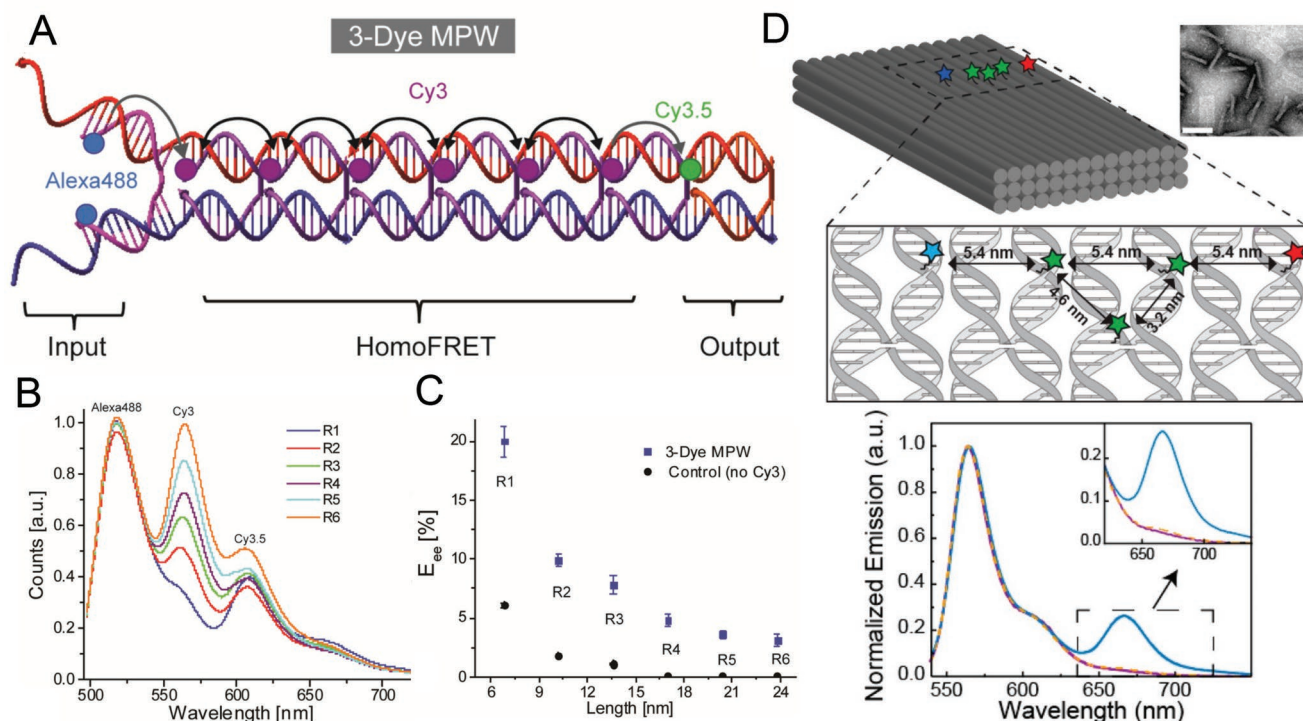


**Figure 8.** Representative MPWs exploiting HomoFRET. A) Schematic of MPW containing a modular HomoFRET relay section. B) Emission spectra of the MPW with increasing HomoFRET repeat (R) sections from R1 to R6. C) End-to-end transfer efficiency of MPW in (B). Reproduced with permission.<sup>[152]</sup> Copyright 2016, Wiley-VCH. D) Schematic representation of the three-layered DNA origami block. In the enlarged region, the scheme indicates the designed locations of the dye molecules with respect to the DNA strands. Possible energy pathways of the photonic wire and their corresponding transfer rates. Normalized emission spectra of the different configurations of the three-color cascade after Alexa488 excitation. Reproduced with permission.<sup>[158]</sup> Copyright 2017, American Chemical Society.

lanthanide-QD systems as detailed below).<sup>[148c,159]</sup> Nevertheless, assembling MPWs that incorporate QDs can still provide multiple inherent advantages. For example, they can act as a centralized nanoscaffold to display multiple equivalent DNA strands around them creating an enhanced efficiency system as compared to other nonhybrid systems.<sup>[148c,154a,160]</sup> Work from our group demonstrated that up to eight identical DNA MPWs could be connected to a 530 nm emitting donor QD, with each arm having four different sequentially arranged donor-acceptor dyes (Cy3, Cy3.5, Cy5, and Cy5.5) creating a system with 41 fluorophores, see **Figure 9A**.<sup>[160]</sup> This system could be further controlled by integrating an intercalating dye (BOBO-3) into the system.<sup>[154a]</sup> By using hybrid peptido-DNA strands that exploit the metal affinity driven self-assembly of poly-histidine peptides onto the surface of QDs that contain  $Zn^{+2}$ , the MPWs could be conjugated in simple mix-together methodologies and still yield ratiometrically controlled QD-DNA<sub>n</sub> mixtures.<sup>[59a]</sup> These structures demonstrated transfer efficiencies of up to 8% over five distinct FRET steps.<sup>[160]</sup> The higher transfer efficiency values were only obtained by conjugating multiple DNA MPWs around the QD scaffold, for example, the same system with half the MPWs (reducing from 8 to 4) decreased efficiency to 5%, see **Figure 9B**.<sup>[160]</sup> The latter improvement arises since the first QD-Cy3 dye step is the most critical and placing more MPWs displaying this first acceptor around the QD increases the probability of this step occurring along with increasing its relative energy transfer efficiency.

Though FRET is the most studied mechanism for MPWs there has been considerable work into other mechanisms; of greatest interest is exploiting coherent ET within organic dyes to obtain transfer speeds and efficiencies unavailable in the weakly coupled FRET regime.<sup>[154b]</sup> This is actually a case of science imitating nature, as the two mechanisms, FRET and coherent transfer, are used in combination in plant and algal photosynthetic systems.<sup>[133b]</sup> Closely spaced dyes, separated by only a few base pairs, or even dye J- or H-aggregates within DNA templates can be exploited to transport photonic excitation.<sup>[161]</sup> In H-aggregates, i.e., head-to-head stacked aggregates, the Coulomb coupling is positive, generally resulting in quenched fluorescence. Conversely, in J-aggregates based on offset head-to-toe aggregates, the Coulomb coupling is negative with no modification of the fluorescence.<sup>[162]</sup> Nature has found ways to exploit this at room temperature, something that human-designed systems are just now beginning to explore. Within appropriately designed DNA structures, dye-labeled DNAs can be separated by only a few Å and when bound to the complementary DNA strand to form dsDNA they become more rigid, maintaining the dyes in a somewhat fixed position and orientation, which is potentially more conducive to coherent transfer. The Häner group has been studying this concept as the basis for potential coherent interactions for nearly a decade; they began much of their investigation by looking at the change in spectroscopic properties upon the formation of

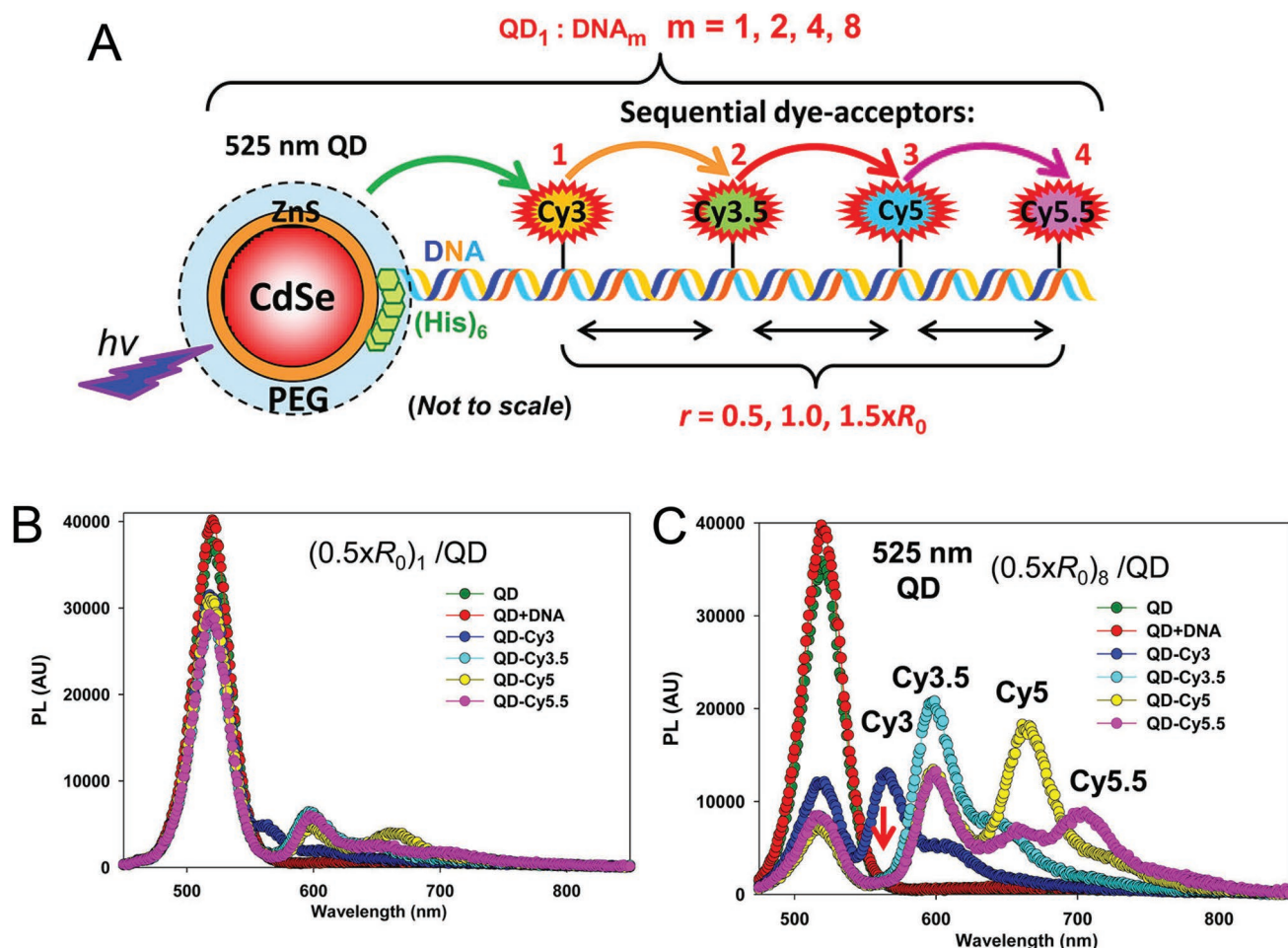


**Figure 9.** Molecular photonic wires incorporating QDs. A) Schematic of a central 525 nm emitting QD donor assembled with a peptide-DNA photonic wire by  $(\text{His})_6$ -metal affinity coordination; only one wire is shown for clarity. Pertinent characteristics that could be varied in these structures include the position and type of dyes, the interfluorophore distances, which were varied as a function of  $0.5 \times$ ,  $1.0 \times$ , and  $1.5 \times R_0$  along with the number of arms displayed around the QD, which were doubled incrementally from 1 to 8. These variables are highlighted in red. Fluorescent intensity profile of the  $0.5 \times R_0$  QD photonic wire when assembled with increasing DNA wires. Representative FRET progression of QD-DNA construct with B) 1 photonic wire per QD and C) 8 photonic wires per QD. Green and red curves correspond to the emission spectrum of DHLA-PEG coated QDs and QDs with an average of 1 dsDNA coupled to the surface, respectively. Subsequent curves show the intensity profile in the presence of additional FRET acceptors with  $0.5 \times R_0$  spacing until the full QD-[Cy3-Cy3.5-Cy5-Cy5.5] $_8$  configuration is reached. Reproduced with permission.<sup>[160]</sup> Copyright 2013, American Chemical Society.

dye-dimers within DNA.<sup>[163]</sup> Strong coupling of dyes in DNA can occur if they are covalently bound to the DNA, intercalated between the bp, or if certain types of artificial bps are utilized as fluorophores.<sup>[161]</sup> Porphyrins are some of the classical dyes used to study this phenomena in MPWs, the other common dyes being cyanines, as they will form H-type aggregates in the MPWs.<sup>[53b,164]</sup> The Häner group looked extensively at DNA templated MPWs with different dyes and an MPW of  $\pi$ -stacked phenanthrenes (up to 8) that could transfer light to the endpoint pyrene dye.<sup>[165]</sup> Continued investigations into these types of systems even demonstrated heteroaggregates systems using perylenediimide and pyrene templated by DNA.<sup>[166]</sup> To address the limitations of quenched fluorescence commonly associated with H-aggregates<sup>[167]</sup> as well as to create programmable systems, Boulais et al. used rigid DNA with special sequences preselected using exhaustive molecular dynamic simulations to organize pseudoisocyanine into J-like strongly coupled

aggregates.<sup>[168]</sup> The aggregate systems were capable of showing delocalized super-radiant exciton states while achieving greater long-range interactions with adjacent acceptors, see **Figure 10**.<sup>[169]</sup> Though at present there are still limitations such as weak binding of the aggregates to the DNA as well as a lack of alternative DNA sequences that may provide other binding templates for aggregates, this avenue of research shows the greatest promise in allowing MPWs to reach the potential efficiency desired from room-temperature coherent mechanisms.

### 6.3. Light Harvesting

Nature uses multiple precisely aligned chromophores within macromolecular photosynthetic complexes to optimize light-capture and subsequent transfer to the reaction centers.<sup>[170]</sup> As stated, investigators seek to use the powerful organizational



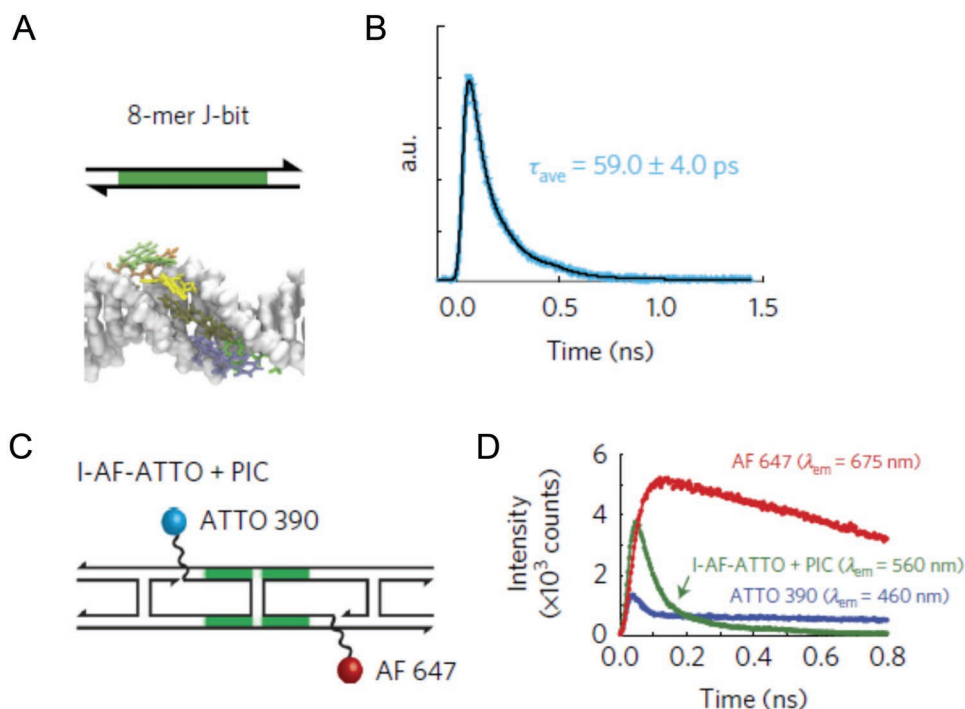


**Figure 10.** J-aggregates and FRET. A) The minimal J-aggregating synthetic DNA template (an 8-mer “J-bit”). B) Experimental fluorescence decay kinetics at 580 nm for the synthesized PIC J-bit. C) Schematic diagrams depicting the DX-tile constructs used to program multi-J-bit excitonic circuits with three-step energy transfer. D) Three-step energy transfer mediated by the multi-J-bit excitonic circuit. The ATTO 390 donor dye is excited with a 400 nm laser. Energy is subsequently transferred to the J-bits templated by the DX-tiles, and onward to the Alexa Fluor 647 acceptor dye. Reproduced with permission.<sup>[168]</sup> Copyright 2017, Springer Nature.

variability offered by DNA nanostructures in an attempt to elucidate the basic design principles that underwrite the near perfect energy transfer efficiencies observed in these assemblies. One of their driving motivations is that these design principles can then be applied to increase the functionality of dye-doped solar cells, for example, by increasing the capture section to most of the available solar spectra and then allow transport of those photons with near 100% efficiency to some type of reaction or charge conversion center. Much of the initial research in this vein overlaps to some extent with the previously discussed MPW research as linear DNA-dye arrangements were utilized as both antennae to capture the light and then relays to direct it downstream to an apex or some representative facsimile of a reaction center. Rather than add the complexity of trying to incorporate an actual macromolecular photosynthetic complex or equivalent into these initial structures, reaction centers are generally represented by red-shifted fluorescent emitters allowing for a far simpler read-out in a test structure. A good metric for comparing the efficiency in these systems is the antenna effect (AE), a measure of the light collecting ability of the dye network. AE is defined as the ratio of the fluorescence intensity of the acceptor ( $I_A$ ) upon excitation of the donor ( $D_{\lambda_{max}}$ ) to that of the direct excitation of the acceptor ( $A_{\lambda_{max}}$ ), with the excitation wavelengths being at or near their respective absorption maxima as given by

$$AE = \frac{I_{A, A_{\lambda_{max}}}}{I_{A, D_{\lambda_{max}}}} \quad (8)$$

An initial example of such a light harvesting MPW was based on a 7-helix origami bundle architecture that demonstrated picosecond time-scale funneling from pyrene through Cy3 to a final AF647 acceptor, see **Figure 11A** for a schematic and some representative data which reported 85% AE at pyrene excitation

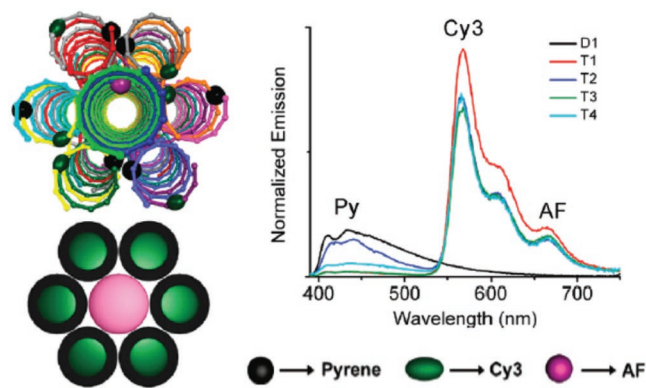


**Figure 11.** Light harvesting DNA constructs. Schematic representation of 7-helix bundle DNA origami light harvester. The black spheres, dark green ovals, and pink spheres represent Py, Cy3, and AF, respectively. The colored circles represent the presence of the dye molecules on the DNA helices. Normalized emission spectra with excitation at 380 nm. D1 – donor only. T1–T4 represent different ratios of each dye incorporated: T1 (6:6:1), T2 (6:3:1), T3 (3:6:1), T4 (1:1:1). Reproduced with permission.<sup>[171]</sup> Copyright 2011, American Chemical Society.



as compared to direct AF647 excitation.<sup>[171]</sup> Other investigations into the antennae capabilities of MPWs included aggregate systems similar to those discussed above.<sup>[165b,172]</sup> For example, 8  $\pi$ -stacked phenanthrenes formed through dsDNA presented 230% AE over direct excitation of a pyrene, though this effect was limited to a  $\approx 2$  nm length construct.<sup>[165a]</sup> Within the light-capture paradigm, dye-aggregates are of particular interest as their absorbance properties are greatly modified, shifting the absorbance peaks and allowing for greater coverage of broad white-light spectra.<sup>[173]</sup> An interesting example of this type was reported by Ensslen et al. who demonstrated a dsDNA wire with ethynyl pyrene, ethynyl perylene, and ethynyl nile red dyes incorporated as modified nucleosides. They showed photonic transfer from pyrene  $\rightarrow$  perylene  $\rightarrow$  nile red, but more surprisingly an electron transfer flowing in the opposite direction from nile red to pyrene or perylene, obtaining a charge separated state on the DNA wire, which is an important step in optimized photochemistry.<sup>[174]</sup>

DNA assemblies that extend beyond 1D structures or linear DNA wires can function to increase dye density and as such increase light harvesting and related capabilities. Assemblies of 2-D or 3-D DNA based on both origami or dendrimeric systems have been extensively studied to understand how to optimize light funneling, antenna effects, and other related properties.<sup>[175]</sup> Antenna effects at the single donor–acceptor level were studied on a DNA origami which allowed for very controlled positioning of multiple donors around a single acceptor. A linear increase in the antenna effect for up to six donor dyes (the maximum number of donors tested) was observed demonstrating that in simple systems the greater the number of donors to acceptor, the better the theoretical light harvesting should be.<sup>[34a]</sup> Detailed work by Buckhout-White et al. focused on resolving this question in systems of increasing complexity by systematically comparing different designs from simple wires through DNA stars and up to dendrimers of varying generations and branching ratios while also varying  $R_0$  values within the structures by altering the placement of dyes relative to each other.<sup>[176]</sup> See **Figure 12A–D** for some representative structures and plots of fluorescence spectra demonstrating the energy transfer. The base structures had up to 5 different dyes arranged in a sequential FRET cascade and the more complex architectures incorporated  $\approx 170$  individual dyes in one dendrimeric DNA. The results were observed using ensemble fluorescent measurements complemented by single-pair FRET and lifetime observations and it was concluded that the best light harvesting performance was obtained through a complex optimization of structural formation efficiency, absorption cross-section increases, and FRET efficiency within the individual steps.<sup>[176]</sup> A fourth generation 2-1 (donor per acceptor) dendrimeric architecture was thus deemed to be the more optimal light harvester than 3-1 or even 4-1 dendrimers, with the corresponding number of donors per sequential acceptor, as it created multiple interconnected and redundant energy transfer pathways in a more compact, better assembled (i.e., higher formation yield) DNA nanostructure. This dendrimer demonstrated a 200-fold increase in light harvesting when compared to a single DNA wire that contained the same variety of dyes (though far less total dyes). Based on these results, this optimized dendrimer scaffold was then

incorporated into multiple different configurations and hybrid nanostructures to test different FRET properties (vide infra).

The lessons learned from HomoFRET studies in linear DNA structures could be applied in light harvesting where it was shown that adding HomoFRET repeat modules into such complex structures also allowed them to act as antennas, see **Figure 13A–C**. This, however, only increased funneling efficiency up to a point as extending the antenna beyond five repeat dyes actually resulted in steady or decreased transfer to the terminus due to the aforementioned competition between directionality and transfer efficiency as the number of transfer steps are increased.<sup>[177]</sup> Nevertheless, hybrid vesicle assemblies formed by interacting dye-DNA structures within either lipid bilayers<sup>[178]</sup> or spermine<sup>[179]</sup> demonstrated high HomoFRET and increased light harvesting properties with nearly 20-fold augmented antenna effects. Such mixed biological structures, especially if a more rigid peptidyl scaffold structure could be incorporated, may be a powerful pathway to achieving nature-level efficiencies, however, this developing field is still challenged by lack of robust mixed (bio) material design and construction methodologies.<sup>[61a]</sup>

Complex multidimensional DNA structures have also been investigated for their ability to incorporate a variety of other photonic materials beyond organic dyes. For example, conjugation of DNA dendrimers to inorganic QDs allowed for the entire structure to function as a light harvester with directed transfer to an end point.<sup>[11g]</sup> The QD was again exploited here for its large extinction coefficient as well as its capability to scaffold or host multiple components around its surface. Light harvesting in this context does not have to be strictly limited to that originating from external photon sources and it can also occur from bioluminescent emitters as elegantly demonstrated by Rao and co-workers when they created luciferase-QD conjugates.<sup>[180]</sup> The bioluminescence arises from the oxidation of a chemical substrate, such as coelenterazine, by enzymes originally found in nature which produce emission spectra generally in the 450–500 nm region, including most commonly the firefly luciferase.<sup>[181]</sup> This concept was expanded by combining it with secondary fluorescent dyes bound to DNA.<sup>[182]</sup> Most bioluminescent emission tend to have very broad peaks making QDs an excellent energy acceptor for this due to their own broad absorption profiles. Placing additional dyes on the QD surface can improve overall cascaded transfer properties by either acting as FRET acceptors to the QD or directly capturing the energy from the luciferase emission themselves. In fact, dendrimeric DNA structures tend to be efficient enough on their own due to their inherent redundancy that they can be combined with a luciferase enzyme directly without requiring a QD to act as a light harvesting and donor relay or intermediary, see **Figure 14**.<sup>[181b]</sup> Depending on whether the bioluminescence resonance energy transfer (BRET)-FRET cascade was directed from the outside $\rightarrow$ in (luciferase on the exterior of the dendrimer) or inside $\rightarrow$ out (luciferase at the center of the dendrimer), the efficiency of harvesting the blue-shifted bioluminescence and delivering it to an apex point (Cy5.5 dye) was either 17% or 15%, respectively. These high transfer efficiencies, almost twice as high as similar cascades that included QDs with transfer efficiencies of  $\approx 9\%$ ,<sup>[181b]</sup> was the result of a greater direct interaction of the luciferase emission with down-stream acceptor dyes in the dendrimer configuration.<sup>[179b]</sup>

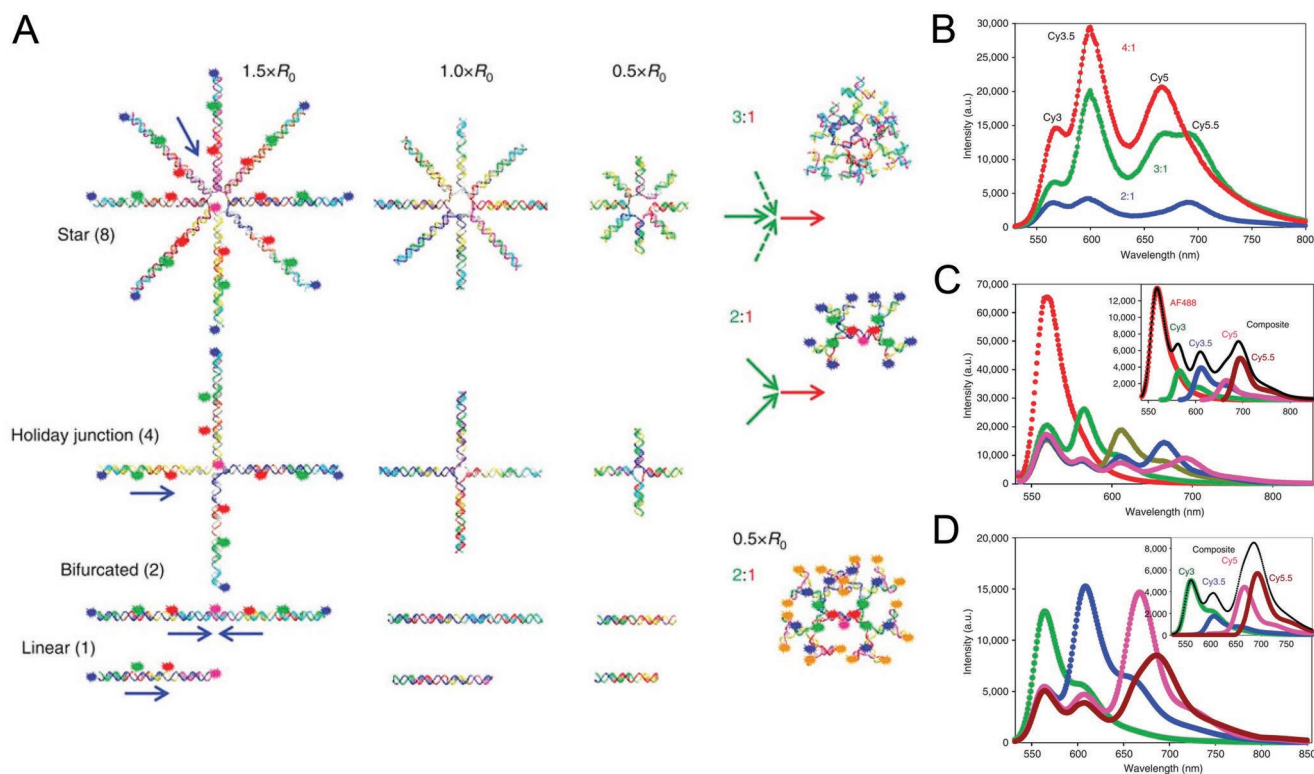


**Figure 12.** DNA light harvesting structures of increasing complexity. A)  $[\text{Cy}3 \rightarrow \text{Cy}3.5 \rightarrow \text{Cy}5]_n \rightarrow \text{Cy}5.5$  four-dye, three FRET step system with sequential donor–acceptor arrangements of Cy3 (blue), Cy3.5 (green), Cy5 (red), and Cy5.5 (pink) in photonic wire configurations. The number of  $[\text{Cy}3 \rightarrow \text{Cy}3.5 \rightarrow \text{Cy}5]_n$  wires leading into each terminal Cy5.5 dye increases similarly from one to eight using linear, bifurcated, Holliday junction and eight-arm star constructs. The blue arrows show the directionality of the FRET cascade(s) along each wire in each structure as they converge on the terminal Cy5.5 acceptor. Donor–acceptor spacing varied as  $0.5 \times$ ,  $1.0 \times$ , and  $1.5 \times R_0$ . The  $1.5 \times R_0$  schematic shows the approximate dye positions. Branched  $0.5 \times R_0$  dendrimer-based FRET systems utilizing Cy3, Cy3.5, Cy5, and Cy5.5 dyes in configurations were each dye preceding the central-terminal Cy5.5 has two or three donors. Donor–acceptor spacing's for the dendrimers were fixed at  $0.5 \times R_0$ , and the 2:1 structure shows approximate dye locations. Dendrimer-based five-dye FRET system utilizing AF488 (orange), Cy3 (blue), Cy3.5 (green), Cy5 (red), and Cy5.5 (pink) dyes in a configuration, where each dye preceding the central-terminal Cy5.5 has two donors shown as bottom 2:1 dendrimer. B) Representative comparative spectral data for the fully assembled 2:1, 3:1, and 4:1  $0.5 \times R_0$  dendrimer structures. Dye stoichiometries for dendrimer structures: 2:1 =  $\text{Cy}3_8 \rightarrow \text{Cy}3.5_4 \rightarrow \text{Cy}5_2 \rightarrow \text{Cy}5.5_1$ ; 3:1 =  $\text{Cy}3_{27} \rightarrow \text{Cy}3.5_9 \rightarrow \text{Cy}5_3 \rightarrow \text{Cy}5.5_1$  and 4:1 =  $\text{Cy}3_{64} \rightarrow \text{Cy}3.5_{16} \rightarrow \text{Cy}5_4 \rightarrow \text{Cy}5.5_1$ . C) Representative spectral data following the evolution of the five-dye 2:1  $0.5 \times R_0$  dendrimer AF488<sub>16</sub>  $\rightarrow$   $\text{Cy}3_8 \rightarrow \text{Cy}3.5_4 \rightarrow \text{Cy}5_2 \rightarrow \text{Cy}5.5_1$  system. Inset in (C) and (D) shows the spectra of fully formed structure along with each of the contributing component dyes. Constructs with Cy3 as the initial dye were excited at 515 nm, while those with AF488 were excited at 465 nm. Reproduced under the terms of the CC-BY license.<sup>[176]</sup> Copyright 2014, The Authors, published by Springer Nature.

The other common source of luminescence that is often times conjugated to DNA nanostructures is that originating from lanthanide ions. Lanthanide ions have interesting fluorescent properties as compared to normal fluorophores, they present multiple sharp emission lines with large Stokes shifts and extremely long excited-state lifetimes that are typically in the high  $\mu\text{s}$  to low ms range.<sup>[183]</sup> Lanthanides have been used as fluorophores within multichromophore DNA nanophotonics systems, both within simple DNA MPWs<sup>[184]</sup> as well as with hybrid lanthanide-dye-QD systems which have been applied to assays and diagnostics.<sup>[59b,185]</sup> Due to the inherent long-lifetimes of lanthanides as well as their generally small extinction coefficients found in the UV portion of the spectrum, they do not function well as relays or acceptors within energy transfer systems, rather they remain excellent initiators of energy cascades. The lanthanide systems are also one of the few cases beyond BRET where QDs can act as efficient FRET acceptors.<sup>[3a]</sup> Their extended lifetimes also open them up to exploitation in

time-gated and logic gate systems demonstrating several unique characteristics as detailed below.

#### 6.4. Molecular Actuators

The third use of DNA-templated multifluorophore systems described here are loosely characterized as actuators and they demonstrate utility primarily for sensing and computation. FRET is utilized extensively as the signal transduction modality within molecular beacons in all their different iterations.<sup>[186]</sup> This is due to the high sensitivity that can be achieved and the simple fluorescent readout that does not require additional assay steps.<sup>[92]</sup> Such DNA biosensors have applications in sensing a myriad of DNA targets as well as RNA; of particular interest currently is the detection of circulating microRNAs which may prove to be a simple diagnostic biomarker for a myriad of infection and disease states.<sup>[187]</sup> However, the small

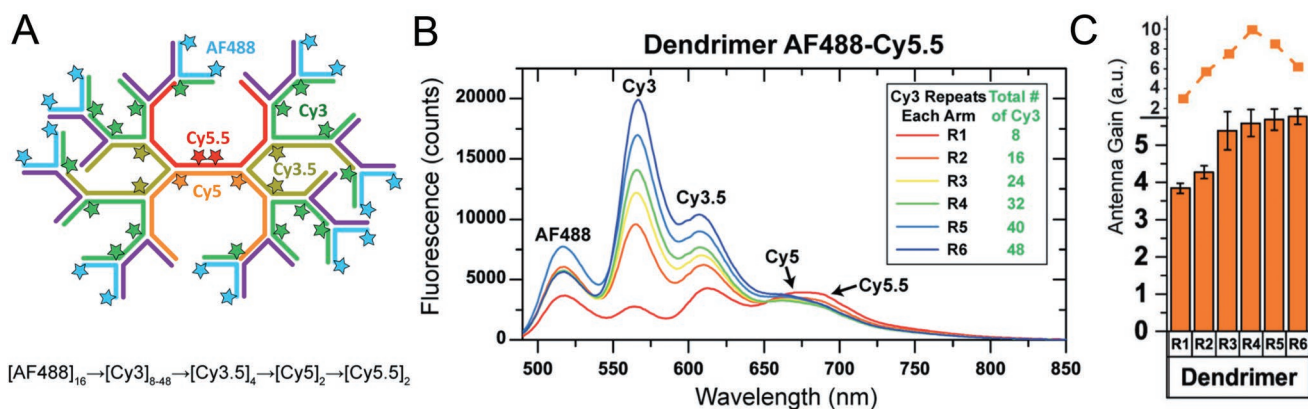


**Figure 13.** DNA dendrimer with increasing number of HomoFRET modules. A) Schematic of DNA dendrimer light harvester with two repeat HomoFRET sections (R2), along with B) the fluorescence spectra and C) antennae gain of the R1–R6 dendrimers as a function of HomoFRET repeat number. Blocks represent the experimental values, while the dots represent the theoretical predictions. Reproduced with permission.<sup>[177]</sup> Copyright 2017, Wiley-VCH.

size and limited number of available bps in these microRNAs make them quite challenging for direct hybridization-based sensing and they often require amplification steps and use of adaptors to extend their sequence length for FRET-based interrogation. The use of lanthanides and QDs as fluorescent probes has provided some success in overcoming these limitations as well as providing multiplexing capabilities.<sup>[188]</sup> Beyond this,

there are many methodologies for both sensing and computing utilizing DNA (based on molecular or Boolean logic), though we limit our focus to multifluorophore systems and recommend other sources to the reader interested in those areas.<sup>[30,189]</sup>

One way to increase the sensitivity toward detecting biomarkers and especially rare targets that may only be present in small copy numbers is to multiply the dye interactions in the

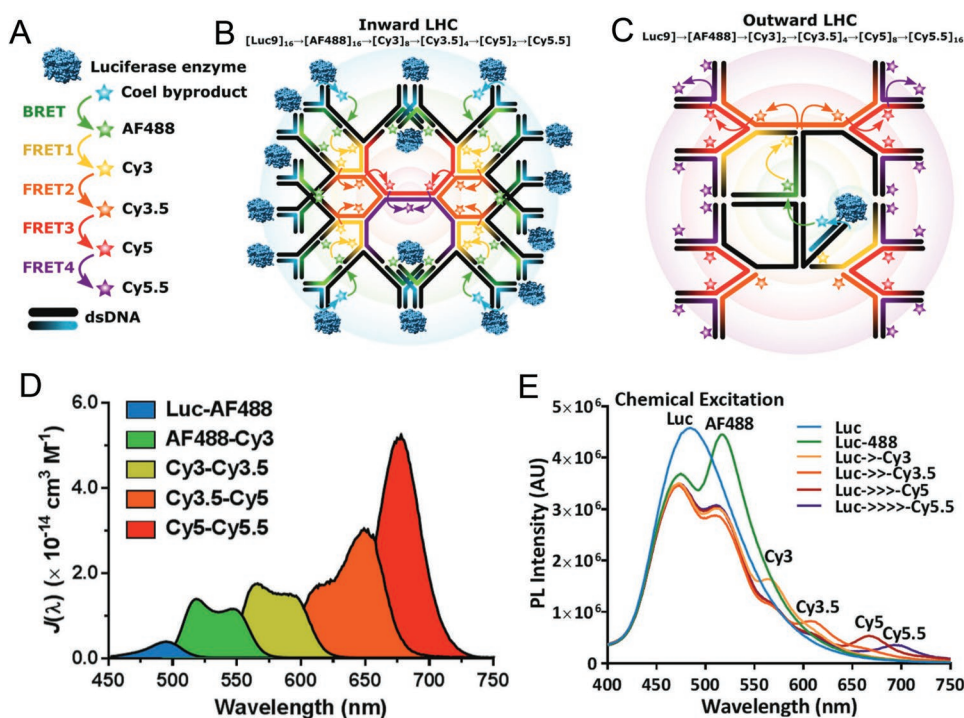


**Figure 14.** DNA light harvesting dendrimers sensitized with luciferase. A) Schematic of the sequential donor–acceptor energy transfer steps. B) Schematic of the inward LHC, in which 16 Luc9 (luciferase enzyme with 9 residues optimized) are displayed on the outside of the dendrimer and energy is transferred toward the terminal Cy5.5 at the center of the dendrimer through the multistep FRET relay with two donors per acceptor. C) Schematic of the outward LHC, in which a single Luc9 is attached in the center and excitons travel from the central Luc9 to the peripheral Cy5.5 dyes via the same FRET cascade but with two acceptors per donor. D) Integrand of the spectral overlap function versus wavelength of selected donor–acceptor fluorophore pairs. E) Emission profile of outward LHC with sequential addition of fluorophores. Arrows in the legends indicate the presence of intermediate. Reproduced with permission.<sup>[181b]</sup> Copyright 2017, Wiley-VCH.



biosensor from those based on a simple one donor–one acceptor configuration to one that incorporates multidye systems. DNA nanostructures provide the capability to arrange multiple copies of the same dyes, for example,<sup>[190]</sup> increasing sensitivity in a pH sensor by threefold.<sup>[191]</sup> Another strategy for greater signal-to-noise ratios is by creating energy cascades that are excited with blue-shifted wavelengths, and as such direct excitation of the acceptor dye can be avoided.<sup>[192]</sup> By using a simple 3-dye system and exploiting the 2-1 dendrimer structure previously discussed above, a  $\approx 20$ -fold increase in signal sensitivity could be achieved.<sup>[192b]</sup> Additionally, use of a dendrimer structure opens up the possibility of multiple types of sensing and read-outs beyond that of simple strand displacement. Indeed, steps such as strand replacement or structural rearrangement in which dyes are not extracted but their transfer efficiency is modified can now be incorporated, see the schematic in **Figure 15A**.<sup>[192b]</sup> The spectra shown in Figure 15B present the strand replacement of the Cy5-labeled DNA in the dendrimer and how a 15-fold change in the relative intensities of the Cy3 and Cy5.5 ratios is achieved. Of greater interest, Figure 15C, shows how

that same structure can be reformed upon returning to the initial fluorescent read-out allowing for dynamic monitoring. Accessing far more dynamic signal changes within the latter types of systems makes them optimal for creating logic gates where changes in their fluorescent readouts serve to reflect their function. Molecular logic gates are the building blocks for more complex computational tasks, but to function they should present robust photonic signals, both in signal intensity and readout speed.<sup>[190,193]</sup> In general, the inputs for DNA logic gates are most often other DNA strands, but RNA, enzymes, or small molecules can all function as input signals.<sup>[192a,194]</sup> Exploiting multistep FRET cascades for these purposes allows for clear threshold cut-offs that differentiate ON or OFF states. Similar to the development path of MPWs, the first examples of this class of structures utilized dsDNA and incorporated FRET pairs with conjugated and intercalating dyes.<sup>[195]</sup> Initial demonstrations from these systems were limited to AND, NAND, and INHIBIT types of logic operations, but the next generation examples also showed OR and NOT operations by using 4-dyes and exploiting DNA hairpin formation.<sup>[196]</sup> Full sets of Boolean

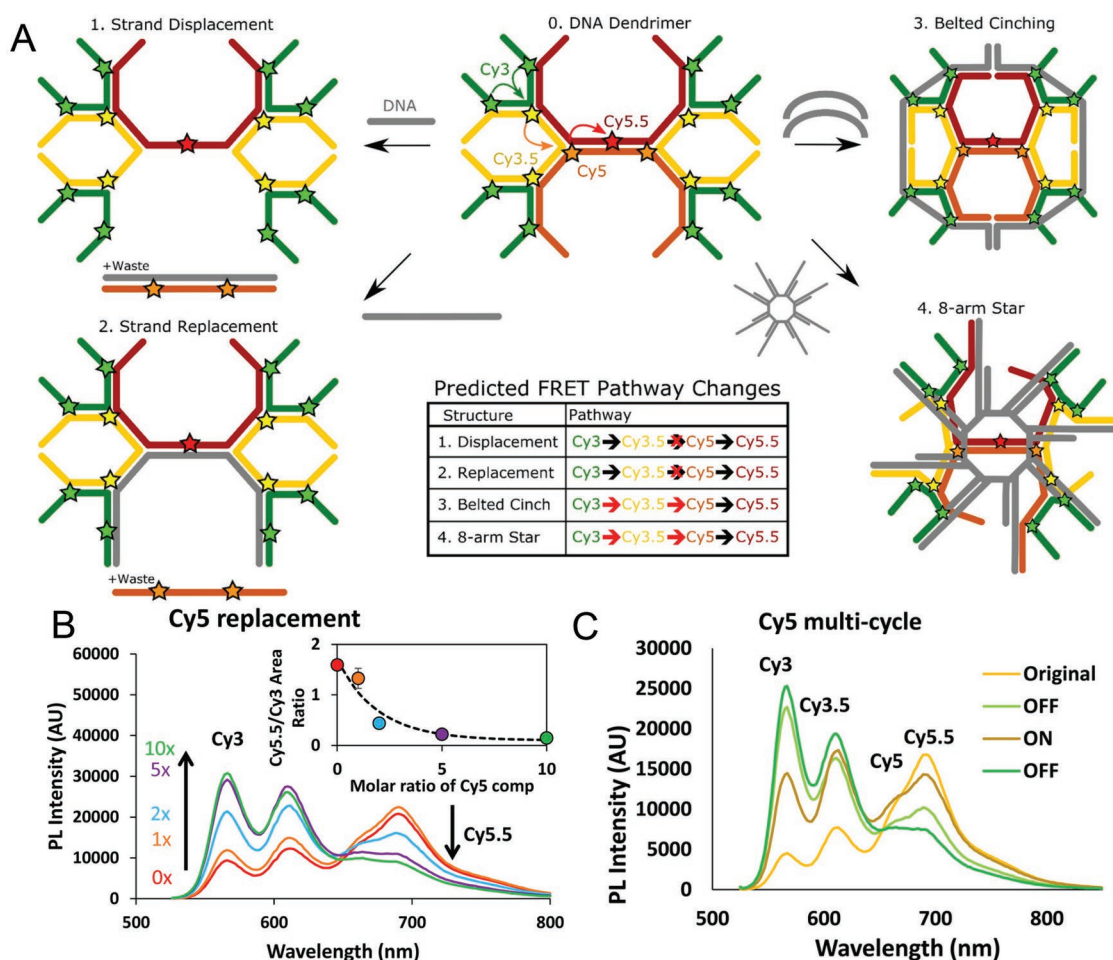


**Figure 15.** FRET and actuators. A) Schematic detailing the structural modification approaches to alter FRET cascades in a DNA dendrimer. The predicted changes to the FRET pathways, where arrows indicate FRET steps, include either altering FRET (red X) or increasing overall FRET efficiency through the cascade (red arrow). B) Strand replacement of the Cy5-labeled DNA strand with an unlabeled DNA strand at range of increasing ratios (1 ×, 2 ×, 5 ×, and 10 ×, with 0 × being the control). C) Multistep sequential cycling of Cy5 replacement. Reproduced with permission.<sup>[192b]</sup> Copyright 2017, American Chemical Society.

logic gates were then shown using DNA templated organic dyes as well as QDs.<sup>[197]</sup> These could be achieved on simple DNA wire structures but use of DNA-triads scaffolds enhanced the interactions of the FRET signals and allowed for far more varied inputs.<sup>[192a,198]</sup> This technology has shown remarkable progress with recent examples from the Reif lab reporting on renewable circuits which provide for multiuse gates as well as including a time-component to the response.<sup>[199]</sup> The dynamic modulation aspect is also the key to molecular photonic switches demonstrated on DNA templates. Using toe-hold mediated displacement, switches capable of more than four changes from ON to OFF with signal ratios in the range of nearly four could be obtained.<sup>[141a,198b]</sup> A particularly interesting use of this technology was described by LaBoda et al. in which a photonic pass gate was assembled where the gate control was actually a photon of a different wavelength.<sup>[200]</sup> By exciting the gate, it was pushed into a non-accepting dark-state opening the gate and allowing the excitation to reach the drain. The photonic modulation occurs at a much greater rate than can be obtained by strand displacement, but the modulation is limited to an ON/OFF ratio of only 1.2. In contrast to this, some of the highest ON/OFF signal ratios can be obtained by exploiting time-gated signals from lanthanide ions in MPWs where ratios in the range of 10 have been reported for three-input AND NAND operations (ratios are generally in the 2–4 range).<sup>[201]</sup> In general, use of lanthanide cryptates provide unique access to the temporal dimension with variable parameters that can extend from the nanosecond to millisecond range and this can certainly increase the richness of accessible molecule logic to include even on-the-fly gate transitions.<sup>[202]</sup> Although this has strong potential, it still remains mostly unexplored due in part to the requirement for specialized types of instrumentation. Other examples show how the hairpin modules of DNA can be used for ternary computing allowing for parallel operations,<sup>[203]</sup> or how exploiting modular localization allows calculation speeds to be decreased from hours to minutes and, of even greater interest, the same hairpins can be utilized across circuits due to the localization allowing for much greater circuit sizes.<sup>[194a]</sup>

## 7. Challenges and Outlook

The field of DNA-based photonic structures is in its initial discovery stage and this means that its potential is still wide open. As highlighted here, the goal is to exploit DNA self-assembly to design and construct nanoscale architectures with sophisticated morphologies and imbue them with customized optical properties that are achieved with nanometer resolutions. To this point, investigators are still primarily focused on demonstrating proof-of-principle research and then formulating optimized design principles and methodologies. As such, it is not clear which of the above application areas will really flesh out and fully develop or remain more of an academic interest. From a materials perspective, the primary challenges arise from the nature of the DNA scaffold itself along with all the optically active elements that need to be assembled on or displayed around the DNA scaffold.

As a scaffolding material, DNA offers unique properties and is unlike any other NMs currently available. This functional uniqueness allows it to be both the key enabling factor for the

above optical applications and also gives rise to many of the challenges faced when working with it. We must remind ourselves that the real-world dynamic picture of these systems does not correlate 100% with the static AFM image or computer rendering of a DNA structure. DNA is a biological material which has been evolutionarily optimized over billions of years to function in the confines of a cell and not in a test tube let alone on an optical table. The simplicity of its assembly chemistry, namely that of hybridization based solely on hydrogen bonding, gives it the ability to assemble itself in a temperature driven manner as so elegantly epitomized by origami formation. This, however, also greatly narrows its effective environmental boundaries and confines it to certain temperature ranges beyond which it is incompatible or, at the least, loses structural integrity. Even at a fixed temperature where a given structure is assumed to be stable, the DNA double helix is still active and often experiences a “breathing” effect which may disrupt the overall stability or otherwise impair optical applications that require very rigid, fixed spacing between individual or grouped optically active elements. This will be especially true with structures displaying lots of junctions and crossovers where the hydrogen bonding is not present for every bp or is under stress to dissociate. Some possible solutions to this may be found either in creating extremely dense DNA structures such as Yin’s bricks which may minimize such breathing<sup>[40]</sup> or, alternatively, chemically cross-linking the DNA strands to each other after formation.<sup>[204]</sup> Indeed some preliminary work utilizing DNA brick nanobreadboard structures to create FRET-based excitonic logic gates capable of repeated dynamic switching have already been reported.<sup>[205]</sup> An important issue to be appreciated in conjugation with the choice of which DNA assembly approach to utilize is that each requires design knowledge and comes with its own set of benefits and liabilities for a given application. Thus DNA bricks may not be a first choice at the current time but may soon increase in popularity if high density over a small structural space is needed. It is especially unclear how DNA devices will be integrated with the hard components of optical devices and what their viable lifetime will be in this configuration. It is possible that the DNA scaffold can either be covalently linked or chemically removed leaving the optical components in the desired architecture in a manner similar to what is done with lithography.<sup>[206]</sup> Another alternative is to align origamis displaying optically active elements with a hard device and functionally integrate them optically, electronically, or both. It is also important to note that DNA is a fundamental material of life and there exists a large application space where these same properties that are looked at as a liability for these applications are actually critically important.

From a higher level perspective, the field of structural DNA technology is still challenged overall by both assembly yields and formation efficiencies. Although a typical laboratory experimental format can produce from billions to trillions or more of DNA constructs, these are still miniscule quantities when considering what is needed for any large-scale optical application or utility. Fortunately, the ever decreasing cost of DNA synthesis and efforts to replace chemical synthesis with enzymatic-based processes can help address this.<sup>[207]</sup> Within a given structure that is formed in an experiment, it is still not clear how much of that structure is correctly formed and what inconsistencies

are present across the ensemble. Moreover, this will be exacerbated as DNA assemblies increase in size.<sup>[41]</sup> Unfortunately, the analytical capabilities and metrologies available to probe DNA structures of such magnitude do not have the requisite capabilities or sensitivity to answer such challenging questions.<sup>[61a,208]</sup> Perhaps, formation efficiencies that are “good enough” to provide a structure demonstrating enough of a requisite property will be sufficient for an application and not be precluded by the need to create and isolate only perfectly formed assemblies.

The above does not take into account the further complications of attaching optically active materials to discrete DNA sequences or attaching them onto already fully formed structures. As mentioned, dyes can range in size from the equivalent of just a few nucleotides while NPs can be on a scale that matches an entire origami and this brings with it many challenges. Compounding this, most chemistries to conjugate DNA with such materials suffer from a range of liabilities that can limit a desired application. Thus, the absolute placement of materials such as fluorescent molecules remains a challenge. Fortunately, strong interest in this and many related fluorescent applications are driving a strong impetus to develop newer, better, and more diverse bioconjugation chemistries in general.<sup>[61g,209]</sup> The growing library of accessible fluorescent nucleic acid analogs that can be incorporated into DNA during synthesis are one promising development toward addressing this issue.<sup>[51,52,210]</sup> Much of the limitations of DNA-fluorescent constructs continues to be in getting better formation efficiencies<sup>[39]</sup> as well as precision placement.<sup>[54]</sup> Additionally DNA is an active template that can interact with the conjugated fluorophores, often times in constructive manners but it can also inhibit the function we seek.<sup>[151]</sup> Pragmatically, the yield of the final functional-labeled material also tends to suffer from the multiple rounds of synthesis and purification needed.

In terms of the challenges faced by the specific applications envisioned here, we note that natural chiral molecules generally have weak chiral optical responses which often limits the scope of expanding their usage beyond studying macromolecules. It is possible that other metallic materials such as gold or silver could be coupled to the chiral molecules to enhance the optical responses. Since metallic materials offer a large number of quasi-free conduction electrons, they can inherently lead to much stronger optical responses. As a result, integrating metallic materials to the DNA double helix could enhance the optical signal beyond the UV range while also increasing response changes above that of the milli-degree range. It is important to note that the combination between DNA and other metallic materials depends on the physical scaffold which is used to hold the materials in place unlike natural molecules in which the bond of individual atoms or its subgroups dictate the overall structure. Since the chiral optical response strongly depends on the structure of the molecule, there is no guarantee that the hybrid chiral molecules/systems will exhibit an expected chiral response in all cases especially if the symmetry and the bond formation are not correctly aligned.<sup>[211]</sup> For plasmonic-based materials, it still remains difficult to construct increased order and complexity between the plasmonic molecules themselves and the scaffolds using both top-down and bottom-up approaches. The following challenges need to be cumulatively addressed in order to transcend to future

generation systems: (i) the capability to create uniform surface chemistry for the plasmonic NP/nanorod with different DNA scaffoldings; (ii) the capability to integrate different binding affinities (ssDNA or polymer) in order to create different shapes and complexities (sphere, rod, prism, cube, etc.); (iii) the capability to incorporate different plasmonic compositions (Au, Ag, Pd, etc.) in order to create broadband optical properties; (iv) and the capability to create isotropic and anisotropic NP of different sizes (5–200 nm) in order to address geometrical constraints. In addition, the vast library of other available NMs, such as QDs and metal oxide or magnetic NPs, have not been extensively explored for their capabilities to contribute to these or even newer applications and they could certainly open up exciting routes for future plasmonic research.

With the ability to create any arbitrary DNA structure, the issues pertinent to creating FRET systems have now become more pragmatic focusing on fluorophore conjugation to the DNA, control over dipole orientation, and achieving fluorophore diversity. As FRET is exquisitely sensitive to even slight sub-nanometer displacements, it is important to again consider the inherent movement or “breathing” of the DNA structures themselves. DNA quenching of certain dyes in a manner that is still not fully understood or predictable is also a continuing issue.<sup>[54]</sup> Additionally, the number and inherent diversity of fluorophores that are available for inserting into the materials is very limited. These issues are epitomized by trying to incorporate both fluorophores and QDs into the same DNA assembly where the inherent size differences present many challenges and constrains what can actually be achieved. The limitations of what FRET processes can contribute in these structures are becoming evident despite the complexity of the structures achieved.<sup>[176]</sup> The more promising area is now that of pursuing coherent interactions between dyes located on DNA scaffolds and within this approach issues of placement, rigidity, and especially orientation become critical to any potential coupling.<sup>[53b,78,154b]</sup> Another fascinating relevant material is that of DNA crystals, which have already been formed with optically active elements such as dyes included into their structure and have even demonstrated FRET process; these certainly have further potential for developing unique optical applications.<sup>[212]</sup>

Although only preliminary, the examples described here and the potential applications they are being developed for represent only a fraction of the possibilities for these materials. For example, a combination of different fluorescence sensing effects could be integrated to the same DNA nanostructure template. And by programming different DNA sequences while using the same number of fluorescence molecules, different sensing effects could be achieved and different nanosensing devices could be constructed. One exciting and largely unexplored possibility in the biosensing realm is to exploit the ability of DNA to perform Boolean and other types of computing via structural rearrangements as part of a sensing application. This could add a smart data processing aspect to any sensor configuration and allow it to differentiate between targets while signaling this to the user or even activating a physical response such as a drug release by a resulting strand displacement. Indeed, a preliminary proof of concept demonstrating this very strategy was recently reported.<sup>[213]</sup> Furthermore structural DNA nanotechnology also shows promise for other types of biomolecular sensing,



fluorescence spectroscopy, diffraction-limited optics, and light harvesting devices. Active plasmonic DNA materials are also of interest for photoacoustic imaging and photothermal therapy in vivo along with constructing biologically based organic light emitting diodes and creating new types of metamaterials.

The application where DNA structures still present perhaps the best near and long-term opportunity is that of acting as a precise scaffold for placement of diverse optically active materials in order to understand their near- and far-field interactions. This can extend to: fluorescent nanodiamonds, fluorescent proteins, photoactive enzymes, carbon and graphene QDs, upconversion NPs, fluorescent gold, and noble metal nanoclusters, for example.<sup>[4b–d,214]</sup> Such combinations present the exciting possibility to harvest via antenna or chemically generated blue light, transfer it across the spectrum to some terminal red-shifted acceptor and then allow it to be converted to useful energy or drive a reaction. This is not to say that dye–dye combinations on DNA do not have ample utility as well. For example, the Knowlton group recently demonstrated an all-optical dye–dye DNA-based excitonic switch, which operated in both the solid and liquid phase repeatedly with almost no fatigue.<sup>[50]</sup> Although the bioconjugation chemistry remains challenging, no other material allows this to be accomplished in such a controlled, massively parallel, and reproducible manner on the nanoscale. As more NMs displaying diverse optical and electronic properties are continuously being reported on almost a monthly basis, this capability to rapidly prototype and test both their near- and far-field optical interactions will certainly remain invaluable.

## Acknowledgements

The authors acknowledge the Office of Naval Research (ONR), the U.S. Naval Research Laboratory (NRL), the NRL-Nanosciences Institute, and the LUCI program through OSD for financial support.

## Conflict of Interest

The authors declare no conflict of interest.

## Keywords

chiral properties, DNA scaffolds, Förster resonance energy transfer, metamaterials, nanoscale optical devices, optically active molecules, plasmonic nanomaterials

Received: April 3, 2019

Revised: May 23, 2019

Published online:

- [1] a) B. J. W. S. Rayleigh, *The Collected Optics Papers of Lord Rayleigh*, Optical Society of America, Washington, DC **1994**; b) M. I. Kolobov, C. Fabre, *Phys. Rev. Lett.* **2000**, *85*, 3789.  
[2] M. C. Daniel, D. Astruc, *Chem. Rev.* **2004**, *104*, 293.  
[3] a) N. Hildebrandt, C. M. Spillmann, W. R. Algar, T. Pons, M. H. Stewart, E. Oh, K. Susumu, S. A. Díaz, J. B. Delehanty,

- I. L. Medintz, *Chem. Rev.* **2017**, *117*, 536; b) X. B. Li, C. H. Tung, L. Z. Wu, *Nat. Rev. Chem.* **2018**, *2*, 160.  
[4] a) S. A. Diaz, D. A. Hastman, I. L. Medintz, E. Oh, *J. Mater. Chem. B* **2017**, *5*, 7907; b) E. Oh, J. B. Delehanty, L. D. Field, A. J. Makinen, R. Goswami, A. L. Huston, I. L. Medintz, *Chem. Mater.* **2016**, *28*, 8676; c) E. Oh, F. K. Fatemi, M. Currie, J. B. Delehanty, T. Pons, A. Fragola, S. Leveque-Fort, R. Goswami, K. Susumu, A. L. Huston, I. L. Medintz, *Part. Part. Syst. Character.* **2013**, *30*, 453; d) E. Oh, A. L. Huston, A. Shabaev, A. Efros, M. Currie, K. Susumu, K. Bussmann, R. Goswami, F. K. Fatemi, I. L. Medintz, *Sci. Rep.* **2016**, *6*, 35538.  
[5] a) D. B. Luo, K. Nakata, A. Fujishima, S. H. Liu, *J. Photochem. Photobiol., C* **2017**, *31*, 139; b) Y. H. Zhang, K. Y. Rhee, D. Hui, S. J. Park, *Composites, Part B* **2018**, *143*, 19.  
[6] C. Hu, Y. Mu, M. Y. Li, J. S. Qiu, *Acta Phys.-Chim. Sin.* **2019**, *35*, 572.  
[7] Z. S. Luo, J. Manders, J. Yurek, *IEEE Spectrum* **2018**, *55*, 28.  
[8] N. J. Greybush, K. Charipar, J. A. Geldmeier, S. J. Bauman, P. Johns, J. Naciri, N. Charipar, K. Park, R. A. Vaia, J. Fontana, *ACS Nano* **2019**, *13*, 3875.  
[9] S. Samai, Z. X. Qian, J. Ling, K. N. Guye, D. S. Ginger, *ACS Appl. Mater. Interfaces* **2018**, *10*, 8976.  
[10] H. Hosokawa, R. Tamaki, T. Sawada, A. Okonogi, H. Sato, Y. Ogomi, S. Hayase, Y. Okada, T. Yano, *Nat. Commun.* **2019**, *10*, 43.  
[11] a) A. P. Alivisatos, W. W. Gu, C. Larabell, *Annu. Rev. Biomed. Eng.* **2005**, *7*, 55; b) A. L. Efros, J. B. Delehanty, A. L. Huston, I. L. Medintz, M. Barbic, T. D. Harris, *Nat. Nanotechnol.* **2018**, *13*, 278; c) L. D. Field, S. A. Walper, K. Susumu, G. Lasarte-Aragones, E. Oh, I. L. Medintz, J. B. Delehanty, *Bioconjugate Chem.* **2018**, *29*, 2455; d) L. Tang, S. E. Kocabas, S. Latif, A. K. Okay, D. S. Ly-Gagnon, K. C. Saraswat, D. A. B. Miller, *Nat. Photonics* **2008**, *2*, 226; e) X. Michalet, F. F. Pinaud, L. A. Bentolila, J. M. Tsay, S. Doose, J. J. Li, G. Sundaresan, A. M. Wu, S. S. Gambhir, S. Weiss, *Science* **2005**, *307*, 538; f) H. A. Nguyen, T. Grange, B. Reznichenko, I. Yeo, P. L. de Assis, D. Tumanov, F. Fratini, N. S. Malik, E. Dupuy, N. Gregersen, A. Auffeves, J. M. Gerard, J. Claudon, J. P. Poizat, *Phys. Rev. B* **2018**, *97*, 201106; g) A. Samanta, S. Buckhout-White, E. Oh, K. Susumu, I. L. Medintz, *Mol. Syst. Des. Eng.* **2018**, *3*, 314; h) J. A. Schuller, T. Taubner, M. L. Brongersma, *Nat. Photonics* **2009**, *3*, 658; i) Z. L. Song, S. M. Xu, J. Y. Liu, Z. X. Hu, N. B. Gao, J. B. Zhang, F. Yi, G. Z. Zhang, S. L. Jiang, H. Liu, *Sens. Actuators, B* **2018**, *271*, 147; j) A. S. Urban, T. Pfeiffer, M. Fedoruk, A. A. Lutich, J. Feldmann, *ACS Nano* **2011**, *5*, 3585; k) N. Yu, E. Cubukcu, L. Diehl, M. A. Belkin, K. B. Crozier, F. Capasso, D. Bour, S. Corzine, G. Hofler, *Appl. Phys. Lett.* **2007**, *91*, 173113.  
[12] R. W. Wagner, J. S. Lindsey, *J. Am. Chem. Soc.* **1994**, *116*, 9759.  
[13] S. Gwo, H. Y. Chen, M. H. Lin, L. Y. Sun, X. Q. Li, *Chem. Soc. Rev.* **2016**, *45*, 5672.  
[14] S. Okazaki, *Microelectron. Eng.* **2015**, *133*, 23.  
[15] a) J. W. Haus, *Fundamentals and Applications of Nanophotonics*, Woodhead Publishing, UK **2016**; b) M. Ohtsu, K. Kobayashi, T. Kawazoe, S. Sangu, T. Yatsui, *IEEE J. Sel. Top. Quantum Electron.* **2002**, *8*, 839.  
[16] a) N. C. Seeman, N. R. Kallenbach, *Biophys. J.* **1983**, *44*, 201; b) P. W. K. Rothmund, *Nature* **2006**, *440*, 297; c) A. V. Pinheiro, D. R. Han, W. M. Shih, H. Yan, *Nat. Nanotechnol.* **2011**, *6*, 763.  
[17] S. M. Douglas, A. H. Marblestone, S. Teerapittayanon, A. Vazquez, G. M. Church, W. M. Shih, *Nucleic Acids Res.* **2009**, *37*, 5001.  
[18] J. D. Watson, F. H. C. Crick, *Nature* **1953**, *171*, 737.  
[19] a) C. Bustamante, S. B. Smith, J. Liphardt, D. Smith, *Curr. Opin. Struct. Biol.* **2000**, *10*, 279; b) C. Bustamante, Z. Bryant, S. B. Smith, *Nature* **2003**, *421*, 423.  
[20] C. D. Mao, W. Q. Sun, N. C. Seeman, *Nature* **1997**, *386*, 137.  
[21] N. C. Seeman, *Nature* **2003**, *421*, 427.

- [22] N. C. Seeman, *J. Theor. Biol.* **1982**, *99*, 237.
- [23] R. Holliday, *Genet. Res.* **1964**, *5*, 282.
- [24] J. H. Chen, N. C. Seeman, *Nature* **1991**, *350*, 631.
- [25] a) B. Sacca, C. M. Niemeyer, *Angew. Chem., Int. Ed.* **2012**, *51*, 58; b) J. Bath, A. J. Turberfield, *Nat. Nanotechnol.* **2007**, *2*, 275; c) T. Liedl, T. L. Sobey, F. C. Simmel, *Nano Today* **2007**, *2*, 36; d) S. Modi, D. Bhatia, F. C. Simmel, Y. Krishnan, *J. Phys. Chem. Lett.* **2010**, *1*, 1994; e) J. Nangreave, D. R. Han, Y. Liu, H. Yan, *Curr. Opin. Chem. Biol.* **2010**, *14*, 608; f) W. M. Shih, C. X. Lin, *Curr. Opin. Struct. Biol.* **2010**, *20*, 276; g) T. Torring, N. V. Voigt, J. Nangreave, H. Yan, K. V. Gothelf, *Chem. Soc. Rev.* **2011**, *40*, 5636; h) F. C. Simmel, *Curr. Opin. Biotechnol.* **2012**, *23*, 516; i) F. Zhang, J. Nangreave, Y. Liu, H. Yan, *J. Am. Chem. Soc.* **2014**, *136*, 11198.
- [26] T. H. LaBean, H. Yan, J. Kopatsch, F. R. Liu, E. Winfree, J. H. Reif, N. C. Seeman, *J. Am. Chem. Soc.* **2000**, *122*, 1848.
- [27] a) S. H. Park, R. Barish, H. Y. Li, J. H. Reif, G. Finkelstein, H. Yan, T. H. LaBean, *Nano Lett.* **2005**, *5*, 693; b) J. H. Reif, *Comput. Sci. Eng.* **2002**, *4*, 32; c) E. Winfree, F. R. Liu, L. A. Wenzler, N. C. Seeman, *Nature* **1998**, *394*, 539; d) Y. He, Y. Chen, H. P. Liu, A. E. Ribbe, C. D. Mao, *J. Am. Chem. Soc.* **2005**, *127*, 12202.
- [28] Y. L. Wang, J. E. Mueller, B. Kemper, N. C. Seeman, *Biochemistry* **1991**, *30*, 5667.
- [29] T. J. Fu, N. C. Seeman, *Biochemistry* **1993**, *32*, 3211.
- [30] C. Mao, T. H. LaBean, J. H. Reif, N. C. Seeman, *Nature* **2000**, *407*, 493.
- [31] P. W. K. Rothmund, N. Papadakis, E. Winfree, *PLoS Biol.* **2004**, *2*, e424.
- [32] Y. He, T. Ye, M. Su, C. Zhang, A. E. Ribbe, W. Jiang, C. D. Mao, *Nature* **2008**, *452*, 198.
- [33] a) H. Y. Li, S. H. Park, J. H. Reif, T. H. LaBean, H. Yan, *J. Am. Chem. Soc.* **2004**, *126*, 418; b) C. X. Lin, Y. Liu, S. Rinker, H. Yan, *ChemPhysChem* **2006**, *7*, 1641.
- [34] a) E. A. Hemmig, C. Creatore, B. Wünsch, L. Hecker, P. Mair, M. A. Parker, S. Emmott, P. Tinnefeld, U. F. Keyser, A. W. Chin, *Nano Lett.* **2016**, *16*, 2369; b) P. Ensslen, H. A. Wagenknecht, *Acc. Chem. Res.* **2015**, *48*, 2724.
- [35] H. Dietz, S. M. Douglas, W. M. Shih, *Science* **2009**, *325*, 725.
- [36] D. R. Han, S. Pal, Y. Liu, H. Yan, *Nat. Nanotechnol.* **2010**, *5*, 712.
- [37] a) F. Zhang, S. X. Jiang, S. Y. Wu, Y. L. Li, C. D. Mao, Y. Liu, H. Yan, *Nat. Nanotechnol.* **2015**, *10*, 779; b) E. Benson, A. Mohammed, J. Gardell, S. Masich, E. Czeizler, P. Orponen, B. Hogberg, *Nature* **2015**, *523*, 441; c) R. Veneziano, S. Ratanalert, K. M. Zhang, F. Zhang, H. Yan, W. Chiu, M. Bathe, *Science* **2016**, *352*, 1534.
- [38] a) R. Veneziano, T. R. Shepherd, S. Ratanalert, L. Bellou, C. Q. Tao, M. Bathe, *Sci. Rep.* **2018**, *8*, 6548; b) X. X. Chen, Q. Wang, J. Peng, Q. P. Long, H. Y. Yu, Z. Li, *ACS Appl. Mater. Interfaces* **2018**, *10*, 24344.
- [39] A. N. Marchi, I. Saaem, B. N. Vogen, S. Brown, T. H. LaBean, *Nano Lett.* **2014**, *14*, 5740.
- [40] Y. G. Ke, L. L. Ong, W. M. Shih, P. Yin, *Science* **2012**, *338*, 1177.
- [41] L. L. Ong, N. Hanikel, O. K. Yaghi, C. Grun, M. T. Strauss, P. Bron, J. Lai-Kee-Him, F. Schueder, B. Wang, P. F. Wang, J. Y. Kishi, C. Myhrvold, A. Zhu, R. Jungmann, G. Bellot, Y. G. Ke, P. Yin, *Nature* **2017**, *552*, 72.
- [42] G. Tikhomirov, P. Petersen, L. Qian, *Nature* **2017**, *552*, 67.
- [43] K. Pan, E. Boulais, L. Yang, M. Bathe, *Nucleic Acids Res.* **2014**, *42*, 2159.
- [44] a) B. X. Shen, M. A. Kostianen, V. Linko, *Langmuir* **2018**, *34*, 14911; b) K. Tapio, J. Leppiniemi, B. X. Shen, V. P. Hytonen, W. Fritzsche, J. J. Toppari, *Nano Lett.* **2016**, *16*, 6780; c) P. F. Wang, T. A. Meyer, V. Pan, P. K. Dutta, Y. G. Ke, *Chem* **2017**, *2*, 359.
- [45] a) C. M. Niemeyer, *Angew. Chem., Int. Ed.* **2010**, *49*, 1200; b) A. Vigovskaya, D. Abt, I. Ahmed, C. M. Niemeyer, C. Barner-Kowollik, L. Fruk, *J. Mater. Chem. B* **2016**, *4*, 442.
- [46] L. Berti, J. Xie, I. L. Medintz, A. N. Glazer, R. A. Mathies, *Anal. Biochem.* **2001**, *292*, 188.
- [47] H. Farrokhpour, S. Abedi, H. Jouypazadeh, *Colloids Surf., B* **2019**, *173*, 493.
- [48] a) D. E. Prasuhn, J. B. Blanco-Canosa, G. J. Vora, J. B. Delehanty, K. Susumu, B. C. Mei, P. E. Dawson, I. L. Medintz, *ACS Nano* **2010**, *4*, 267; b) D. E. Prasuhn, A. Feltz, J. B. Blanco-Canosa, K. Susumu, M. H. Stewart, B. C. Mei, A. V. Yakovlev, C. Loukov, J. M. Mallet, M. Oheim, P. E. Dawson, I. L. Medintz, *ACS Nano* **2010**, *4*, 5487.
- [49] *Bioconjugate Techniques* (Ed: G. T. Hermanson), 3rd ed., Academic Press, San Diego **2013**.
- [50] N. Venkatesan, S. J. Kim, B. H. Kim, *Curr. Med. Chem.* **2003**, *10*, 1973.
- [51] M. S. Wranne, A. F. Fuchtbauer, B. Dumat, M. Bood, A. H. El-Sagheer, T. Brown, H. Graden, M. Groth, L. M. Wilhelmsson, *J. Am. Chem. Soc.* **2017**, *139*, 9271.
- [52] K. Borjesson, S. Preus, A. H. El-Sagheer, T. Brown, B. Albinsson, L. M. Wilhelmsson, *J. Am. Chem. Soc.* **2009**, *131*, 4288.
- [53] a) J. S. Melinger, A. Khachatryan, M. G. Ancona, S. Buckhout-White, E. R. Goldman, C. M. Spillmann, I. L. Medintz, P. D. Cunningham, *ACS Photonics* **2016**, *3*, 659; b) P. D. Cunningham, Y. C. Kim, S. A. Díaz, S. Buckhout-White, D. Mathur, I. L. Medintz, J. S. Melinger, *J. Phys. Chem. B* **2018**, *122*, 5020.
- [54] S. Sindbert, S. Kalinin, H. Nguyen, A. Kienzler, L. Clima, W. Bannwarth, B. Appel, S. Müller, C. A. M. Seidel, *J. Am. Chem. Soc.* **2011**, *133*, 2463.
- [55] a) H. Gudnason, M. Dufva, D. D. Bang, A. Wolff, *Nucleic Acids Res.* **2007**, *35*, e127; b) I. L. Medintz, B. M. Paegel, R. G. Blazej, C. A. Emrich, L. Berti, J. R. Scherer, R. A. Mathies, *Electrophoresis* **2001**, *22*, 3845; c) S. H. I. Yeung, I. L. Medintz, S. A. Greenspoon, R. A. Mathies, *Clin. Chem.* **2008**, *54*, 1080.
- [56] J. C. Love, L. A. Estroff, J. K. Kriebel, R. G. Nuzzo, G. M. Whitesides, *Chem. Rev.* **2005**, *105*, 1103.
- [57] a) E. Oh, J. B. Delehanty, C. A. Klug, K. Susumu, W. R. Algar, R. Goswami, I. L. Medintz, *Chem. Commun.* **2018**, *54*, 1956; b) E. Oh, K. Susumu, A. J. Mäkinen, J. R. Deschamps, A. L. Huston, I. L. Medintz, *J. Phys. Chem. C* **2013**, *117*, 18947.
- [58] K. Boeneman, J. R. Deschamps, S. Buckhout-White, D. E. Prasuhn, J. B. Blanco-Canosa, P. E. Dawson, M. H. Stewart, K. Susumu, E. R. Goldman, M. Ancona, I. L. Medintz, *ACS Nano* **2010**, *4*, 7253.
- [59] a) J. B. Blanco-Canosa, M. Wu, K. Susumu, E. Petryayeva, T. L. Jennings, P. E. Dawson, W. R. Algar, I. L. Medintz, *Coord. Chem. Rev.* **2014**, *263–264*, 101; b) J. Guo, X. Qiu, C. Mingoos, J. R. Deschamps, K. Susumu, I. L. Medintz, N. Hildebrandt, *ACS Nano* **2019**, *13*, 505.
- [60] J. C. Breger, M. Muttenthaler, J. B. Delehanty, D. A. Thompson, E. Oh, K. Susumu, J. R. Deschamps, G. P. Anderson, L. D. Field, S. A. Walper, P. E. Dawson, I. L. Medintz, *Nanoscale* **2017**, *9*, 10447.
- [61] a) K. E. Sapsford, W. R. Algar, L. Berti, K. B. Gemmill, B. J. Casey, E. Oh, M. H. Stewart, I. L. Medintz, *Chem. Rev.* **2013**, *113*, 1904; b) W. R. Algar, D. E. Prasuhn, M. H. Stewart, T. L. Jennings, J. B. Blanco-Canosa, P. E. Dawson, I. L. Medintz, *Bioconjugate Chem.* **2011**, *22*, 825; c) M. R. Jones, K. D. Osberg, R. J. Macfarlane, M. R. Langille, C. A. Mirkin, *Chem. Rev.* **2011**, *111*, 3736; d) N. L. Rosi, C. A. Mirkin, *Chem. Rev.* **2005**, *105*, 1547; e) J. J. Storhoff, C. A. Mirkin, *Chem. Rev.* **1999**, *99*, 1849; f) *Chemoselective and Bioorthogonal Ligation Reactions: Concepts and Applications* (Eds: W. R. Algar, P. E. Dawson, I. L. Medintz), Wiley-VCH, Weinheim, Germany **2017**; g) M. Madsen, K. V. Gothelf, *Chem. Rev.* **2019**, *119*, 6384.
- [62] E. M. Heckman, J. A. Hagen, P. P. Yaney, J. G. Grote, F. K. Hopkins, *Appl. Phys. Lett.* **2005**, *87*, 211115.
- [63] R. Khazaeinezhad, S. Hosseinzadeh Kassani, B. Paulson, H. Jeong, J. Gwak, F. Rotermond, D.-I. Yeom, K. Oh, *Sci. Rep.* **2017**, *7*, 41480.

- [64] J. A. Hagen, W. Li, A. J. Steckl, J. G. Grote, *Appl. Phys. Lett.* **2006**, *88*, 171109.
- [65] a) Y.-C. Hung, D. M. Bauer, I. Ahmed, L. Fruk, *Methods* **2014**, *67*, 105; b) F. Ouchen, I. Rau, F. Kajzar, E. Heckman, J. G. Grote, presented at *SPIE OPTO*, San Francisco, California, USA **2018**, p. 105290L.
- [66] Y.-C. Hung, T.-Y. Lin, W.-T. Hsu, Y.-W. Chiu, Y.-S. Wang, L. Fruk, *Opt. Mater.* **2012**, *34*, 1208.
- [67] D. Mathur, A. Samanta, E. Oh, S. A. Diaz, K. Susumu, M. G. Ancona, I. L. Medintz, *Chem. Mater.* **2017**, *29*, 5762.
- [68] T. Šmidlehner, I. Piantanida, G. Pescitelli, *Beilstein J. Org. Chem.* **2017**, *14*, 84.
- [69] a) E. A. Jares-Erijman, T. M. Jovin, *J. Mol. Biol.* **1996**, *257*, 597; b) C. Chen, M. Li, Y. Xing, Y. Li, C.-C. Joedecke, J. Jin, Z. Yang, D. Liu, *Langmuir* **2012**, *28*, 17743.
- [70] V. I. Doderio, Z. B. Quirolo, M. A. Sequeira, *Front. Biosci.* **2011**, *16*, 61.
- [71] L. D. Barron, *Strategies of Life Detection*, Springer, Berlin **2008**, p. 187.
- [72] L. A. Nguyen, H. He, C. Pham-Huy, *Int. J. Biomed. Sci.* **2006**, *2*, 85.
- [73] M. Balaz, S. Tannir, K. Varga, *Coord. Chem. Rev.* **2017**, *349*, 66.
- [74] Y. Gao, S. Or, A. Toop, I. Wheeldon, *Langmuir* **2017**, *33*, 2033.
- [75] a) K. Dutta, T. Fujimoto, M. Inoue, D. Miyoshi, N. Sugimoto, *Chem. Commun.* **2010**, *46*, 7772; b) C. X. Lin, Y. G. Ke, Z. Li, J. H. Wang, Y. Liu, H. Yan, *Nano Lett.* **2009**, *9*, 433.
- [76] A. H. J. Wang, G. J. Quigley, F. J. Kolpak, J. L. Crawford, J. H. Vanboom, G. Vandermarel, A. Rich, *Nature* **1979**, *282*, 680.
- [77] T. Biver, B. Garcia, J. M. Leal, F. Secco, E. Turriani, *Phys. Chem. Chem. Phys.* **2010**, *12*, 13309.
- [78] P. D. Cunningham, W. P. Bricker, S. A. Diaz, I. L. Medintz, M. Bathe, J. S. Melinger, *J. Chem. Phys.* **2017**, *147*, 055101.
- [79] a) M. M. Bhanjadeso, A. K. Nayak, U. Subudhi, *Biochem. Biophys. Res. Commun.* **2017**, *482*, 916; b) A. K. Nayak, A. Mishra, B. S. Jena, B. K. Mishra, U. Subudhi, *Sci. Rep.* **2016**, *6*, 26855.
- [80] Y. M. Chang, C. K. M. Chen, M. H. Hou, *Int. J. Mol. Sci.* **2012**, *13*, 3394.
- [81] L. Alarcón, Y. Baena, R. Manzo, *Sci. Pharm.* **2017**, *85*, 1.
- [82] S.-I. Shin, S. Ham, J. Park, S. H. Seo, C. H. Lim, H. Jeon, J. Huh, T.-Y. Roh, *DNA Res.* **2016**, *23*, 477.
- [83] a) M. Govindaraju, F. S. Monica, R. Berrocal, K. R. S. Sambasiva Rao, K. S. Rao, *Curr. Trends Biotechnol. Pharm.* **2012**, *6*, 204; b) A. Suram, J. K. S. Rao, K. S. Latha, M. A. Viswamitra, *NeuroMol. Med.* **2002**, *2*, 289.
- [84] a) P. Charoenphol, H. Bermudez, *Acta Biomater.* **2014**, *10*, 1683; b) D. Mathur, I. L. Medintz, *Adv. Healthcare Mater.* **2019**, *8*, 1801546.
- [85] M. Rezaee, R. K. Oskuee, H. Nassirli, B. Malaekhe-Nikouei, *J. Controlled Release* **2016**, *236*, 1.
- [86] T. K. Prasad, V. Gopal, N. Madhusudhana Rao, *Biochim. Biophys. Acta, Gen. Subj.* **2003**, *1619*, 59.
- [87] N. J. Zuidam, Y. Barenholz, A. Minsky, *FEBS Lett.* **1999**, *457*, 419.
- [88] N. S. Chiaramoni, L. C. Baccarini, M. C. Taira, S. Del V. Alonso, *J. Biol. Phys.* **2008**, *34*, 179.
- [89] H. Yin, R. L. Kanasty, A. E. Eltoukhy, A. J. Vegas, J. R. Dorkin, D. G. Anderson, *Nat. Rev. Genet.* **2014**, *15*, 541.
- [90] C. Zhang, W. M. Wu, X. Li, C. Tian, H. Qian, G. S. Wang, W. Jiang, C. D. Mao, *Angew. Chem., Int. Ed.* **2012**, *51*, 7999.
- [91] C. D. Mao, W. Q. Sun, Z. Y. Shen, N. C. Seeman, *Nature* **1999**, *397*, 144.
- [92] I. Medintz, N. Hildebrandt, *FRET – Förster Resonance Energy Transfer: From Theory to Applications*, Wiley-VCH Verlag GmbH, Weinheim, Germany **2013**.
- [93] A. Rajendran, M. Endo, K. Hidaka, H. Sugiyama, *J. Am. Chem. Soc.* **2013**, *135*, 1117.
- [94] F. Zhang, C. R. Simmons, J. Gates, Y. Liu, H. Yan, *Angew. Chem., Int. Ed.* **2018**, *57*, 12504.
- [95] a) U. Resch-Genger, M. Grabolle, S. Cavaliere-Jaricot, R. Nitschke, T. Nann, *Nat. Methods* **2008**, *5*, 763; b) R. P. Haugland, *The Handbook: A Guide to Fluorescent Probes and Labeling Technologies*, Invitrogen, San Diego **2005**.
- [96] Y. Choi, T. Kang, L. P. Lee, *Nano Lett.* **2009**, *9*, 85.
- [97] S. Zhang, D. A. Genov, Y. Wang, M. Liu, X. Zhang, *Phys. Rev. Lett.* **2008**, *101*, 047401.
- [98] S. A. Maier, *Plasmonics: Fundamentals and Applications*, Springer Science & Business Media, New York, NY **2007**.
- [99] a) C. F. Bohren, D. R. Huffman, *Absorption and Scattering of Light by Small Particles*, Wiley-VCH, New York, NY **1983**; b) J. Fontana, B. R. Ratna, *Appl. Phys. Lett.* **2014**, *105*, 011107.
- [100] E. Cubukcu, E. A. Kort, K. B. Crozier, F. Capasso, *Appl. Phys. Lett.* **2006**, *89*, 093120.
- [101] a) M. W. Knight, N. S. King, L. Liu, H. O. Everitt, P. Nordlander, N. J. Halas, *ACS Nano* **2014**, *8*, 834; b) C. Gong, M. S. Leite, *ACS Photonics* **2016**, *3*, 507; c) Y. Wang, A. Capretti, L. Dal Negro, *Opt. Mater. Express* **2015**, *5*, 2415; d) A. Agrawal, S. H. Cho, O. Zandi, S. Ghosh, R. W. Johns, D. J. Milliron, *Chem. Rev.* **2018**, *118*, 3121.
- [102] a) A. L. González, C. Noguez, J. Beránek, A. S. Barnard, *J. Phys. Chem. C* **2014**, *118*, 9128; b) C. L. Nehl, J. H. Hafner, *J. Mater. Chem.* **2008**, *18*, 2415; c) J. Fontana, R. Nita, N. Charipar, J. Naciri, K. Park, A. Dunkelberger, J. Owrutsky, A. Piqué, R. Vaia, B. Ratna, *Adv. Opt. Mater.* **2017**, *5*, 1700335.
- [103] a) K.-S. Lee, M. A. El-Sayed, *J. Phys. Chem. B* **2006**, *110*, 19220; b) A. B. Taylor, P. Zijlstra, *ACS Sens.* **2017**, *2*, 1103; c) B. Doherty, M. Thiele, S. Warren-Smith, E. Schartner, H. Ebendorff-Heidepriem, W. Fritzsche, M. A. Schmidt, *Opt. Lett.* **2017**, *42*, 4395.
- [104] a) N. J. Halas, S. Lal, W. S. Chang, S. Link, P. Nordlander, *Chem. Rev.* **2011**, *111*, 3913; b) A. Kuzyk, R. Jungmann, G. P. Acuna, N. Liu, *ACS Photonics* **2018**, *5*, 1151.
- [105] P. Nordlander, C. Oubre, E. Prodan, K. Li, M. I. Stockman, *Nano Lett.* **2004**, *4*, 899.
- [106] M. A. El-Sayed, P. K. Jain, W. Y. Huang, *Nano Lett.* **2007**, *7*, 2080.
- [107] L. Gunnarsson, E. J. Bjerneld, H. Xu, S. Petronis, B. Kasemo, M. Käll, *Appl. Phys. Lett.* **2001**, *78*, 802.
- [108] O. Perez-Gonzalez, N. Zabala, A. G. Borisov, N. J. Halas, P. Nordlander, J. Aizpurua, *Nano Lett.* **2010**, *10*, 3090.
- [109] a) L. O. Herrmann, V. K. Valev, C. Tserkezis, J. S. Barnard, S. Kasera, O. A. Scherman, J. Aizpurua, J. J. Baumberg, *Nat. Commun.* **2014**, *5*, 4568; b) J. Fontana, N. Charipar, S. R. Flom, J. Naciri, A. Piqué, B. R. Ratna, *ACS Photonics* **2016**, *3*, 904.
- [110] J. Fontana, B. R. Ratna, *Appl. Opt.* **2015**, *54*, F61.
- [111] N. Yu, F. Capasso, *Nat. Mater.* **2014**, *13*, 139.
- [112] S. Linic, P. Christopher, D. B. Ingram, *Nat. Mater.* **2011**, *10*, 911.
- [113] N. Engheta, *Science* **2007**, *317*, 1698.
- [114] a) Z. Xuming, C. Yu Lim, L. Ru-Shi, T. Din Ping, *Rep. Prog. Phys.* **2013**, *76*, 046401; b) W. Hou, S. B. Cronin, *Adv. Funct. Mater.* **2013**, *23*, 1612.
- [115] a) K. Kneipp, Y. Wang, H. Kneipp, L. T. Perelman, I. Itzkan, R. Dasari, M. S. Feld, *Phys. Rev. Lett.* **1997**, *78*, 1667; b) K. Kneipp, H. Kneipp, V. B. Kartha, R. Manoharan, G. Deinum, I. Itzkan, R. R. Dasari, M. S. Feld, *Phys. Rev. E* **1998**, *57*, R6281; c) J. D. Caldwell, O. Glembocki, F. J. Bezares, N. D. Bassim, R. W. Rendell, M. Feygelson, M. Ukaegbu, R. Kasica, L. Shirey, C. Hosten, *ACS Nano* **2011**, *5*, 4046; d) J. Fontana, J. Livener, F. J. Bezares, J. D. Caldwell, R. Rendell, B. R. Ratna, *Appl. Phys. Lett.* **2013**, *102*, 201606; e) W. Lee, S. Y. Lee, R. M. Briber, O. Rabin, *Adv. Funct. Mater.* **2011**, *21*, 3424.
- [116] a) M. P. Cecchini, V. A. Turek, J. Paget, A. A. Kornyshev, J. B. Edel, *Nat. Mater.* **2013**, *12*, 165; b) W. Xie, B. Walkenfort, S. Schlücker, *J. Am. Chem. Soc.* **2013**, *135*, 1657.



- [117] a) V. B. Koman, P. Liu, D. Kozawa, A. T. Liu, A. L. Cottrill, Y. Son, J. A. Lebron, M. S. Strano, *Nat. Nanotechnol.* **2018**, *13*, 819; b) J. Geldmeier, P. Johns, N. Greybush, J. Naciri, J. Fontana, *Phys. Rev. B* **2018**, *99*, 081112(R).
- [118] a) N. Liu, T. Liedl, *Chem. Rev.* **2018**, *118*, 3032; b) M. Pilo-Pais, G. P. Acuna, P. Tinnefeld, T. Liedl, *MRS Bull.* **2017**, *42*, 936; c) S. J. Tan, M. J. Campolongo, D. Luo, W. L. Cheng, *Nat. Nanotechnol.* **2011**, *6*, 268; d) A. Ceconello, L. V. Besteiro, A. O. Govorov, I. Willner, *Nat. Rev. Mater.* **2017**, *2*, 17039; e) J. M. Ou, H. J. Tan, X. D. Chen, Z. Chen, *Nanomaterials* **2018**, *8*, 994; f) C. Zhou, X. Y. Duan, N. Liu, *Acc. Chem. Res.* **2017**, *50*, 2906.
- [119] a) J. P. Zhang, Y. Liu, Y. G. Ke, H. Yan, *Nano Lett.* **2006**, *6*, 248; b) J. W. Zheng, P. E. Constantinou, C. Micheel, A. P. Alivisatos, R. A. Kiehl, N. C. Seeman, *Nano Lett.* **2006**, *6*, 1502; c) J. Sharma, R. Chhabra, A. Cheng, J. Brownell, Y. Liu, H. Yan, *Science* **2009**, *323*, 112.
- [120] a) Y. Y. Pinto, J. D. Le, N. C. Seeman, K. Musier-Forsyth, T. A. Taton, R. A. Kiehl, *Nano Lett.* **2005**, *5*, 2399; b) Q. Liu, C. Song, Z. G. Wang, N. Li, B. Q. Ding, *Methods* **2014**, *67*, 205.
- [121] S. Pal, Z. T. Deng, B. Q. Ding, H. Yan, Y. Liu, *Angew. Chem., Int. Ed.* **2010**, *49*, 2700.
- [122] A. J. Mastroianni, S. A. Claridge, A. P. Alivisatos, *J. Am. Chem. Soc.* **2009**, *131*, 8455.
- [123] R. Elghanian, J. J. Storhoff, R. C. Mucic, R. L. Letsinger, C. A. Mirkin, *Science* **1997**, *277*, 1078.
- [124] a) B. Q. Ding, Z. T. Deng, H. Yan, S. Cabrini, R. N. Zuckermann, J. Bokor, *J. Am. Chem. Soc.* **2010**, *132*, 3248; b) S. Pal, Z. T. Deng, H. N. Wang, S. L. Zou, Y. Liu, H. Yan, *J. Am. Chem. Soc.* **2011**, *133*, 17606.
- [125] a) M. Pilo-Pais, S. Goldberg, E. Samano, T. H. LaBean, G. Finkelstein, *Nano Lett.* **2011**, *11*, 3489; b) R. Schreiber, S. Kempter, S. Holler, V. Schuller, D. Schiffels, S. S. Simmel, P. C. Nickels, T. Liedl, *Small* **2011**, *7*, 1795.
- [126] W. Sun, E. Boulais, Y. Hakobyan, W. L. Wang, A. Guan, M. Bathe, P. Yin, *Science* **2014**, *346*, 717.
- [127] a) A. Kuzyk, R. Schreiber, Z. Y. Fan, G. Pardatscher, E. M. Roller, A. Hoge, F. C. Simmel, A. O. Govorov, T. Liedl, *Nature* **2012**, *483*, 311; b) Z. T. Li, Z. N. Zhu, W. J. Liu, Y. L. Zhou, B. Han, Y. Gao, Z. Y. Tang, *J. Am. Chem. Soc.* **2012**, *134*, 3322; c) X. B. Shen, C. Song, J. Y. Wang, D. W. Shi, Z. A. Wang, N. Liu, B. Q. Ding, *J. Am. Chem. Soc.* **2012**, *134*, 146; d) J. Elbaz, A. Ceconello, Z. Y. Fan, A. O. Govorov, I. Willner, *Nat. Commun.* **2013**, *4*, 2000; e) R. Schreiber, N. Luong, Z. Y. Fan, A. Kuzyk, P. C. Nickels, T. Zhang, D. M. Smith, B. Yurke, W. Kuang, A. O. Govorov, T. Liedl, *Nat. Commun.* **2013**, *4*, 2948; f) C. C. Rao, Z. G. Wang, N. Li, W. Zhang, X. C. Xu, B. Q. Ding, *Nanoscale* **2015**, *7*, 9147; g) G. B. Yao, J. Li, J. Chao, H. Pei, H. J. Liu, Y. Zhao, J. Y. Shi, Q. Huang, L. H. Wang, W. Huang, C. H. Fan, *Angew. Chem., Int. Ed.* **2015**, *54*, 2966; h) R. Schreiber, I. Santiago, A. Ardavan, A. J. Turberfield, *ACS Nano* **2016**, *10*, 7303; i) C. Vietz, B. Lalkens, G. P. Acuna, P. Tinnefeld, *New J. Phys.* **2016**, *18*, 045012; j) B. Liu, C. Y. Song, D. Zhu, X. Wang, M. Z. Zhao, Y. J. Yang, Y. N. Zhang, S. Su, J. Y. Shi, J. Chao, H. J. Liu, Y. Zhao, C. H. Fan, L. H. Wang, *Small* **2017**, *13*, 1603991; k) P. F. Zhan, P. K. Dutta, P. F. Wang, G. Song, M. J. Dai, S. X. Zhao, Z. G. Wang, P. Yin, W. Zhang, B. Q. Ding, Y. G. Ke, *ACS Nano* **2017**, *11*, 1172; l) C. Zhou, X. Duan, N. Liu, *Acc. Chem. Res.* **2017**, *50*, 2906.
- [128] X. B. Shen, P. F. Zhan, A. Kuzyk, Q. Liu, A. Asenjo-Garcia, H. Zhang, F. J. G. de Abajo, A. Govorov, B. Q. Ding, N. Liu, *Nanoscale* **2014**, *6*, 2077.
- [129] X. Lan, X. X. Lu, C. Q. Shen, Y. G. Ke, W. H. Ni, Q. B. Wang, *J. Am. Chem. Soc.* **2015**, *137*, 457.
- [130] a) S. Etcheverry, L. F. Araujo, G. K. B. da Costa, J. M. B. Pereira, A. R. Camara, J. Naciri, B. R. Ratna, I. Hernández-Romano, C. J. S. de Matos, I. C. S. Carvalho, W. Margulis, J. Fontana, *Optica* **2017**, *4*, 864; b) J. Fontana, G. K. B. da Costa, J. M. Pereira, J. Naciri, B. R. Ratna, P. Palffy-Muhoray, I. C. S. Carvalho, *Appl. Phys. Lett.* **2016**, *108*, 081904.
- [131] A. Kuzyk, M. J. Urban, A. Idili, F. Ricci, N. Liu, *Sci. Adv.* **2017**, *3*, e1602803.
- [132] C. Zhou, X. Y. Duan, N. Liu, *Nat. Commun.* **2015**, *6*, 8102.
- [133] a) G. E. Hoffman, M. V. Sanchez-Puerta, C. F. Delwiche, *BMC Evol. Biol.* **2011**, *11*, 101; b) B. S. Rolczynski, H. Zheng, V. P. Singh, P. Navotnaya, A. R. Ginzburg, J. R. Caram, K. Ashraf, A. T. Gardiner, S.-H. Yeh, S. Kais, R. J. Cogdell, G. S. Engel, *Chem* **2018**, *4*, 138.
- [134] N. Keren, Y. Paltiel, *Trends Plant Sci.* **2018**, *23*, 497.
- [135] A. Dietrich, V. Buschmann, C. Müller, M. Sauer, *Rev. Mol. Biotechnol.* **2002**, *82*, 211.
- [136] C. M. Spillmann, I. L. Medintz, *J. Photochem. Photobiol., C* **2015**, *23*, 1.
- [137] J. R. Lakowicz, *Principles of Fluorescence Spectroscopy*, Springer, New York, NY **2006**.
- [138] a) E. A. Jares-Erijman, T. M. Jovin, *Nat. Biotechnol.* **2003**, *21*, 1387; b) W. R. Algar, N. Hildebrandt, S. S. Vogel, I. L. Medintz, *Nat. Methods* **2019**; c) C. E. Rowland, J. B. Delehanty, C. L. Dwyer, I. L. Medintz, *Mater. Today* **2017**, *20*, 131; d) C. E. Rowland, C. W. Brown, I. L. Medintz, J. B. Delehanty, *Methods Appl. Fluoresc.* **2015**, *3*, 042006.
- [139] I. L. Medintz, A. R. Clapp, F. M. Brunel, T. Tiefenbrunn, H. T. Uyeda, E. L. Chang, J. R. Deschamps, P. E. Dawson, H. Mattoussi, *Nat. Mater.* **2006**, *5*, 581.
- [140] C. Devadoss, P. Bharathi, J. S. Moore, *J. Am. Chem. Soc.* **1996**, *118*, 9635.
- [141] a) E. Graugnard, D. L. Kellis, H. Bui, S. Barnes, W. Kuang, J. Lee, W. L. Hughes, W. B. Knowlton, B. Yurke, *Nano Lett.* **2012**, *12*, 2117; b) B. Albinsson, J. K. Hannestad, K. Borjesson, *Coord. Chem. Rev.* **2012**, *256*, 2399; c) W. R. Algar, H. Kim, I. L. Medintz, N. Hildebrandt, *Coord. Chem. Rev.* **2014**, *263–264*, 65; d) B. Hotzer, I. L. Medintz, N. Hildebrandt, *Small* **2012**, *8*, 2297; e) Y. N. Teo, E. T. Kool, *Chem. Rev.* **2012**, *112*, 4221; f) P. Tinnefeld, M. Heilemann, M. Sauer, *ChemPhysChem* **2005**, *6*, 217; g) R. Varghese, H. A. Wagenknecht, *Chem. Commun.* **2009**, *19*, 2615; h) F. Wang, C. H. Lu, I. Willner, *Chem. Rev.* **2014**, *114*, 2881.
- [142] a) M. Dai, in *3D DNA Nanostructure: Methods and Protocols*, Vol. 1500 (Eds: Y. Ke, P. Wang), Springer, New York, NY **2017**, p. 185; b) E. Turriani, C. Höbartner, T. M. Jovin, *Nucleic Acids Res.* **2015**, *43*, 40; c) D. Mathur, E. R. Henderson, *Sci. Rep.* **2016**, *6*, 27413.
- [143] Y. Ohya, K. Yabuki, M. Hashimoto, A. Nakajima, T. Ouchi, *Bioconjugate Chem.* **2003**, *14*, 1057.
- [144] S. Vyawahare, S. Eyal, K. D. Mathews, S. R. Quake, *Nano Lett.* **2004**, *4*, 1035.
- [145] G. Sánchez-Mosteiro, E. M. H. P. van Dijk, J. Hernando, M. Heilemann, P. Tinnefeld, M. Sauer, F. Koberlin, M. Patting, M. Wahl, R. Erdmann, N. F. van Hulst, M. F. García-Parajó, *J. Phys. Chem. B* **2006**, *110*, 26349.
- [146] M. Heilemann, R. Kasper, P. Tinnefeld, M. Sauer, *J. Am. Chem. Soc.* **2006**, *128*, 16864.
- [147] G. D. Todor, K. Stefka, J. V. Juan, *Recent Pat. Mater. Sci.* **2009**, *2*, 1.
- [148] a) J. K. Hannestad, S. R. Gerrard, T. Brown, B. Albinsson, *Small* **2011**, *7*, 3178; b) J. K. Hannestad, P. Sandin, B. Albinsson, *J. Am. Chem. Soc.* **2008**, *130*, 15889; c) T. C. Lim, V. J. Bailey, Y. P. Ho, T. H. Wang, *Nanotechnology* **2008**, *19*, 075507.
- [149] a) I. H. Stein, C. Steinhauer, P. Tinnefeld, *J. Am. Chem. Soc.* **2011**, *133*, 4193; b) W. Su, C. R. Bagshaw, G. A. Burley, *Sci. Rep.* **2013**, *3*, 1883.
- [150] C. M. Spillmann, S. Buckhout-White, E. Oh, E. R. Goldman, M. G. Ancona, I. L. Medintz, *Chem. Commun.* **2014**, *50*, 7246.
- [151] B. J. Harvey, M. Levitus, *J. Fluoresc.* **2009**, *19*, 443.

- [152] S. A. Díaz, S. Buckhout-White, M. G. Ancona, C. M. Spillmann, E. R. Goldman, J. S. Melinger, I. L. Medintz, *Adv. Opt. Mater.* **2016**, 4, 399.
- [153] a) S. Kalinin, T. Peulen, S. Sindbert, P. J. Rothwell, S. Berger, T. Restle, R. S. Goody, H. Gohlke, C. A. M. Seidel, *Nat. Methods* **2012**, 9, 1218; b) S. Preus, K. Kilså, F. A. Miannay, B. Albinsson, L. M. Wilhelmsson, *Nucleic Acids Res.* **2013**, 41, e18; c) P. Moroz, W. P. Klein, K. Akers, A. Vore, N. Kholmicheva, N. Razgoniaeva, D. Khon, S. A. Díaz, I. L. Medintz, M. Zamkov, *J. Phys. Chem. C* **2017**, 121, 26226.
- [154] a) K. Boeneman, D. E. Prasuhn, J. B. Blanco-Canosa, P. E. Dawson, J. S. Melinger, M. Ancona, M. H. Stewart, K. Susumu, A. Huston, I. L. Medintz, *J. Am. Chem. Soc.* **2010**, 132, 18177; b) P. D. Cunningham, A. Khachatrian, S. Buckhout-White, J. R. Deschamps, E. R. Goldman, I. L. Medintz, J. S. Melinger, *J. Phys. Chem. B* **2014**, 118, 14555.
- [155] S. A. Díaz, S. M. Oliver, D. A. Hastman, I. L. Medintz, P. M. Vora, *J. Phys. Chem. Lett.* **2018**, 9, 3654.
- [156] S. Ranjit, K. Gurunathan, M. Levitus, *J. Phys. Chem. B* **2009**, 113, 7861.
- [157] a) Z. Gholami, Q. Hanley, *Bioconjugate Chem.* **2014**, 25, 1820; b) Z. Zolmajd-Haghighi, Q. S. Hanley, *Biophys. J.* **2014**, 106, 1457.
- [158] F. Nicoli, A. Barth, W. Bae, F. Neukirchinger, A. H. Crevenna, D. C. Lamb, T. Liedl, *ACS Nano* **2017**, 11, 11264.
- [159] H. Lu, O. Schöps, U. Woggon, C. M. Niemeyer, *J. Am. Chem. Soc.* **2008**, 130, 4815.
- [160] C. M. Spillmann, M. G. Ancona, S. Buckhout-White, W. R. Algar, M. H. Stewart, K. Susumu, A. L. Huston, E. R. Goldman, I. L. Medintz, *ACS Nano* **2013**, 7, 7101.
- [161] H. Asanuma, T. Fujii, T. Kato, H. Kashida, *J. Photochem. Photobiol., C* **2012**, 13, 124.
- [162] N. J. Hestand, F. C. Spano, *Chem. Rev.* **2018**, 118, 7069.
- [163] a) D. Wenger, V. L. Malinovskii, R. Haner, *Chem. Commun.* **2011**, 47, 3168; b) V. L. Malinovskii, D. Wenger, R. Haner, *Chem. Soc. Rev.* **2010**, 39, 410.
- [164] M. Vybornyi, A. L. Nussbaumer, S. M. Langenegger, R. Häner, *Bioconjugate Chem.* **2014**, 25, 1785.
- [165] a) F. Garo, R. Häner, *Bioconjugate Chem.* **2012**, 23, 2105; b) F. Garo, R. Häner, *Angew. Chem., Int. Ed.* **2012**, 51, 916.
- [166] C. B. Winiger, S. M. Langenegger, G. Calzaferrri, R. Häner, *Angew. Chem., Int. Ed.* **2015**, 54, 3643.
- [167] B. L. Cannon, L. K. Patten, D. L. Kellis, P. H. Davis, J. Lee, E. Graugnard, B. Yurke, W. B. Knowlton, *J. Phys. Chem. A* **2018**, 122, 2086.
- [168] É. Boulais, N. P. D. Sawaya, R. Veneziano, A. Andreoni, J. L. Banal, T. Kondo, S. Mandal, S. Lin, G. S. Schlau-Cohen, N. W. Woodbury, H. Yan, A. Aspuru-Guzik, M. Bathe, *Nat. Mater.* **2018**, 17, 159.
- [169] J. L. Banal, T. Kondo, R. Veneziano, M. Bathe, G. S. Schlau-Cohen, *J. Phys. Chem. Lett.* **2017**, 8, 5827.
- [170] T. Mirkovic, E. E. Ostroumov, J. M. Anna, R. van Grondelle, Govindjee, G. D. Scholes, *Chem. Rev.* **2017**, 117, 249.
- [171] P. K. Dutta, R. Varghese, J. Nangreave, S. Lin, H. Yan, Y. Liu, *J. Am. Chem. Soc.* **2011**, 133, 11985.
- [172] M. Probst, S. M. Langenegger, R. Haner, *Chem. Commun.* **2014**, 50, 159.
- [173] B. L. Cannon, D. L. Kellis, L. K. Patten, P. H. Davis, J. Lee, E. Graugnard, B. Yurke, W. B. Knowlton, *J. Phys. Chem. A* **2017**, 121, 6905.
- [174] P. Ensslen, F. Brandl, S. Sezi, R. Varghese, R. J. Kutta, B. Dick, H. A. Wagenknecht, *Chem. - Eur. J.* **2015**, 21, 9349.
- [175] N. T. Anderson, P. H. Dinolfo, X. Wang, *J. Mater. Chem. C* **2018**, 6, 2452.
- [176] S. Buckhout-White, C. M. Spillmann, W. R. Algar, A. Khachatrian, J. S. Melinger, E. R. Goldman, M. G. Ancona, I. L. Medintz, *Nat. Commun.* **2014**, 5, 5615.
- [177] W. P. Klein, S. A. Díaz, S. Buckhout-White, J. S. Melinger, P. D. Cunningham, E. R. Goldman, M. G. Ancona, W. Kuang, I. L. Medintz, *Adv. Opt. Mater.* **2018**, 6, 1700679.
- [178] J. G. Woller, J. K. Hannestad, B. Albinsson, *J. Am. Chem. Soc.* **2013**, 135, 2759.
- [179] C. D. Bösch, J. Jevric, N. Bürki, M. Probst, S. M. Langenegger, R. Häner, *Bioconjugate Chem.* **2018**, 29, 1505.
- [180] Y. Zhang, M. K. So, A. M. Loening, H. Yao, S. S. Gambhir, J. Rao, *Angew. Chem., Int. Ed.* **2006**, 45, 4936.
- [181] a) J. G. Mild, L. R. Fernandez, O. Gayet, J. Iovanna, N. Dusetti, M. M. Edreira, *Mol. Biotechnol.* **2018**, 60, 369; b) C. W. Brown, A. Samanta, S. A. Díaz, S. Buckhout-White, S. A. Walper, E. R. Goldman, I. L. Medintz, *Adv. Opt. Mater.* **2017**, 5, 1700181.
- [182] a) C. L. Dwyer, S. A. Díaz, S. A. Walper, A. Samanta, K. Susumu, E. Oh, S. Buckhout-White, I. L. Medintz, *Chem. Mater.* **2015**, 27, 6490; b) R. Alam, J. Zylstra, D. M. Fontaine, B. R. Branchini, M. M. Maye, *Nanoscale* **2013**, 5, 5303.
- [183] N. Hildebrandt, K. D. Wegner, W. R. Algar, *Coord. Chem. Rev.* **2014**, 273–274, 125.
- [184] M. Massey, M. G. Ancona, I. L. Medintz, W. R. Algar, *ACS Photonics* **2015**, 2, 639.
- [185] a) S. A. Díaz, G. Lasarte Aragonés, S. Buckhout-White, X. Qiu, E. Oh, K. Susumu, J. S. Melinger, A. L. Huston, N. Hildebrandt, I. L. Medintz, *J. Phys. Chem. Lett.* **2017**, 8, 2182; b) X. Qiu, J. J. Guo, Z. W. Jin, A. Petreto, I. L. Medintz, N. Hildebrandt, *Small* **2017**, 13, 1700332; c) Y. T. Wu, X. Qiu, S. Lindbo, K. Susumu, I. L. Medintz, S. Hober, N. Hildebrandt, *Small* **2018**, 14, 1802266.
- [186] J. Zheng, R. Yang, M. Shi, C. Wu, X. Fang, Y. Li, J. Li, W. Tan, *Chem. Soc. Rev.* **2015**, 44, 3036.
- [187] S. Raghunath, A. Prasad, R. Tevatia, J. R. Gunther, S. Roy, S. Krishnan, R. F. Saraf, *ChemElectroChem* **2018**, 5, 429.
- [188] a) X. Qiu, J. Guo, Z. Jin, A. Petreto, I. L. Medintz, N. Hildebrandt, *Small* **2017**, 13, 1700332; b) X. Qiu, J. Guo, J. Xu, N. Hildebrandt, *J. Phys. Chem. Lett.* **2018**, 9, 4379.
- [189] a) X. Su, X. Xiao, C. Zhang, M. Zhao, *Appl. Spectrosc.* **2012**, 66, 1249; b) A. Padirac, T. Fujii, Y. Rondelez, *Curr. Opin. Biotechnol.* **2013**, 24, 575; c) S. G. Harroun, C. Prévost-Tremblay, D. Lauzon, A. Desrosiers, X. Wang, L. Pedro, A. Vallée-Bélisle, *Nanoscale* **2018**, 10, 4607.
- [190] D. Selnihhin, S. M. Sparvath, S. Preus, V. Birkedal, E. S. Andersen, *ACS Nano* **2018**, 12, 5699.
- [191] Y. Choi, L. Kotthoff, L. Olejko, U. Resch-Genger, I. Bald, *ACS Appl. Mater. Interfaces* **2018**, 10, 23295.
- [192] a) S. Buckhout-White, C. Person, I. L. Medintz, E. R. Goldman, *ACS Omega* **2018**, 3, 495; b) C. W. Brown, S. Buckhout-White, S. A. Díaz, J. S. Melinger, M. G. Ancona, E. R. Goldman, I. L. Medintz, *ACS Sens.* **2017**, 2, 401.
- [193] a) H. Bui, S. Shah, R. Mokhtar, T. Song, S. Garg, J. Reif, *ACS Nano* **2018**, 12, 1146; b) H. Bui, V. Miao, S. Garg, R. Mokhtar, T. Song, J. Reif, *Small* **2017**, 13, 1602983.
- [194] a) G. Chatterjee, N. Dalchau, R. A. Muscat, A. Phillips, G. Seelig, *Nat. Nanotechnol.* **2017**, 12, 920; b) A. P. de Silva, S. Uchiyama, *Nat. Nanotechnol.* **2007**, 2, 399.
- [195] A. Saghatelian, N. H. Völcker, K. M. Guckian, V. S. Y. Lin, M. R. Ghadiri, *J. Am. Chem. Soc.* **2003**, 125, 346.
- [196] T. Nishimura, Y. Ogura, J. Tanida, *Appl. Phys. Lett.* **2012**, 101, 233703.
- [197] a) R. M. Zadegan, M. D. E. Jepsen, L. L. Hildebrandt, V. Birkedal, J. Kjems, *Small* **2015**, 11, 1811; b) X. He, Z. Li, M. Chen, N. Ma, *Angew. Chem., Int. Ed.* **2014**, 53, 14447.
- [198] a) S. Buckhout-White, C. W. Brown, D. A. Hastman, M. G. Ancona, J. S. Melinger, E. R. Goldman, I. L. Medintz, *RSC Adv.* **2016**, 6, 97587; b) S. Buckhout-White, J. C. Claussen, J. S. Melinger, Z. Dunningham, M. G. Ancona, E. R. Goldman, I. L. Medintz, *RSC Adv.* **2014**, 4, 48860.

- [199] a) S. Garg, S. Shah, H. Bui, T. Song, R. Mokhtar, J. Reif, *Small* **2018**, *14*, 1801470; b) X. Song, A. Eshra, C. Dwyer, J. Reif, *RSC Adv.* **2017**, *7*, 28130.
- [200] C. D. LaBoda, A. R. Lebeck, C. L. Dwyer, *Nano Lett.* **2017**, *17*, 3775.
- [201] M. Massey, I. L. Medintz, M. G. Ancona, W. R. Algar, *ACS Sens.* **2017**, *2*, 1205.
- [202] a) J. C. Claussen, W. R. Algar, N. Hildebrandt, K. Susumu, M. G. Ancona, I. L. Medintz, *Nanoscale* **2013**, *5*, 12156; b) J. C. Claussen, N. Hildebrandt, K. Susumu, M. G. Ancona, I. L. Medintz, *ACS Appl. Mater. Interfaces* **2014**, *6*, 3771.
- [203] R. Orbach, S. Lilienthal, M. Klein, R. D. Levine, F. Remacle, I. Willner, *Chem. Sci.* **2015**, *6*, 1288.
- [204] H. B. Rycenga, D. T. Long, *Curr. Opin. Pharmacol.* **2018**, *41*, 20.
- [205] B. L. Cannon, D. L. Kellis, P. H. Davis, J. Lee, W. Kuang, W. L. Hughes, E. Graugnard, B. Yurke, W. B. Knowlton, *ACS Photonics* **2015**, *2*, 398.
- [206] A. Gopinath, P. W. K. Rothmund, *ACS Nano* **2014**, *8*, 12030.
- [207] a) R. A. Hughes, A. D. Ellington, *Cold Spring Harbor Perspect. Biol.* **2017**, *9*, a023812; b) S. Kosuri, G. M. Church, *Nat. Methods* **2014**, *11*, 499.
- [208] a) D. Mathur, I. L. Medintz, *Anal. Chem.* **2017**, *89*, 2646; b) K. E. Sapsford, K. M. Tyner, B. J. Dair, J. R. Deschamps, I. L. Medintz, *Anal. Chem.* **2011**, *83*, 4453.
- [209] I. Medintz, *Nat. Mater.* **2006**, *5*, 842.
- [210] M. Wilhelmsson, Y. Tor, *Fluorescent Analogs of Biomolecular Building Blocks: Design and Applications*, Wiley, Hoboken, New Jersey **2016**.
- [211] M. Hentschel, M. Schaferling, X. Y. Duan, H. Giessen, N. Liu, *Sci. Adv.* **2017**, *3*, e1602735.
- [212] a) J. S. Melinger, R. Sha, C. Mao, N. C. Seeman, M. G. Ancona, *J. Phys. Chem. B* **2016**, *120*, 12287; b) B. Chu, D. Zhang, W. Hwang, P. J. Paukstelis, *J. Am. Chem. Soc.* **2018**, *140*, 16291.
- [213] H. Bui, C. W. Brown III, S. Buckhout-White, S. A. Díaz, M. H. Stewart, K. Susumu, E. Oh, M. G. Ancona, E. R. Goldman, I. L. Medintz, *Small* **2019**, *15*, 1805384.
- [214] a) E. Oh, F. K. Fatemi, M. Currie, J. B. Delehanty, T. Pons, A. Fragola, S. Lévêque-Fort, R. Goswami, K. Susumu, A. L. Huston, *Part. Part. Syst. Character.* **2013**, *30*, 453; b) S. Bhuckory, E. Hemmer, Y. T. Wu, A. Yahia-Ammar, F. Vetrone, N. Hildebrandt, *Eur. J. Inorg. Chem.* **2017**, *2017*, 5186.